The Institute of Paper Chemistry

Appleton, Wisconsin

Doctor's Dissertation

Turbulent Tube Flow of Dilute Fiber Suspensions

Truman L. Seely

January, 1968

TURBULENT TUBE FLOW OF DILUTE FIBER SUSPENSIONS

A thesis submitted by

Truman L. Seely

B.S. 1963, California Institute of Technology
M.S. 1965, Lawrence University

in partial fulfillment of the requirements
of The Institute of Paper Chemistry
for the degree of Doctor of Philosophy
from Lawrence University,
Appleton, Wisconsin

January, 1968

TABLE OF CONTENTS

SUMMARY

An experimental investigation of wood fiber suspensions in turbulent tube flow is described in the following text along with an empirical treatment of the data obtained.

Turbulent tube flow of dilute fiber suspensions (0.05 to 0.50 g./100 ml.) is divided into three distinct regions on the basis of pressure drop-flow rate correlations and velocity profiles. These regions are designated plug turbulence, damped turbulence, and Newtonian turbulence.

Some evidence is presented to suggest the presence of a coherent fiber network during plug turbulent flow which is notably lacking in the other two forms of suspension turbulence.

Damped turbulence is a flow region characterized by an apparently constant value of the friction factor over a wide range of flow rates. Within the turbulent core, a logarithmic distribution law similar to the universal velocity profile for a Newtonian fluid in turbulent flow is obeyed. However, the apparent von Kármán constant, κ, is lower than its Newtonian value and increases with flow rate. An empirical expression relating κ to the friction factor in this region, β, and to the conventional Reynolds number is:

$$\kappa = \left(\frac{\sqrt{\beta/2}}{1 - 13\sqrt{\beta/2}}\right)\left[\ln\left(\frac{Re\sqrt{\beta/2}}{60}\right) - \frac{3}{2}\right] \qquad (1) .$$

Newtonian turbulence is so designated because velocity profiles and $\underline{f}$ vs. $\underline{Re}$ correlations in this region are indistinguishable from the corresponding behavior of water alone. If β is replaced with $\underline{f}$, Equation (1) is valid in this region.

In addition to experimental data and empirical analyses, a flow loop and associated instruments are described in detail.

Special equipment to create known flow fields in creeping motion is described. A mathematical analysis of certain flow fields containing spherical fiber networks is presented to obtain an estimate of the stress applied to the network by the fluid motion. Experiments in specified flow fields are discussed in detail; and one quantitative estimate of network strength is reported. This estimate is considered to be in good agreement with flow loop data taken in plug turbulence.

A number of directions are suggested for possible future work.

INTRODUCTION

It is manifestly impossible to operate a present-day pulp or paper mill without large quantities of water to serve as a dispersing, transporting, and handling medium for the fibers which ultimately become the paper sheet. This rather straightforward observation has led a number of people to comment on and study the behavior of suspensions of fibers in water. Despite the efforts of these people, relatively little is known of the momentum transport properties or small-scale structure of flowing suspensions.

The lack of quantitative knowledge of suspension flow has apparently not prevented wide industrial use of fiber suspensions, particularly in pulp and paper manufacture. Doubtless this is partly due to the similarity of turbulent dilute suspension flow to turbulent water flow. It must also be due in part to the accumulation of practical experience with fiber suspensions over hundreds of years of papermaking.

It follows that design of most process equipment involving fiber suspensions must be based on repeated experiment and prior art. While valid, the cut-and-dry method is costly and time consuming, and often does not yield the optimum system for a specific task.

If the objective is to be the improvement of design criteria for process equipment and operating conditions, investigations of fiber suspension behavior should be directed toward the development of general rules which may be applied with confidence to specific situations.

This thesis deals with momentum transport in fully developed flow of dilute fiber suspensions. From momentum transport rules it is often possible to predict heat and mass transfer characteristics of a flowing fluid or suspension.

This work is far from being the first investigation of momentum transfer in suspensions. Without offering the reader an exhaustive survey of the literature, a few of the more important previous studies will be mentioned here.

The field is a bit confused in the sense that it is often not possible to attribute a discovery to a particular investigator. Of necessity, previous authors have often had to rely on qualitative impressions, and little systematic analysis of quantitative data has been presented.

Probably the most extensive investigation of momentum transfer in fiber suspensions has been carried out by the M.I.T. Hydrodynamics Laboratory under a TAPPI contract (1-4). Some of this work deals with rigid particle suspensions as well. An extensive survey of the previous literature may be found in reference (1).

The M.I.T. studies contain a great many friction factor-Reynolds number correlations, some of these suggesting the existence of two types of turbulent flow behavior. Attempts to obtain velocity profiles using a standard impact tube with a wide, flat face to prevent clogging by fibers are reported. In addition, turbulence measurements of a sort are mentioned. Unfortunately, neither the velocity profiles nor the turbulence measurements are thought to be quantitatively reliable and were not so interpreted by the authors. Transition to turbulence was also a subject of the M.I.T. investigations, and the interpretation presented is different than usually found in suspension studies. The transition problem has never really been clarified and will not be further discussed here.

Some additional work in the field has been carried out at McGill University (5, 6). The subject of these investigations is usually the phenomenon of flocculation, or small-scale consistency variation in suspension flow and its prevention. In addition, though, "impressions" of velocity profiles based on direct observation

and high-speed photographs are mentioned. These qualitative descriptions are correct so far as they go and indicate two types of suspension turbulence as well as the familiar laminar plug flow.

Another study also directed at flocculation is that of Wollwage (7). It is of interest here simply because it includes the first and only known attempt to measure the attractive force between two fibers in contact in water. While Wollwage does report an attractive force, it is rather small (about 10^{-4} dynes) and may have been beyond the limits of resolution of the apparatus used.

More recent and much more closely connected to this work is the paper by Mih and Parker (8) describing a special impact probe for determining local velocity in fiber suspensions and in addition providing a number of velocity profiles in fiber suspensions.

These profiles show conclusively that at low turbulent flow rates a central plug flow region may be present which shrinks as flow rate increases and perhaps finally vanishes. The turbulent portions of these profiles appear to obey a logarithmic distribution law as do turbulent profiles of Newtonian fluids. The apparent von Kármán constant is lower for these suspensions than for Newtonian fluids, and appears to vary with fiber consistency and type.

This seems a good place to discuss briefly the turbulent tube flow of ordinary fluids. There is no existing theoretical treatment. At best, existing knowledge may be thought of as semiempirical. Employing as variables the distance from the tube wall, s, the time mean local fluid velicity, $\bar{v}$, fluid density, ρ, and kinematic viscosity ν, along with the wall shear stress, τ_o, the following dimensionless variables may be formed:

$$s^+ = \frac{s\sqrt{\tau_o/\rho}}{\nu} \qquad (2),$$

$$v^+ = \frac{\bar{v}}{\sqrt{\tau_o/\rho}} \qquad (3).$$

Flow in the tube is divided into three regions with appropriate boundaries. In the laminar sublayer, momentum transfer is by viscosity alone; in the buffer zone the situation is mixed, and in the turbulent core, Reynolds stresses are the predominant vehicle of momentum transfer:

$$0 < s^+ < 5 \Rightarrow v^+ = s^+ \qquad (4);$$

$$5 < s^+ < 26 \Rightarrow v^+ = \int_o^{s^+} \frac{ds^+}{1 + n^2 v^+ s^+ (1 - \exp\{-n^2 v^+ s^+\})} \qquad (5);$$

$$26 < s^+ \Rightarrow v^+ = \frac{1}{\kappa} \ln (s^+) + b \qquad (6).$$

Equations (4) and (5) are of the form suggested by Deissler to cope with this region. Equation (5) is wholly empirical with no theoretical significance. The same may be said for Equation (6), which has been employed by many investigators. The choice of boundary positions is a bit arbitrary, but κ, b, and n are regarded as dimensionless constants applying universally to Newtonian fluids.

In some semiempirical mathematical models, special significance is attached to the dimensionless constant κ. For example, in Prandtl's mixing length theory:

$$\tau_{xy} = -\rho\kappa^2 y^2 \left|\frac{d\bar{v}_x}{dy}\right| \frac{d\bar{v}_x}{dy} \qquad (7),$$

where of course the situation is a "two-dimensional" flow in the x direction with a boundary at $y = 0$. In the same sort of "two-dimensional" flow, without the requirement of a boundary a $y = 0$, the von Kármán similarity hypothesis results in:

$$\tau_{xy} = -\rho\kappa^2 \left| \left(\frac{d\bar{v}_x}{dy}\right)^3 \Big/ \left(\frac{d^2\bar{v}_x}{dy^2}\right)^2 \right| \frac{d\bar{v}_x}{dy} \qquad (8) .$$

A fairly complete discussion of some of the common semiempirical approaches may be found in Schlichting's book (9).

This thesis consists mostly of experimental work carried out in a flow loop, which in turn is tied to some additional semiquantitative experiments in other types of flow. Experimental data are used to construct an empirical description of suspension flow by recourse to conventional fluid mechanics.

Before going into detail, it would probably be useful to make a few qualitative comments about the flow of dilute fiber suspensions. By dilute we shall mean roughly the range 0.05 to 0.5% consistency.

The first observation one might make is that such suspensions do not look very dilute. Owing to the high length-to-diameter ratio characteristic of wood fibers, dilute suspensions exhibit some degree of coherence. The laminar flow of such suspensions is roughly similar to Bingham plastic behavior. A clear water gap is formed between the container boundary and the fiber network, and within this gap virtually all of the shear occurs. Gap width increases with increasing shear stress, but not necessarily in a regular or predictable manner. Also, this deformation is not completely elastic. Thus, the laminar portion of the log f vs. log Re diagram is characterized by a negative slope much steeper than that of a Newtonian fluid.

Turbulent tube flow of suspensions exhibits two or three different flow regions. On the log f-log Re diagram, they correspond to straight lines, first of slightly negative slope, then horizontal, then very nearly following the Newtonian fluid curve (Fig. 1).

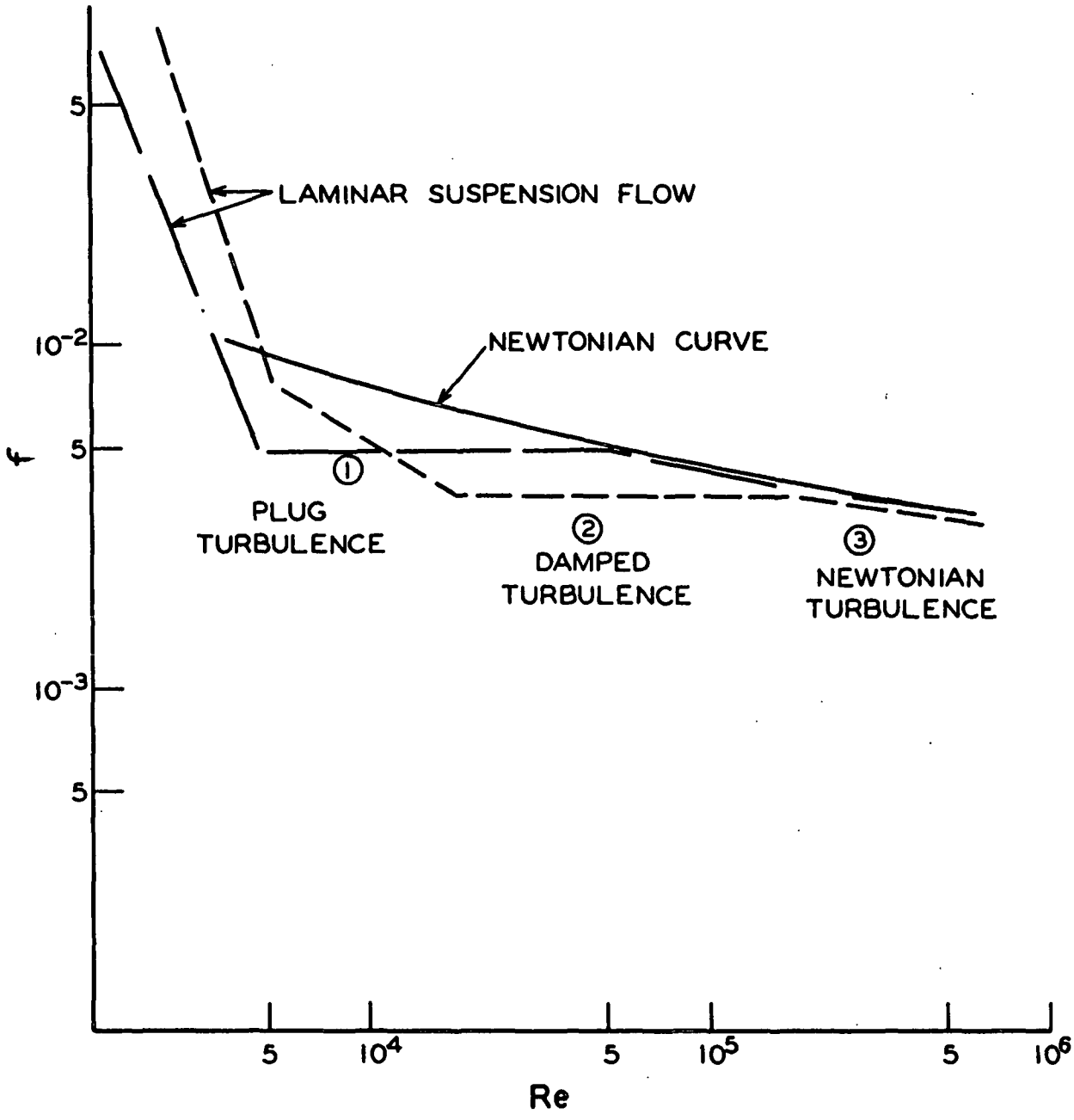

Figure 1. Characteristic Friction Factor-Reynolds Number Curves for Fiber Suspensions

Two different yet somewhat related points will be discussed on the following pages. First, can a fiber network of dilute consistency in water truly be thought of as having strength and continuity; and, if so, can the strength be quantitatively assessed? Second, what momentum transfer characteristics of the suspension are responsible for the observed turbulent flow behavior, and how can they best be characterized?

The discussion will no doubt sometimes appear to be ranging far from the main track. There is little which can be done for this except to note that the result is often a pertinent observation concerning the behavior of a fiber suspension.

FIBER NETWORKS IN SPECIFIABLE FIELDS OF FLOW

At the time when work on this thesis was initiated, a similar project was being carried out by Mih and Parker (8). These workers had at that time conclusively shown the existence of a flow region consisting of a central plug surrounded by turbulent flow in the annular region between the plug and the tube wall. The interesting possibility that this plug is due to a fiber network which supports the applied shear stress and carries along included water was soon suggested.

Assuming the usual linear distribution of shear stress across the tube radius, it is possible to determine the shear stress at the plug boundary, this boundary being rather sharp and well defined. The size of the plug shrinks as the wall shear stress increases, and one is led to suggest that the fiber network forming the core can exist only in regions where the applied shear stress is less than some critical value.

To test this idea independently, it would be necessary to subject a directly observable fiber network to a hydrodynamically applied shear stress and to observe its response. For this test to have any meaningful value, a reasonable estimate of the magnitude of the applied shear stress must accompany the observation.

It is extremely difficult, if not impossible, to obtain direct measurement of the shear stresses applied to a fiber network in a moving fluid. Indirect methods are indicated.

The easiest form of viscous fluid motion to deal with analytically is Stokes flow or creeping motion, in which the inertial terms of the Navier-Stokes equations may be neglected.

If possible, the ideal procedure involves subjecting an isolated fiber network to some definable velocity field within the Stokes region. This motion should

exert some predictable shear stress upon the network. In addition, it would be nice if the network were not subjected to a net body force or moment and therefore would remain stationary in the field of observation.

There happens to be a velocity field which will approximately satisfy the above criteria. It is called the hyperbolic field and will be discussed in detail later.

It is further desirable to have a second field related to the first in which the network may undergo translation and rotation in response to fluid motion. The obvious choice is a linear or Couette velocity field.

Construction of equipment to generate the fields will be described in a later section. It should be mentioned that a similar set of equipment was built for Taylor (10) some time ago for his studies on a drop of one fluid suspended in a second immiscible fluid.

Before discussing the equipment and results, a mathematical description of the fluid motion and the stresses exerted upon the network will be presented.

THE SPHERICAL FIBER NETWORK IN CREEPING FLUID MOTION

This discussion begins with the problem of a spherical fiber network located at the origin of a hyperbolic velocity field in a viscous fluid. The motion is assumed to be in the Stokes region and the rate of shear, α, is assumed known. Fluid motion inside and outside the network and the corresponding state of stress of the network must be determined.

The network is assumed to be isotropic and homogeneous. It is further assumed that Darcy's Law governs fluid motion within the network.

The derivation begins with a statement of the equations and boundary conditions to be used, where $\underline{x}$, $\underline{y}$, $\underline{z}$ are right-handed Cartesian coordinates with velocity components $\underline{u}$, $\underline{v}$, $\underline{w}$, respectively.

For $\underline{r} > \underline{a}$ (external to the network),

$$\nabla \cdot \vec{V} = 0 \qquad (9),$$

$$\mu\nabla^2 u = \frac{\partial p}{\partial x}, \quad \mu\nabla^2 v = \frac{\partial p}{\partial y}, \quad \mu\nabla^2 w = \frac{\partial p}{\partial z} \qquad (10),$$

while for $\underline{r} < \underline{a}$ (inside the network),

$$\nabla \cdot \vec{V}_* = 0 \qquad (11),$$

$$u_r = \frac{-k}{\mu}\frac{\partial p}{\partial x}, \quad v_r = \frac{-k}{\mu}\frac{\partial p}{\partial y}, \quad w_r = \frac{-k}{\mu}\frac{\partial p}{\partial z} \qquad (12).$$

The external equations are quite common and need no explanation here. The internal equations are less common. The vector $\vec{V}_*$ is called the superficial velocity of the fluid in the porous medium. It is an average of fluid velocity over an appropriately large region, the average being over total volume rather than fluid-occupied volume. Equation (11) is the equation of continuity, but is strictly valid only under steady flow conditions and when averaged over an appropriately large volume.

The vector $\vec{V}_r$ refers to the superficial velocity of the fluid relative to the porous medium, while ∇p is the pressure gradient in the fluid. The second equation is the usual form of Darcy's Law for a Newtonian fluid. The equation as written holds only for isotropic, homogeneous porous media. The porosity, ε, and the permeability coefficient, k, may not vary with position or direction.

For the time being, the porous sphere will be considered incompressible and stationary at the center of the reference coordinate system. Obviously, under these conditions, $\vec{V}_r = \vec{V}_*$, and there is the important result:

$$\nabla^2 p = 0 \quad \text{for all } r \quad . \tag{13}$$

The boundary conditions are easily expressed. Far from the network the velocity tends toward the applied hyperbolic field. In addition, the pressure must be finite everywhere, while pressure and superficial velocity must be continuous across the sphere boundary. The last two conditions may be regarded as arbitrary, but seem the most reasonable choices from a physical point of view.

Writing out the boundary conditions:

$r \gg a$

$$u \to \frac{\alpha x}{2} \tag{14a}$$

$$v \to \frac{-\alpha y}{2} \tag{14b}$$

$$w \to 0 \tag{14c}$$

$r = a$

$$\vec{V}_{*\text{int}} = \vec{V}_{\text{ext}} \tag{15}$$

$$p_{\text{int}} = p_{\text{ext}} \tag{16}$$

$$p \quad \text{finite everywhere} \quad .$$

The problem as formulated is not especially difficult to solve. Probably the easiest approach is the method of spherical harmonics, which is well described by Lamb (11). Briefly, this method depends upon the fact that the velocity of a

fluid in Stokes motion may be found by applying prescribed differential operators to a series of scalar harmonic functions. In problems of spherical symmetry, spherical harmonics are employed. From the boundary conditions, the user must select the spherical harmonics of the necessary orders and determine the coefficients which must be applied. Since in this problem the internal pressure is also a harmonic function, it is fairly easy to determine.

Using Lamb's (11) notation, the external velocity field should be generated by the spherical harmonic functions:

$$\varphi_2 = \frac{\alpha(x^2 - y^2)}{4} \tag{17}$$

$$\varphi_{-3} = B_{-3} \frac{a^5(x^2 - y^2)}{r^5} \tag{18}$$

$$p_{-3} = A_{-3} \frac{\mu a^3(x^2 - y^2)}{r^5} \tag{19}$$

The internal pressure must match the external at the sphere boundary and remain finite at $\underline{r} = 0$. Therefore, for the internal pressure:

$$p_2 = \frac{\mu A_2}{a^2} (x^2 - y^2) \tag{20}$$

A clever mathematician could probably write down the coefficients by inspection. A less elegant but equally certain way to determine them is to proceed by successive approximations beginning with the solid sphere values derived by Einstein (12). The internal pressure is determined by requiring that it match the external pressure at $\underline{r} = \underline{a}$. The velocity condition is then not satisfied and the external field must be adjusted, etc. The results, valid for all $\underline{k}$ and $\underline{a}$ are:

$$A_{-3} = A_2 = -\frac{5\alpha}{2(1 + 10\frac{k}{a^2})} \tag{21}$$

$$B_{-3} = - \frac{\alpha}{4\left(1 + \frac{10k}{a^2}\right)} \qquad (22) \ .$$

This in essence completes the solution.

It may be instructive, however, to carry things one step further and introduce another harmonic function to the external field in accordance with Lamb's notation:

$$\chi_1 = \frac{-\alpha z}{2} \qquad (23) \ .$$

The effect of this function is to give the external field an angular velocity:

$$\vec{\omega} = \frac{-\alpha \vec{k}}{2} \qquad (24) \ .$$

The boundary conditions may be matched by giving both the porous sphere and the fluid within it an identical angular velocity.

An additional assumption is made in this approach that both centripedal and Correolis accelerations are effectively negligible. This assumption is not necessarily equivalent to the discarding of inertial terms in the Navier-Stokes equations as is done in introducing creeping motion.

The velocity field far from the sphere now tends to:

$$u = \frac{\alpha}{2}(x + y) \qquad (25a)$$

$$v = \frac{-\alpha}{2}(x + y) \qquad (25b)$$

$$w = 0 \qquad (25c) \ .$$

This field is immediately recognized as linear Couette flow in the $\underline{xy}$ plane with streamlines at a $45°$ angle to the $\underline{x}$ axis (Fig. 2).

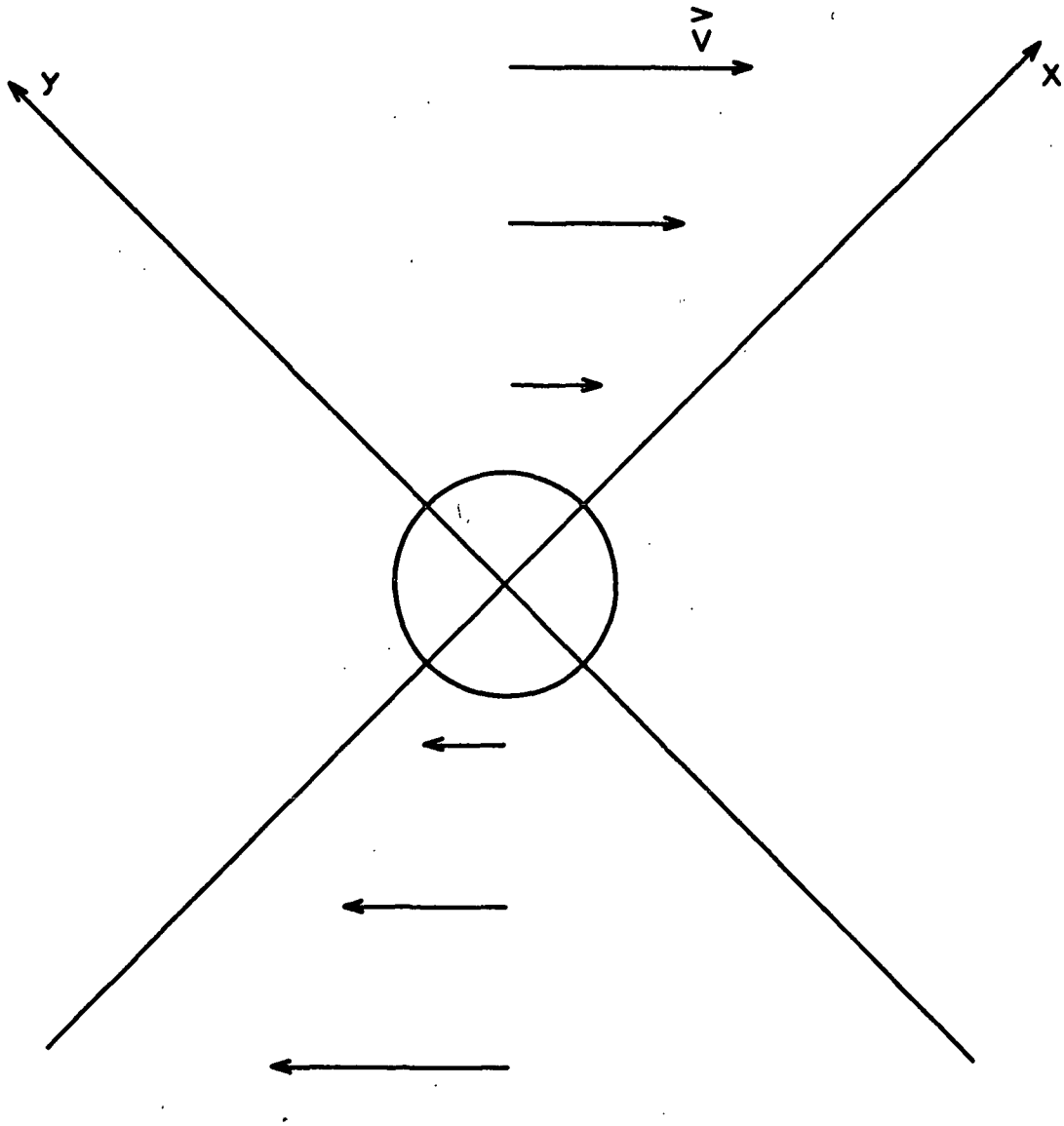

Figure 2. Spherical Network in Linear Velocity Field

It is evident that the results indicated have more potential uses than just determination of a state of stress. For example, with appropriate manipulation one may extract the viscosity of a suspension of porous spheres from the given results. When such a manipulation was carried out, the results were found to be useful in explaining the hydrodynamic behavior of certain dilute polymer solutions. This finding became the subject of a paper recently accepted for publication by the Journal of Polymer Science (13). Interested readers should refer to that paper for the details.

Now to return to the problem at hand — the state of stress of a porous sphere immersed in a fluid with a hyperbolic velocity field — the stress at the surface of the sphere may be evaluated without too much difficulty. However, due to the reduction of order in the differential equations describing the fluid flow inside the sphere, it is not possible to attribute any shear stresses to the fluid within the sphere. In other words, only the stress directed normal to the sphere surface is continuous across the interface. The entire shear stress discontinuity should therefore be attributed to the structural material of the sphere itself.

To compute the traction force at the surface of the sphere, it is necessary to resort to Lamb's equation:

$$rP_{rx} = \Sigma\left\{\frac{n-1}{2n+1}\, r^2\, \frac{\partial p_n}{\partial x} + \frac{(2n^2+4n+3)r^{2n+3}}{(n+1)(2n+1)(2n+3)}\, \frac{\partial}{\partial x}\left(\frac{p_n}{r^{2n+1}}\right)\right.$$

$$\left. + 2\mu\Sigma(n-1)\frac{\partial \varphi_n}{\partial x} + \mu\Sigma(n-1)\left(y\,\frac{\partial \chi_n}{\partial z} - z\,\frac{\partial \chi_n}{\partial y}\right)\right\} \qquad (26),$$

where P_{rx} is the x component of the traction at point (x, y, z) exerted across an infinitesimal portion of a spherical surface, the sphere center being the origin. Plugging in the appropriate harmonics and evaluating at $r = a$, the stress at the sphere surface is expressed:

$$P_{rx}\Big|_a = \frac{\mu\alpha x}{a}\left(1 + \frac{3}{2(1 + \frac{10k}{a^2})}\right) \qquad (27a),$$

$$P_{ry}\Big|_a = \frac{-\mu\alpha y}{a}\left(1 + \frac{3}{2(1 + \frac{10k}{a^2})}\right) \qquad (27b),$$

$$P_{rz}\Big|_a = 0 \qquad (27c).$$

Now this vector represents the stress acting across a segment of the spherical surface at the point $(\underline{x}, \underline{y}, \underline{z})$. By transforming to spherical coordinates, one may arrive at the normal and tangential stress components. Accordingly, the following coordinate transformation is defined:

$$\left.\begin{aligned} x &= r \sin\theta \cos\varphi \\ y &= r \sin\theta \sin\varphi \\ z &= r \cos\theta \end{aligned}\right\} \qquad (28).$$

$$\left.\begin{aligned} r &= (x^2 + y^2 + z^2)^{1/2} \\ \theta &= \tan^{-1}\left[\frac{(x^2 + y^2)^{1/2}}{z}\right] \\ \varphi &= \tan^{-1}(y/x) \end{aligned}\right\}$$

And using the transformation rule for contravarient vectors: $\underline{A}^{\underline{i}}(\underline{x}) = \Sigma \frac{\partial \underline{x}^{\underline{i}}}{\partial \underline{y}^{\underline{j}}} \underline{A}^{\underline{j}}(\underline{y})$, we arrive at the following scheme to represent the traction in terms of the new local direct basis:

	P_{rx}	P_{ry}	P_{rz}
P_{rr}	x/a	y/a	z/a
$P_{r\theta}$	$\frac{xz}{a^2(a^2 - z^2)^{1/2}}$	$\frac{yz}{a^2(a^2 - z^2)^{1/2}}$	$\frac{-(a^2 - z^2)^{1/2}}{a^2}$
$P_{r\varphi}$	$\frac{-y}{a^2 - z^2}$	$\frac{+x}{a^2 - z^2}$	0

The local direct basis is not normalized:

$$\vec{a}_1 = \vec{e}_r \tag{29a}$$

$$\vec{a}_2 = r\vec{e}_\theta \tag{29b}$$

$$\vec{a}_3 = (x^2 + y^2)^{1/2}\,\vec{e}_\varphi \tag{29c}$$

So that finally the representation of the stress in terms of unit vectors in a spherical coordinate system is defined by:

	P_{rx}	P_{ry}	P_{rz}
P_{rr}	x/a	y/a	z/a
$P_{r\theta}$	$\dfrac{xz}{a^2(1 - \frac{z^2}{a^2})^{1/2}}$	$\dfrac{yz}{a^2(1 - \frac{z^2}{a^2})^{1/2}}$	$-(1 - \frac{z^2}{a^2})^{1/2}$
$P_{r\varphi}$	$\dfrac{-y}{a(1 - \frac{z^2}{a^2})^{1/2}}$	$\dfrac{x}{a(1 - \frac{z^2}{a^2})^{1/2}}$	0

Then the traction at $\underline{r} = \underline{a}$ is reexpressed as:

$$P_{rr}\Big|_a = \frac{\mu\alpha}{a^2}\left[1 + \frac{3}{2(1 + \frac{10k}{a^2})}\right](x^2 - y^2) \tag{30a}$$

$$P_{r\theta}\Big|_a = \frac{\mu\alpha}{a^2}\left[1 + \frac{3}{2(1 + \frac{10k}{a^2})}\right]\frac{z(x^2 - y^2)}{(1 - \frac{z^2}{a^2})^{1/2}} \tag{30b}$$

$$P_{r\varphi}\Big|_a = \frac{2\mu\alpha}{a^2}\left[1 + \frac{3}{2(1 + \frac{10k}{a^2})}\right]\frac{xy}{(1 - \frac{z^2}{a^2})^{1/2}} \tag{30c}$$

Clearly, the latter two stresses must be attributed to the network structure once the interface is passed. Change in component $\underline{P_{rr}}$ must be interpreted as additional loading of the network.

Under the conditions of the experimental program $\frac{10\underline{k}}{\underline{a}^2} \ll 1$, so the situation becomes simplified:

$$P_{rr}\Big|_{r=a} = \frac{5\mu\alpha}{2}\,\frac{(x^2 - y^2)}{a^2} \tag{31a}$$

$$P_{r\theta}\Big|_{r=a} = \frac{5\mu\alpha}{2}\,\frac{z(x^2 - y^2)}{a^3\left(1 - \frac{z^2}{a^2}\right)^{1/2}} \tag{31b}$$

$$P_{r\varphi}\Big|_{r=a} = \frac{5\mu\alpha}{a^2}\,\frac{xy}{\left(1 - \frac{z^2}{a^2}\right)^{1/2}} \tag{31c}$$

But, according to assumption, the normal stresses exerted on the network are zero at the surface and a maximum at the sphere center. Ignoring the shear stresses applied at the surface, one finds at the center of the sphere:

$$\begin{Bmatrix} \frac{5\mu\alpha}{2} & 0 & 0 \\ 0 & \frac{-5\mu\alpha}{2} & 0 \\ 0 & 0 & 0 \end{Bmatrix} = \tau \tag{32}$$

which corresponds to a shear stress of equal magnitude at 45° to the principal axes.

One may with some confidence maintain that the maximum shear stress to which the network is subjected is on the close order of $5\mu\alpha/2$, an approximation that satisfies the present purpose.

EXPERIMENTS IN SPECIFIED FIELDS OF FLOW

Two pieces of apparatus were constructed to create, respectively, hyperbolic and Couette velocity fields.

The hyperbolic field is generated by the device pictured in Fig. 3. It consists of a Lucite box 10 in. square and 4-1/2 in. deep. Mounted through the top of the box are four brass cylinders with their axes parallel to each other and perpendicular to the plane of the box lid. The cylinders are arranged at the corners of a square 3 in. on a side which is itself centered on the lid. Portions of the cylinders projecting into the box are 2 in. in diameter. The cylinders are mounted on pillow blocks and driven by a one-sided timing belt in such a way that adjacent cylinders rotate in opposite directions.

A small, spherical network at the center of this device should be subject to approximately the same stresses as described in the previous section.

The device is driven by a Zeromax electric motor rated at 1/8 hp.

The Couette flow apparatus consists of the Lucite box and brass roller assembly shown in Fig. 4. The continuous belts are of Fluorglass and the drive rollers are driven by a one-sided timing belt. This device is also driven by a 1/8-hp. Zeromax electric motor.

In the Couette apparatus, the rate of shear, α, may be measured directly from the belt velocity and gap width. In the other device, the shear rate should be related nearly linearly to the rate of rotation of the cylinders, but the constant of proportionality must be determined experimentally.

The first experiment was performed in the hyperbolic flow device using a mixture of Karo sirup and water which was not well stirred. Streamlines became

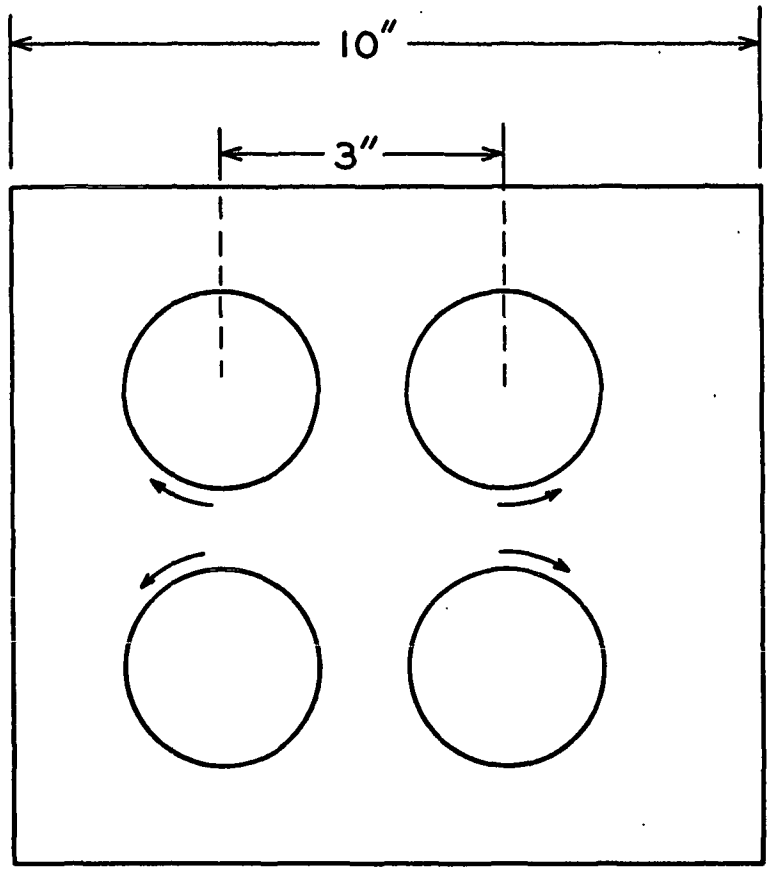

Figure 3. The Hyperbolic Flow Device

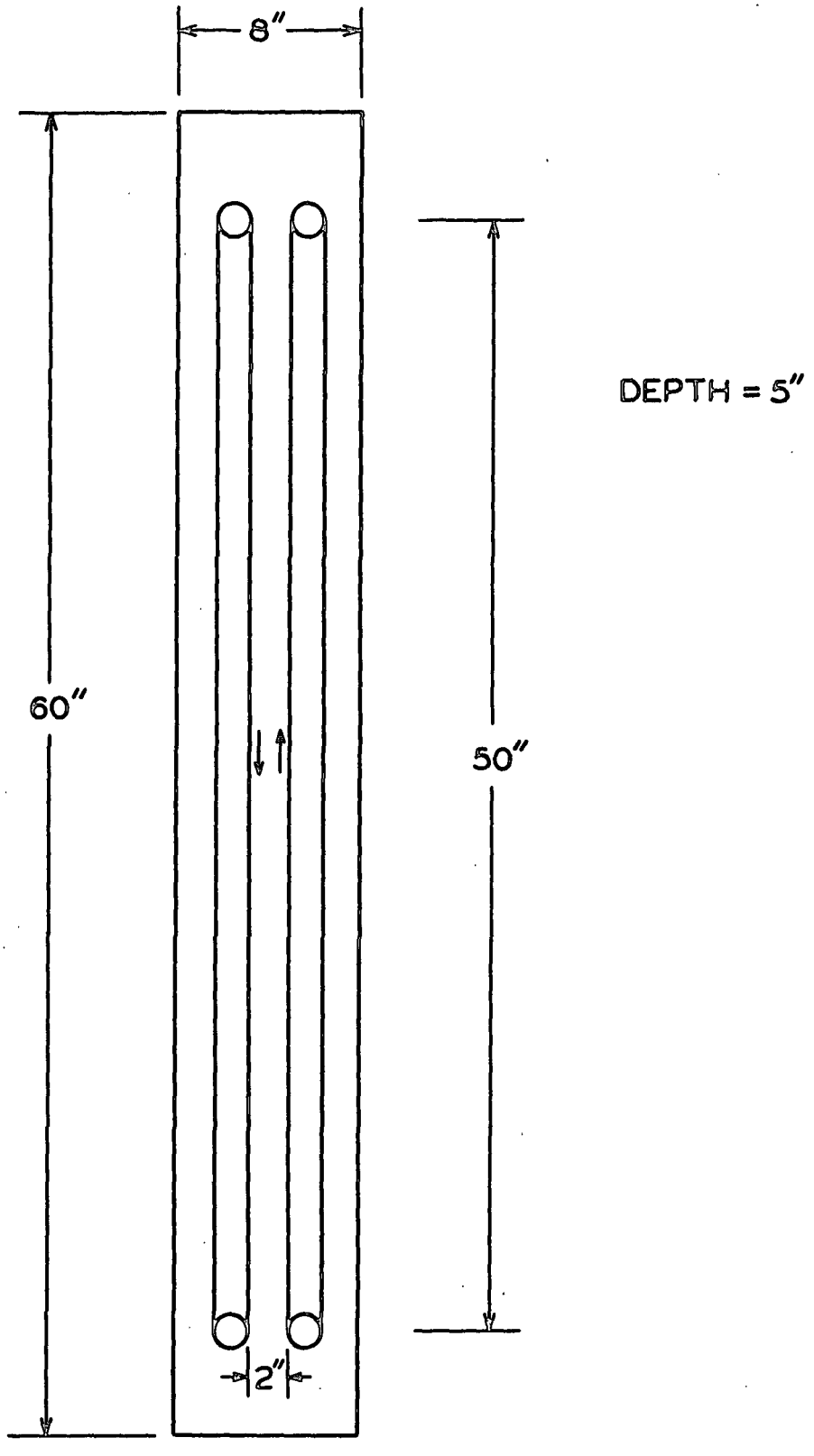

Figure 4. The Couette Flow Device

visible due to differences in optical density and were found to be quite similar to rectangular hyperbolas, as required.

In later experiments, a constant of proportionality between shear rate and timing belt period was approximately established by timing the passage of small particles through portions of the field. The results of this determination are listed in Table I.

TABLE I

DETERMINATION OF α AS A FUNCTION OF BELT REVOLUTION PERIOD, $\underline{R}$

$\underline{R}$, sec.	$\Delta\underline{x}$, cm.	$\Delta\underline{t}$, sec.	$\alpha/2$, sec.$^{-1}$
69	1/2 to 2	7	0.20
69	1/3 to 2	8	0.22
69	1/4 to 2	10	0.21
69	1/2 to 1	3	0.23
25	1/2 to 2	2.4	0.58

Since $\frac{d\underline{x}}{d\underline{t}} = \alpha\underline{x}/2$, $\ln \underline{x}_2/\underline{x}_1 = \frac{\alpha}{2}\Delta\underline{t}$. Then, $\alpha = 29/\underline{R}$ sec.$^{-1}$

The solutions used in the controlled flow experiments were prepared from Karo sirup (purchased) and tap water. Solutions formed appear to be Newtonian and range in viscosity at 24°C. from 30 poises to about 1 centipoise. Specific gravity may not be varied independently and ranges from 1.00 to 1.35 (see Fig. 5). Since the density of cellulose is about 1.55 g./cc., it has not been possible to work with neutrally buoyant suspensions.

When a network is centered in the apparatus, slight deviations from symmetry may cause it to move off to one side or the other. To prevent this and to keep the fibers from settling, it was necessary to provide support for the network. This

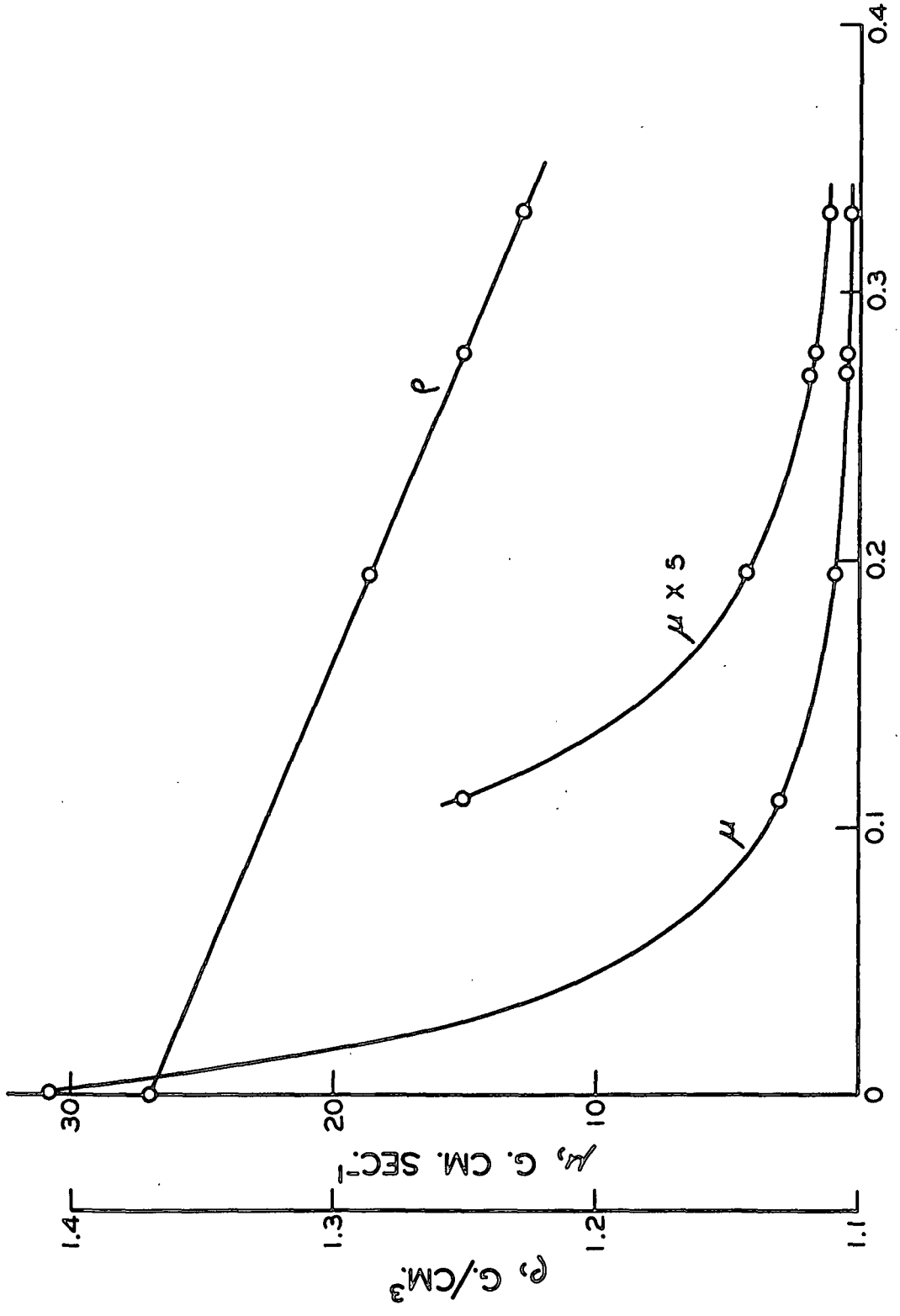

Figure 5. The Viscosity and Density of Karo Sirup-Water Solutions; $\underline{T}$ = 24°C.

may be accomplished by forming the network about a thin wire of glass or steel belled out slightly at the bottom. This holder is shaped to provide minimum support and shielding against fluid stresses.

As can readily be seen, no attempt has been made to control the colloidal environment in the system.

Samples are prepared by dipping the holder into a dispersed suspension of fibers (0.1 to 0.5% consistency) in a 1:1 solution of sirup and water. They are mounted near the surface of the solution in the box until the fluid within the network has reached about the same density as the initially more concentrated solution in the box. The network is then immersed to a point about halfway between the bottom of the box and the surface of the fluid, and is carefully centered. Using fine wires, the investigator then fluffs and teases the network into spherical shape, at the same time increasing the porosity as much as possible without tearing the network. The fluid viscosity is adjusted through repeated trials so that disruption of the network occurs at low but measurable shear rates.

Observations are made as shear rate is increased. The relative shape of the network, its tendency to lose material, and its stability are recorded at a given rate of shear. These qualitative observations give a good indication of what happens:

1. At very low shear, the sphere remains undeformed.
2. As shear increases, there is a rather sharp change in network shape over a narrow range of shear stress.
3. The deformed network takes an ellipsoidal shape, and the deformation is inelastic.
4. At this stage, the network may rupture, or deformation may continue with increasing shear. Axis ratios as high as 5 and as low as 1.5 have been observed immediately prior to rupture.

5. The shear rate at which inelastic deformation becomes apparent is strongly dependent both on consistency within the network and upon fiber length.

6. Despite whatever care is taken in forming the networks, there is quite a bit of variance in the shear rate required to produce inelastic deformation.

Quantitative data from this apparatus are rather limited. The apparent shear stress required to produce inelastic deformation is identified as a yield stress, τ_y. It proved necessary to combine yield stress and consistency determinations to obtain meaningful data. The results listed in Table II should be considered close estimates rather than exact values.

TABLE II

CONSISTENCY AND YIELD STRESS DETERMINATIONS
IN THE HYPERBOLIC FLOW DEVICE

Consistency Determinations

No. of Spheres in Test	Total Volume, $cm.^3$	Mass, mg.	Γ, g./100 ml.
3	2.41	8.8	0.37
5	4.20	13.4	0.32
6	5.70	18.9	0.33

Yield Stress Determinations

Sphere	Yield Belt Period, sec.	τ_y, $g.\ cm.^{-1}\ sec.^{-2}$
1	20	
2	25	
3	21	
4	15	
Average	20	1.45

In spite of the small amount of quantitative data produced, the hyperbolic flow experiments have considerable importance. They show that fiber networks can resist hydrodynamic shear stress at rather low consistencies, and they provide a good estimate of the yield stress for one particular case. Furthermore, additional qualitative experiments using this equipment indicate that the yield stress is strongly dependent on fiber length and consistency of the network.

Work with Couette flow fields was limited to qualitative observation. The equipment used included Mason's (14) concentric cylinder device in addition to the parallel band apparatus already described.

Several small, loose fiber networks were introduced into the gap in the concentric cylinder device. The device had been partially filled with a heavy organic liquid, then completely filled by adding Karo sirup solutions. Fiber networks would float at the interface.

When the rate of shear was high enough to deform the networks, they appeared as rotating ellipsoids of varying eccentricity. The direction which the greatest elongation would occur along a given axis was at 45° to the flow direction, as expected. The networks would break down as bundles of fibers were pulled out in the direction of greatest elongation and then swept away as the mass rotated. Reduction in the size of a network did not increase its stability.

The parallel band device was used in a somewhat different manner. The Lucite box was filled with enough water (about 26 liters) to bring the level close to the tops of the bands. Sufficient fiber (Sample 2578, a Weyerhaeuser bleached softwood sulfite) was added to form a settled network of about 0.5% consistency, the surface of which lay about 1/2 in. below the water surface. The viscosity of the solution was increased when necessary by siphoning off liquid and replacing it with Karo sirup.

The experimental situation was considerably different from the previous cases. Rather than being a small network completely surrounded by fluid, this network extended to all boundaries of the container.

At low viscosity, the fiber network resisted shear as a whole, and at low belt speeds, the edges of the network were definitely in contact with the moving belts. Occasionally, small cylindrical portions of the network near a belt and in contact with it would begin to rotate and translate in the direction of belt travel, increasing in size as they went. Some of these rotational bodies reached a diameter of almost half the gap width before either coming to rest or moving out of the observation region. As these bodies swept out material, large clear water gaps developed at the moving belts and the situation became static.

As the viscosity was increased, the network showed a tendency to deflect from the moving belts. At a viscosity of 3-4 cp., this deflection became sufficient to prevent the formation of rolling cylindrical bodies at the belt surfaces. The size of the clear gap caused by deflection increased with both rate of shear and viscosity. When the belts were stopped, the network was able to recover most of this deflection.

Increasing the viscosity of the fluid had little effect for a while, only increasing the gap width at a given rate of shear. Slowly with increasing viscosity, however, it became evident that the network could no longer resist without motion the shear stresses applied to it. The structure of the network would become blotchy in appearance and at high stress would actually rupture, with adjacent portions moving slowly relative to one another along irregular slip surfaces. At the highest viscosity reached, about 16 cp., a belt speed of 0.25 ft. $sec.^{-1}$ caused motion in a portion of the network while a central core appeared to be stationary. At a belt speed of 0.4 ft. $sec.^{-1}$, the highest used, the entire network is in intermittent and irregular motion.

All of the observations refer to a region near the center of the test box. Despite the large size of the box, end effects are probably appreciable because of the continuous network. Also, at higher shear stress, there is a definite tendency for fibers to be piled up at either end of the box.

No quantitative data regarding the applied shear stress are available from these experiments. It is not clear how such data could be interpreted, anyway.

THE FLOW LOOP

In order to learn much about momentum transfer in turbulent flow, it is necessary to obtain information under steady flow conditions in a known geometry. Considering past investigations and available equipment, the obvious choice of geometry is cylindrical tubing. Most of the information necessary to describe momentum transfer in dilute fiber suspensions could be obtained from pressure drop-flow rate correlations and velocity profiles in tube flow.

Accordingly, a flow loop was constructed in the Chemical Engineering Laboratory to obtain the necessary data. The flow loop and most of the associated instrumentation are pictured in Fig. 6-8. It is a vertical loop to minimize gravitational effects and includes two different pipe diameters, 1.875 and 1.400 in. i.d. The tubing is seamless, hydraulically smooth stainless steel of rather uniform diameter. The maximum tube diameter is limited by the 22-ft. vertical clearance available. The suspension is pumped through the loop by two Jabsco pumps hooked in parallel, each pump being driven through a continuously variable speed pulley system by a 3-hp. electric motor. Maximum discharge rate is about 150 g.p.m. at 30 ft. of head. In addition, the loop is equipped with a 2-in. magnetic flowmeter, a jacketed stock chest, and a calibrated discharge tank. Temperature can be held constant within 0.3°C. by manual control of cooling-water and steam feeds. Pressure differentials are read on standard liquid-liquid manometers.

Pressure drops along a straight length of tubing during flow are easily measured using static pressure taps. Combined with flow rates from the calibrated flowmeter, these data yield wall shear stress and Reynolds number-friction factor correlations.

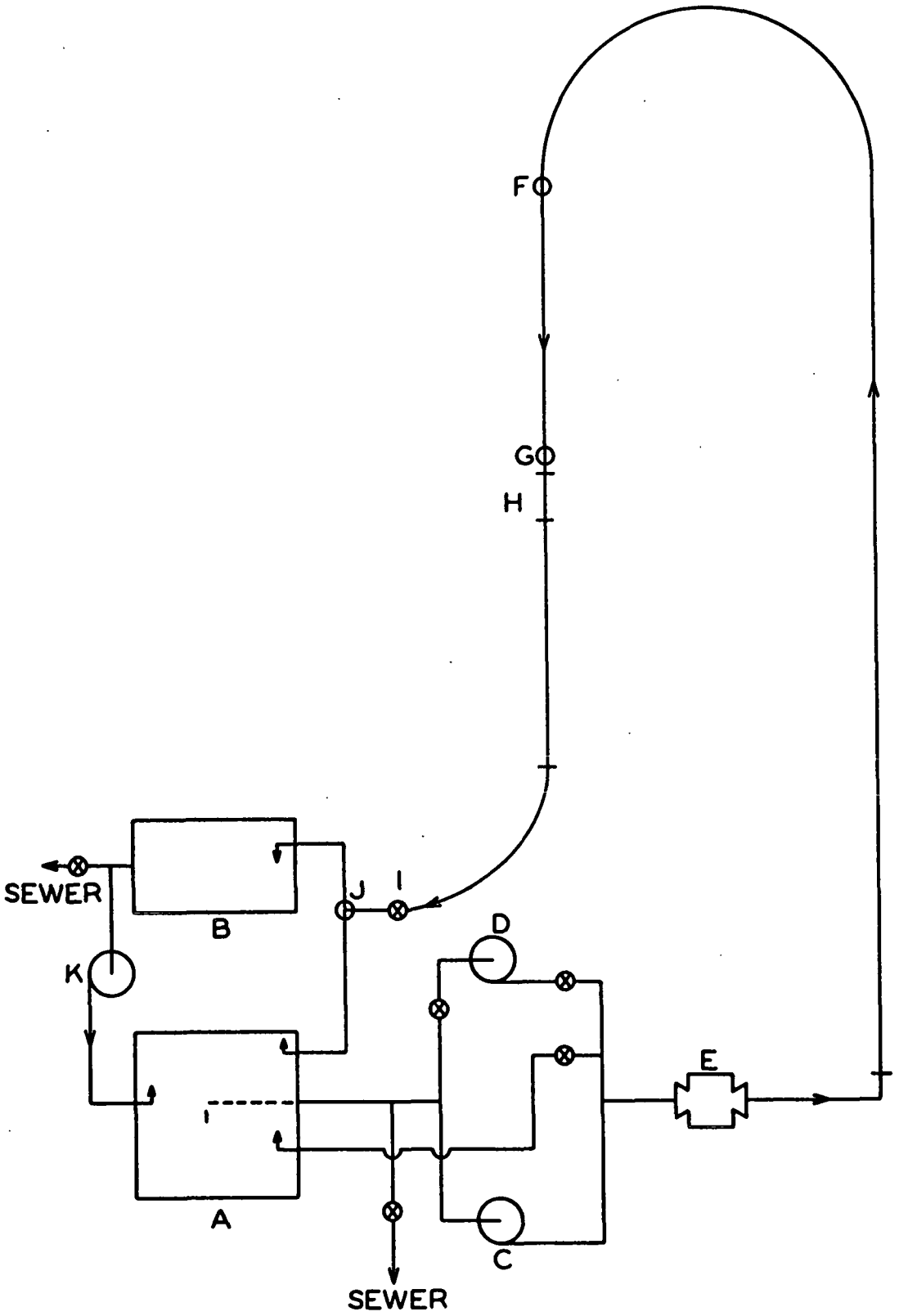

Figure 6. Flow Loop Diagram

Key to Figure 6

A	Stock chest, stainless steel, jacketed, open depth 3 ft., diameter 5 ft.
B	Volumetric discharge tank, stainless steel, open depth 3 ft., diameter 1 ft. 6 in.
C,D	Jabsco Model 3200-01, size 2 in. ball-bearing rotary pumps, each driven through a speed selector variable-speed drive no. 409°-510. 267 r.p.m. to 2400 r.p.m., by a 3-h.p., 1150 r.p.m. NEMA frame 215, squirrel-cage motor wound 3-60-208/220/440.
E	Foxboro dynalog magnetic flowmeter, 2 inch
F	Upstream pressure tap, 3 positions
G	Downstream pressure tap, 3 positions (separation from F, 7 ft. 4 in.)
H	Lucite test section
I	2-in. diaphragm valve keeps static pressure in loop positive
J	Quick-opening 3-way ball valve
K	Recycle pump

The loop is constructed of 2-in. o.d., 1.875-in. i.d. stainless steel tubing mounted vertical on unistrut. Other piping is 2-in. brass.

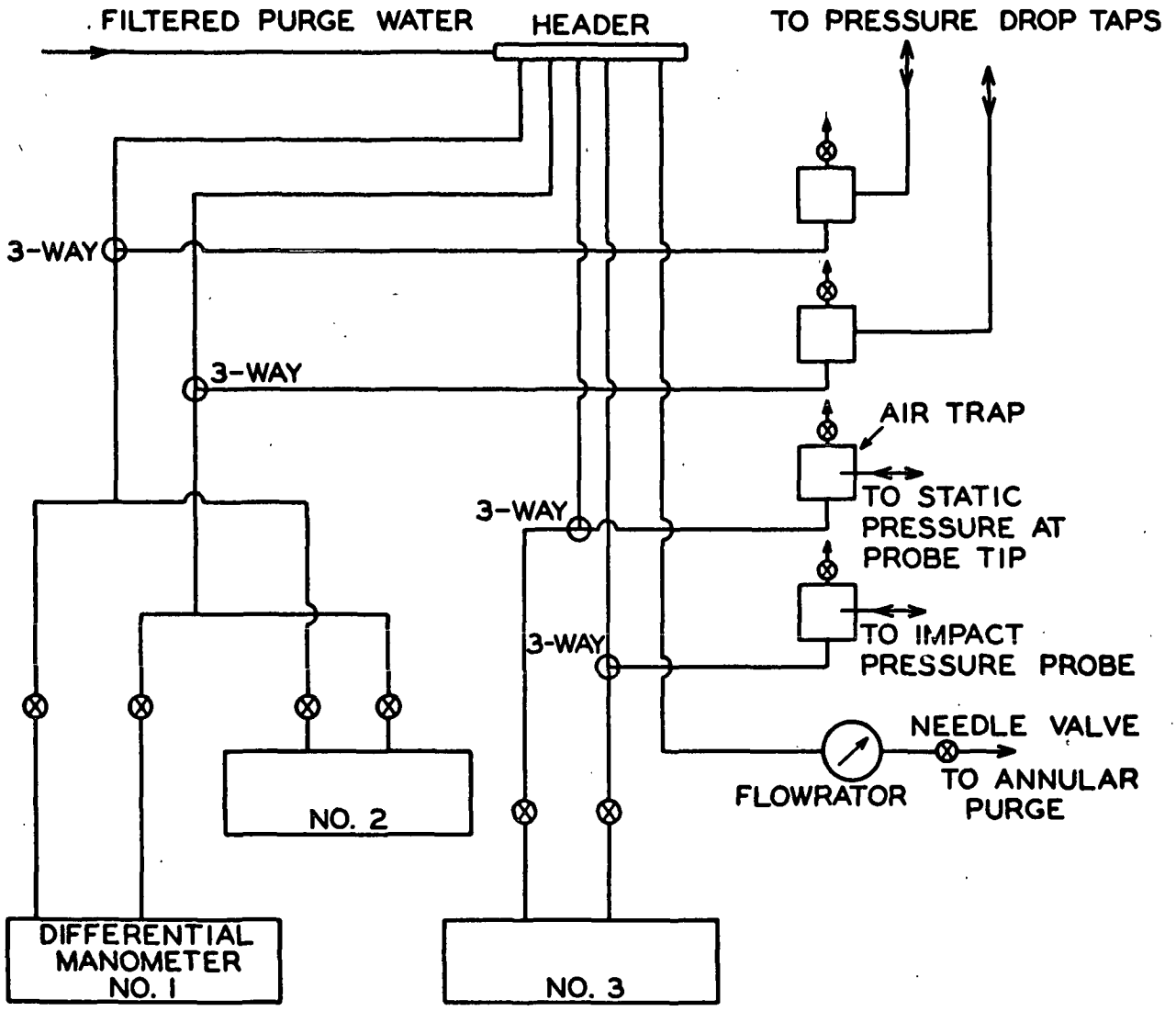

MATERIALS — 1/8" x 1/4" IMPERIAL TUBING WITH APPROPRIATE VALVES AND FITTINGS. AIR TRAPS ARE LUCITE

Figure 7. Instrumentation System for Flow Loop

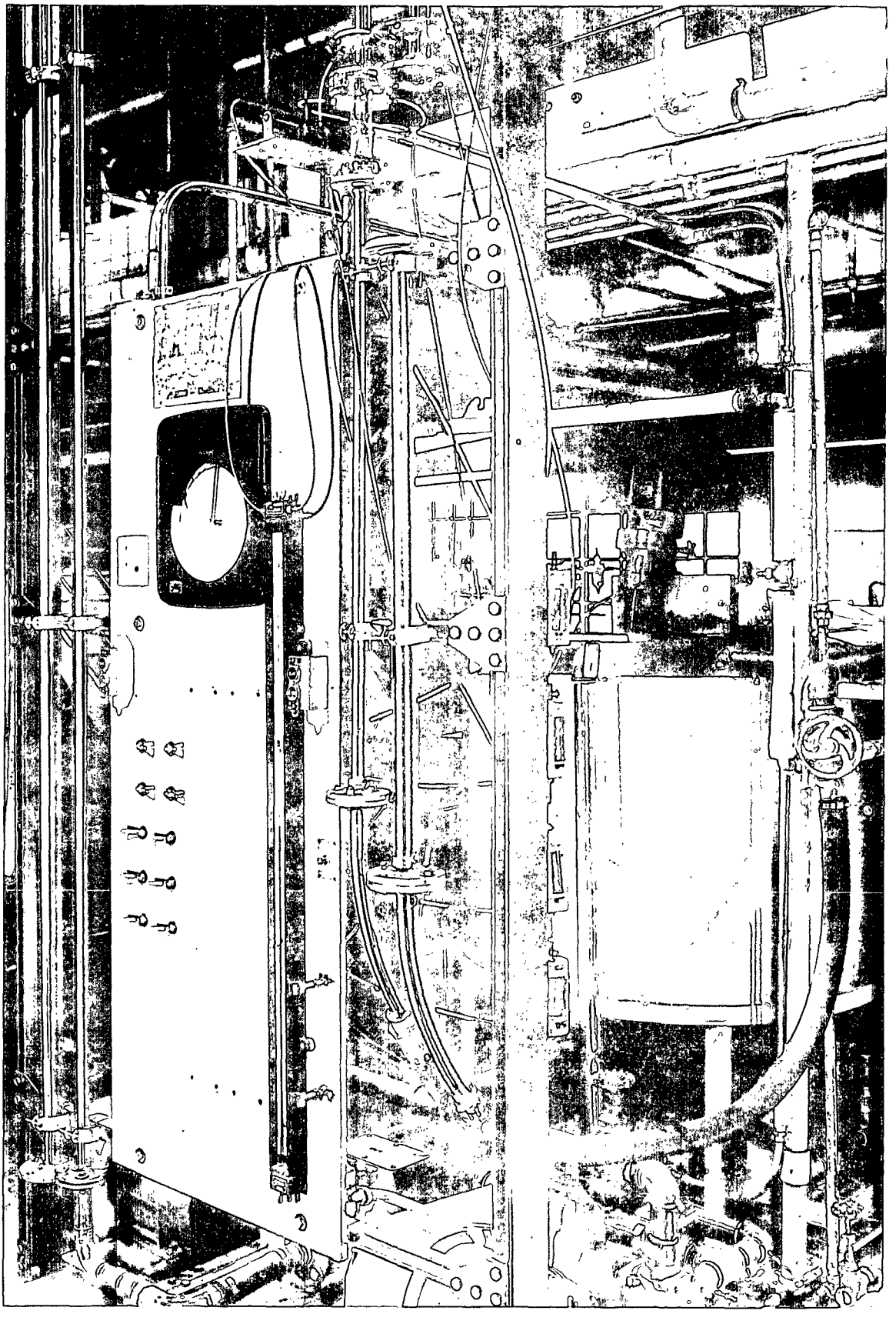

Figure 8. The Flow Loop

Velocity profiles prove more difficult to obtain. Normally, these are measured by a traversing impact probe; but fibers will pile up on the tip of such a probe, causing false readings and rendering the instrument useless in suspension. The annular purge impact probe described by Mih and Parker (8) and used in this work overcomes this difficulty. When this probe is in operation, a jet of water emerges from an annular jacket surrounding a conventional impact probe. This effecitvely prevents fiber build-up; and provided that the jet velocity is low enough compared to the oncoming fluid velocity, the impact pressure is unaffected by the jet. In this work, two of the probes were employed, the linear dimensions of one being half as large as the other. The probes are pictured in Fig. 9 and 10. The smaller probe made it possible to obtain velocity profiles across virtually the entire turbulent core region.

The impact probes were connected to an external mounting assembly as shown in Fig. 11. This assembly made it possible to determine the position of the probe to within about 1/64th inch.

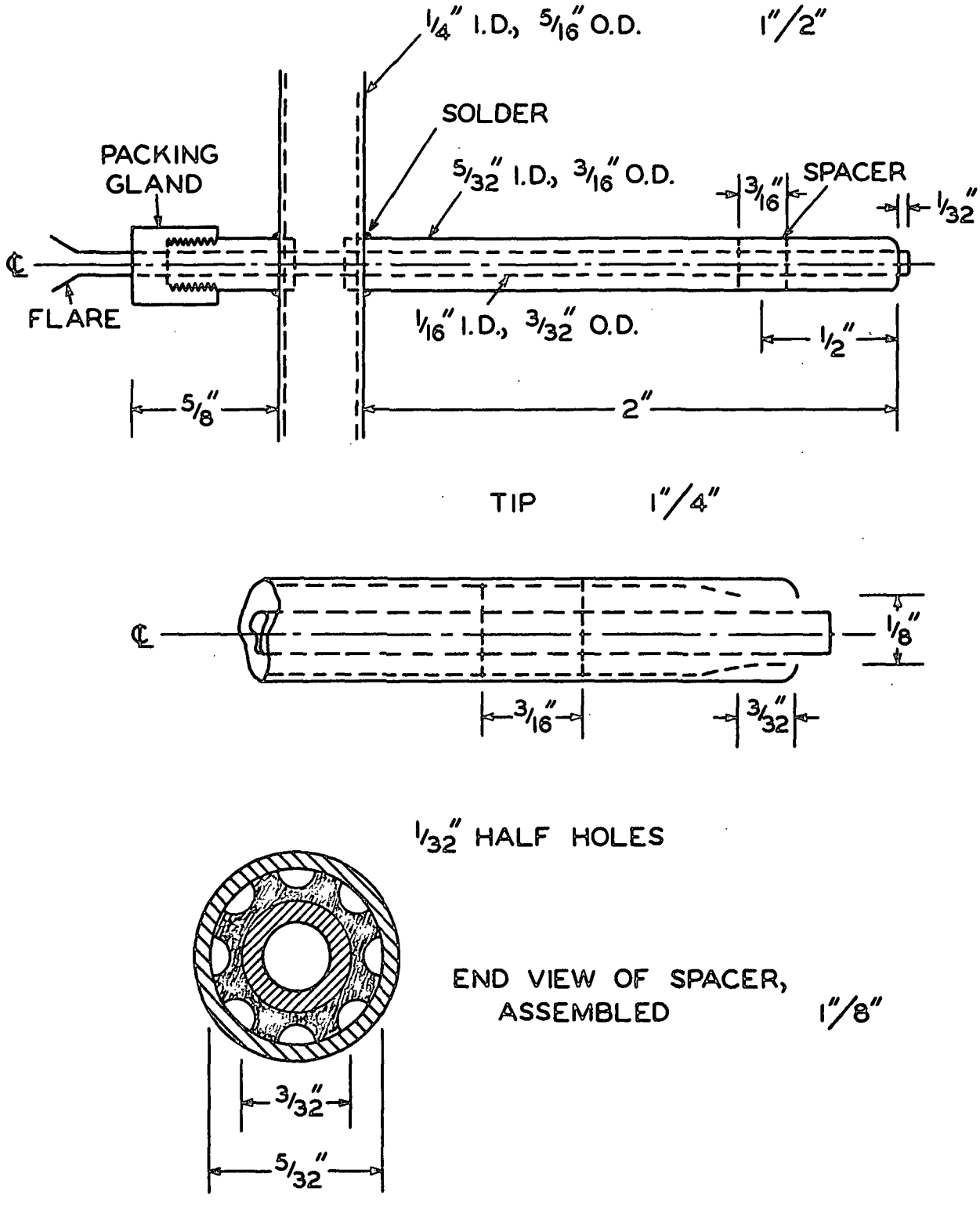

Figure 9. Large Annular Purge Impact Probe

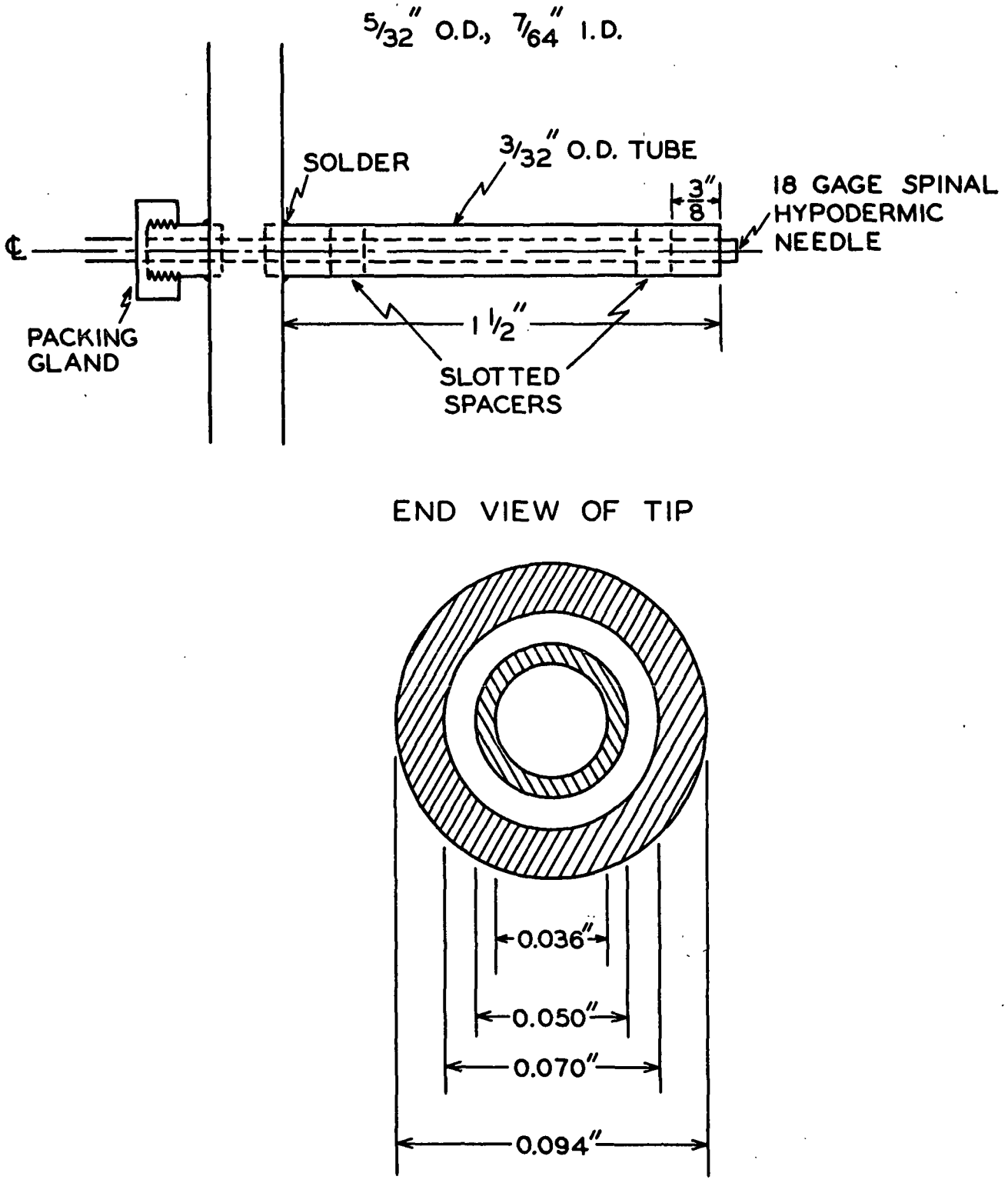

Figure 10. Small Impact Probe (No Scale)

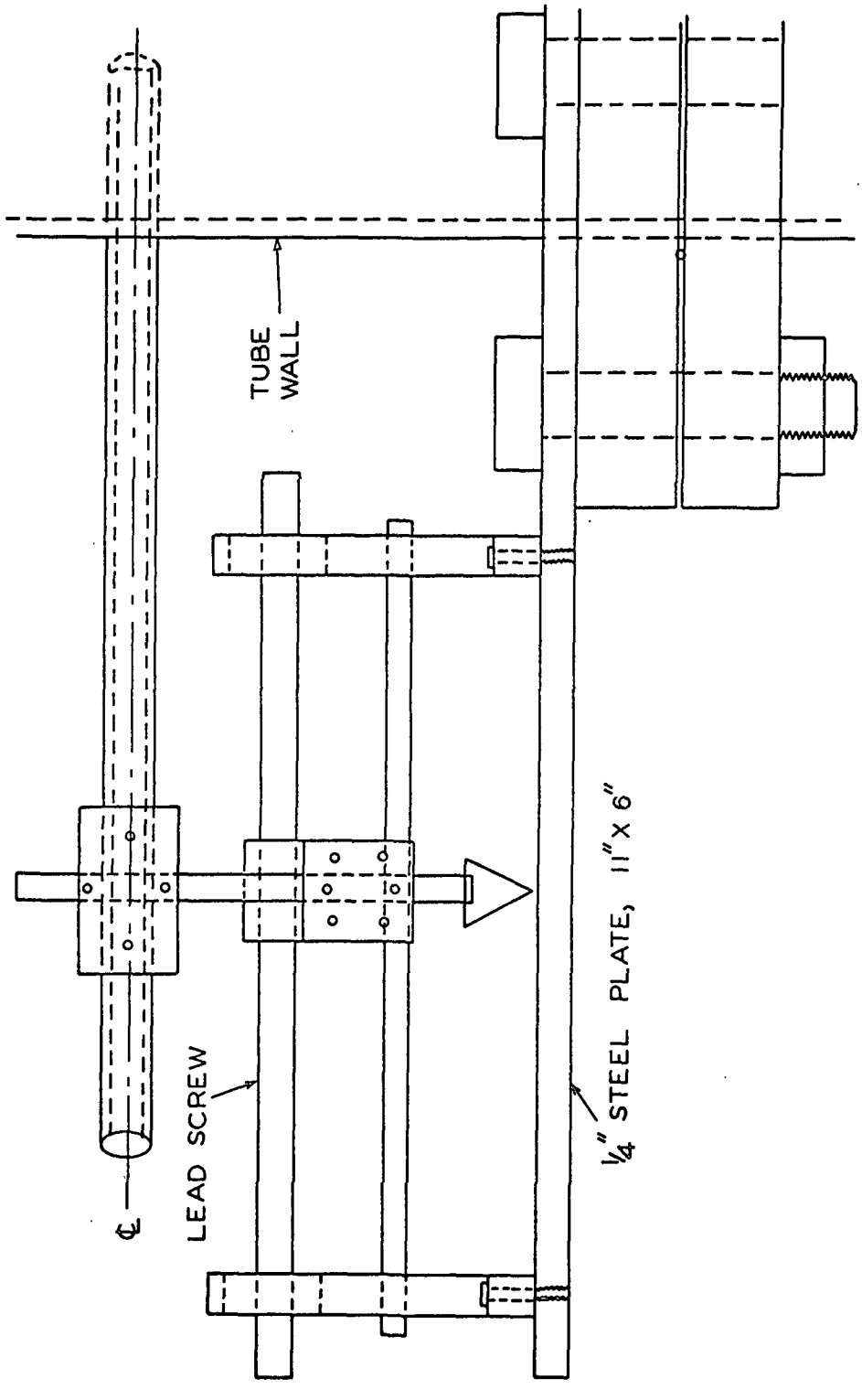

Figure 11. Traversing Feed for Impact Probe (Scale 1 in./1 in.)

EXPERIMENTAL PROCEDURES AND DATA

After the loop was built, it was necessary to be certain that it would function as anticipated. This was accomplished using water as the test fluid. All experimental runs, whether with water or suspension were carried out at 20°C. unless otherwise specified.

Three liquid-liquid manometers were employed, the heavy fluid being mercury in one and carbon tetrachloride in the other two. One of the carbon tetrachloride manometers was hooked up to the impact probe, while the other two manometers were connected to the static pressure taps, as indicated in the instrumentation sketch (Fig. 7).

In testing the loop, the magnetic flowmeter was first calibrated, using the discharge tank (Table III). Pressure drops between static pressure taps at known flow rates were converted to friction factors and plotted against Reynolds number (Fig. 12). Agreement with the long-established correlation was excellent and indicates that the two tubes are indeed hydraulically smooth.

Impact probes of both sizes were tested in water flow. With the larger probe, the mean annular jet velocity was carefully determined by placing a calibrated rotameter on the purge water line. Impact pressure as a function of annular jet velocity is shown in Fig. 13. By varying the flow rate in the tube and changing the probe position in the tube, it was possible to ascertain that the impact pressure-jet velocity relation is virtually independent of the velocity gradient in the fluid. Further testing showed that this relation is also unaffected by close proximity of the tube wall.

TABLE III

MAGNETIC FLOWMETER CALIBRATION

Flowmeter Reading	Q, $ft.^3\ sec.^{-1}$
10.0	0.0119
18.0	0.0210
27.0	0.0312
37.0	0.0428
38.0	0.0451
52.0	0.0596
56.5	0.0645
72.0	0.0817
72.5	0.0827
100.0	0.114
118.0	0.132
131.0	0.1475
153.0	0.174
219.0	0.250

Dye injection studies (8) have shown that the impact pressure suddenly swings negative when the annular purge jet pinches off, merging in front of the probe tip. Determining the effects of the various parameters upon the occurrence of this jet pinch would be an interesting study in itself.

The measured velocity profiles in turbulent flow were checked by comparing them in reduced form to the universal velocity profile for tube flow of Newtonian fluids, and in addition by comparing integrated velocity profiles to measured discharge rates. The results for the smaller probe are summarized in Table IV and Fig. 14. Once again, agreement must be considered very good.

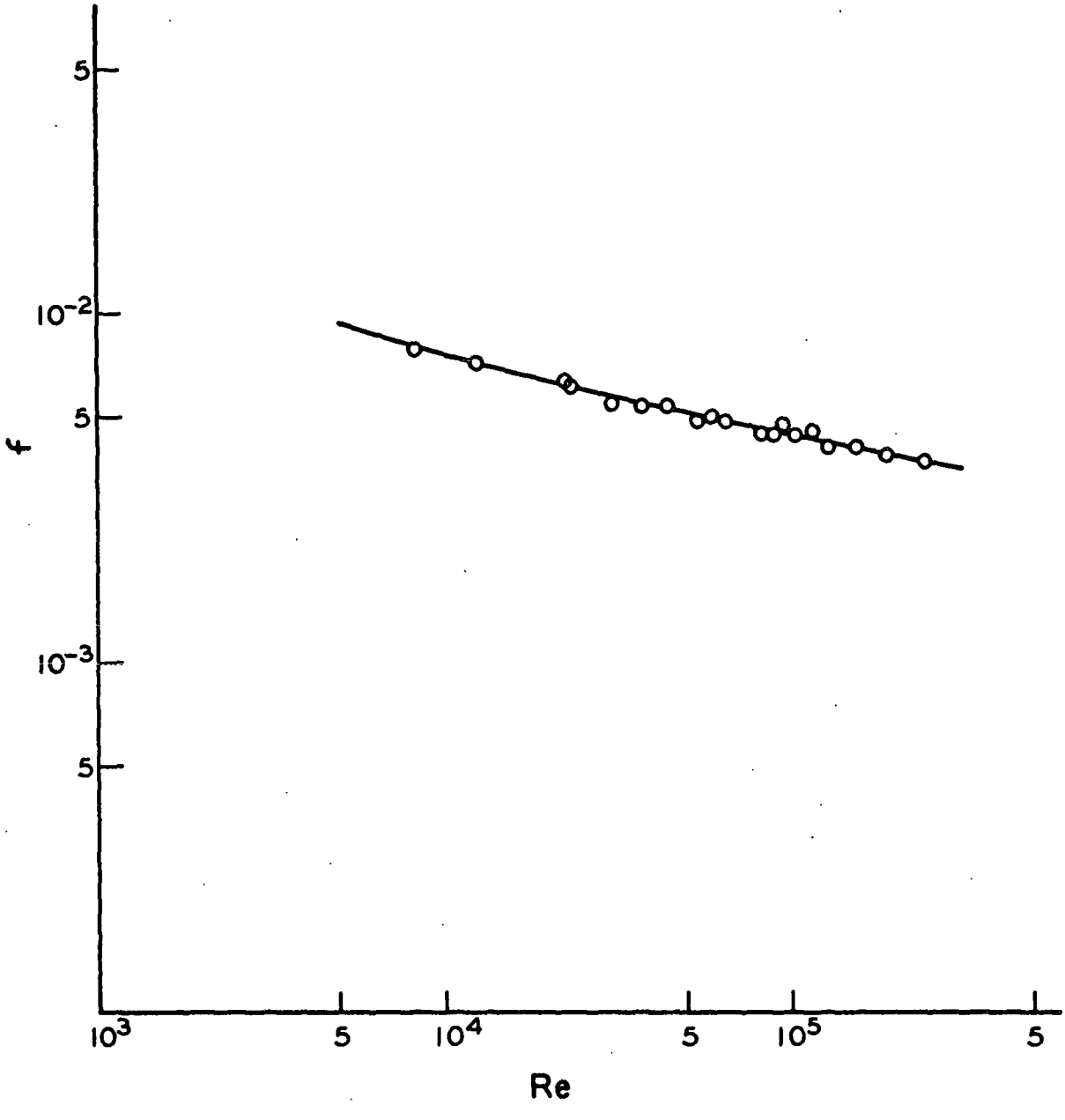

Figure 12. Friction Factor vs. Reynolds Number (Water at 20°C.)
D = 1.875 in., 1.400 in.

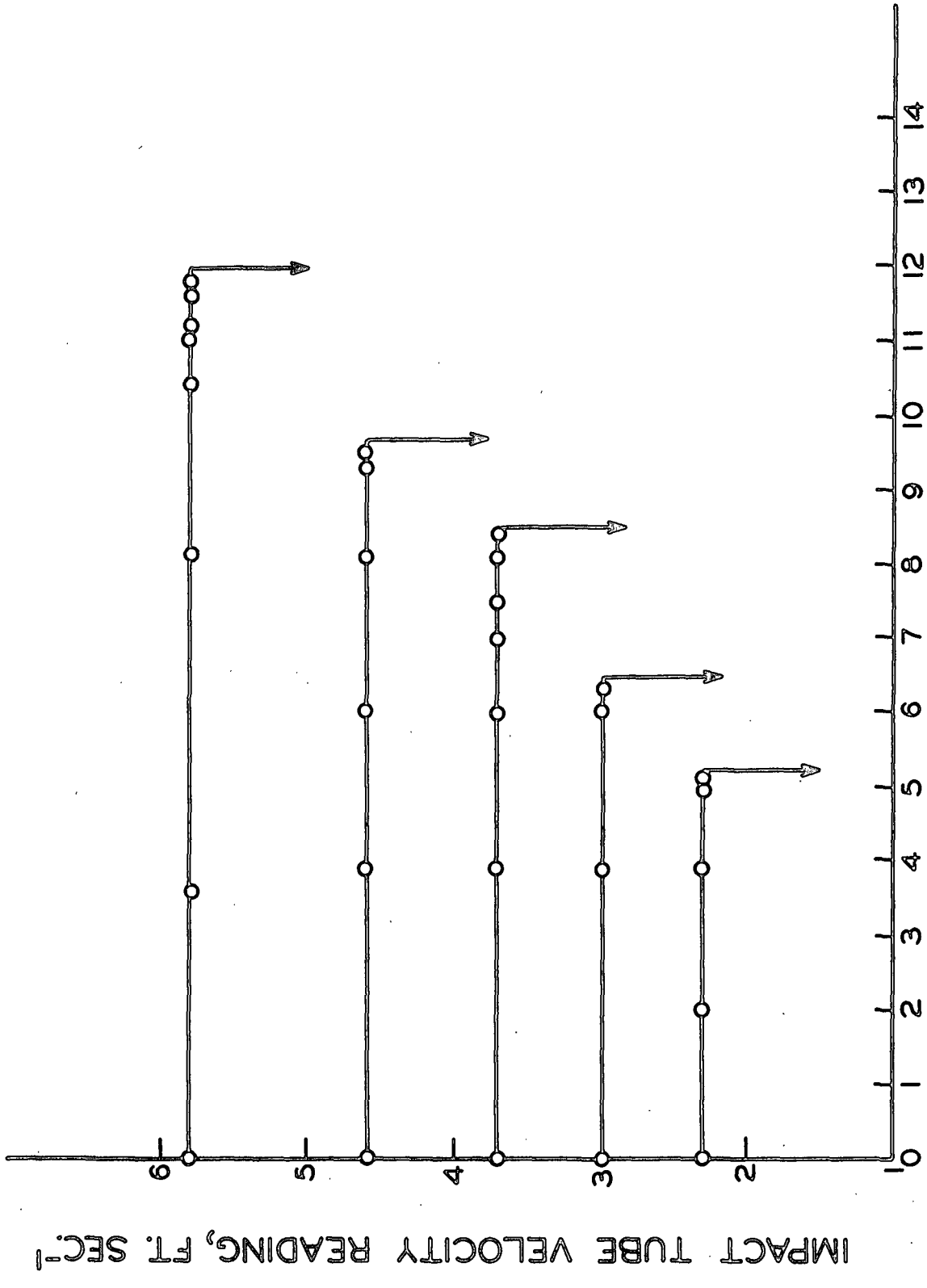

Figure 13. Stability of Annular Purge Impact Tube Readings (Large Probe in Water at 25°C.)

TABLE IV

COMPARISON OF INTEGRATED VELOCITY PROFILES TO VOLUMETRIC FLOW RATES

D, inches	Γ, g./100 ml.	Q, ft.^{3} sec.$^{-1}$	$\int_0^R 2\pi r\bar{v}dr$, ft.^{3} sec.$^{-1}$	Sample
1.875	0.00	0.0375	0.0382	
		0.0630	0.0631	
		0.0645	0.0650	
		0.113	0.114	
	0.100	0.0407	0.0407	2578
		0.0610	0.0610	
	0.157	0.0350	0.0334	2578
		0.0661	0.0635	
		0.115	0.114	
		0.137	0.142	
	0.310	0.0595	0.0616	2578
		0.0700	0.0700	
		0.111	0.107	
		0.147	0.142	
	0.580	0.0630	0.0614	2578
		0.123	0.124	
		0.145	0.144	
	0.113	0.0380	0.0383	2
		0.0590	0.0591	
		0.0745	0.0730	
		0.0905	0.0890	
		0.1095	0.1090	

After the loop was found to be in satisfactory operating condition, the switch to fiber suspensions was carried out. The only additional modification of the loop was the mounting of a 1/4-hp. Lightnin' mixer over the stock chest to maintain agitation.

Two wood fibers, designated Samples 2578 and 2, were used in this work. The characterization of physical properties of these pulps may be found in Appendix I. Both fibers are well-bleached, commercial, softwood sulfite pulps and differ

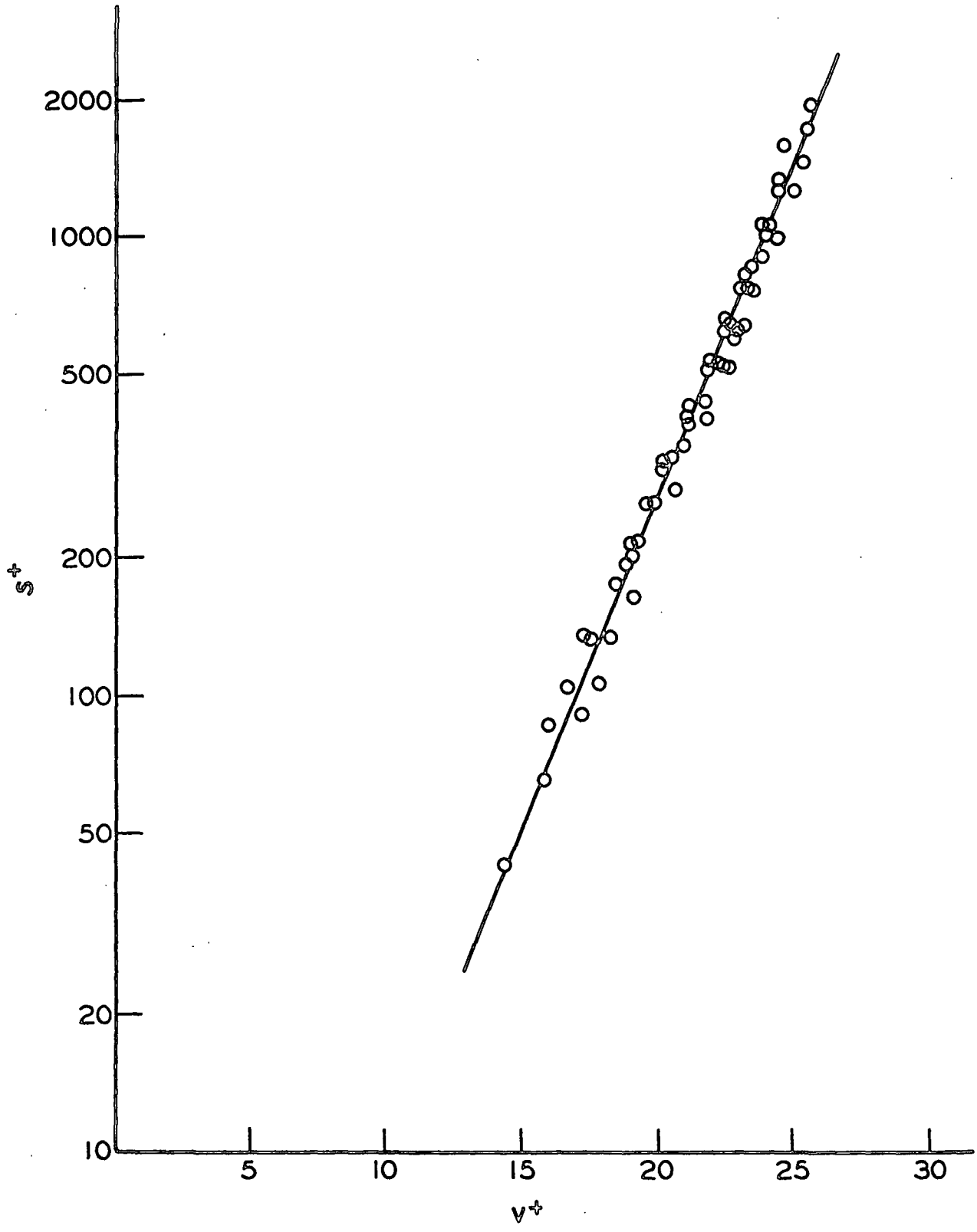

Figure 14. Reduced Position vs. Reduced Velocity
(Water at 20°C., $\overline{D}$ = 1.875 in., 1.400 in.)

from one another primarily in length distribution. As can readily be seen, these experiments do not provide a great deal of contrast in length distribution or tube diameter, but they were not intended to do so. The principal objective of the experiments is to provide a basis for expressing momentum transfer in dilute fiber suspensions, not to conclusively establish functional relationships.

Experiments were carried out at consistencies ranging from 0.05 to 0.6 g./100 ml. Reynolds numbers based on water density and viscosity range from about 1×10^4 to 2.5×10^5. The quantitative information obtained includes velocity profiles and pressure drop-flow rate relationships.

One attempt was made to measure the turbulence-induced fluctuation in impact pressure. A Pace KP 15 pressure transducer was connected to the impact pressure lines in place of Manometer no. 3. The signal was recorded on a fast-response chart recorder. Unfortunately, when the chambers on either side of the diaphragm in the instrument are filled with water, a natural vibration frequency of about 10 cp. is observed. This frequency effectively masks the turbulence-induced fluctuations, and the attempt was regarded as a failure.

The raw data from the flow loop are presented in Appendices II and III. Sufficient information is provided for complete treatment of these data.

Refining effects of the pumps and stirrer on the fibers proved negligible. Table V summarizes the changes in some physical properties of Fiber 2578 after circulation in the loop for fifteen hours at 0.157 g./100 ml. No significant changes were noted.

Appendix IV presents sample calculations of reduced velocity profiles. Fluid properties are assumed to be those of water, so that one may interpret the deviations from Newtonian behavior as effects of the fibers.

TABLE V

SOME PHYSICAL PROPERTIES OF PULP 2578

Arithmetic average fiber length, mm.	= 1.07
Weighted average fiber length, mm.	= 1.83
[a]Swollen specific surface, $\underline{S}_w$, cm.^{2}/g.	= 9900
[a]Swollen specific volume, $\underline{\bar{v}}$, cc./g.	= 2.42

After 15 hr. circulation in the loop at 0.157 g./100 ml.:

Arithmetic average fiber length, mm.	= 1.08
Weighted average fiber length, mm.	= 1.76
[a]Swollen specific surface, $\underline{S}_w$, cm.^{2}/g.	= 9900
[a]Swollen specific volume, $\underline{\bar{v}}$, cc./g.	= 2.42

[a]Values supplied by B. D. Andrews.

Reynolds number-friction factor correlations proved to be of the two general types shown in Fig. 1. These diagrams may be divided into three turbulent flow regions, as labeled in Fig. 1. Region 1 will hereafter be called plug turbulence, Region 2 damped turbulence, and Region 3 Newtonian turbulence. Regions 1 and 2 have often been noted in the past, but this is apparently the first time that the reluctance of the suspension curve to cross the Newtonian line has been observed. This reluctance is here interpreted as an approach to normal Newtonian behavior.

In plug turbulence, Mih and Parker commented, a central plug exists, the size of which shrinks as flow rate increases. These experiments confirm this observation and show in addition that no central plug is present in damped turbulence.

When one prepares a semilog plot of reduced position vs. reduced velocity following the common practice for Newtonian fluids, a straight line is obtained

in the turbulent core area of the tube regardless of whether the flow region is plug turbulence, damped turbulence, or Newtonian turbulence. Of course in plug turbulence two lines are obtained in a given profile, the plug exhibiting constant velocity and the outer annulus line showing a finite slope. For Newtonian fluids in tube flow, all data will of course fall on the same line regardless of flow rate, viscosity, tube diameter, etc. For fiber suspensions, this is not the case.

As Mih and Parker observed, the slope and position of the line are different for suspensions than for Newtonian fluids, the slope in general implying a lower von Kármán constant, κ, for suspensions. Mih and Parker chose to characterize suspension flow by applying a new von Kármán constant which varies with consistency and fiber type, further explaining Regions 1 and 2 by introducing an artificial roughness factor.

Data from this work show that the apparent κ values for dilute suspensions are not in fact independent of flow rate but vary with it in a nearly linear fashion throughout the damped turbulence region and in a more complicated fashion in plug turbulence. As Newtonian turbulence is approached, the nearly linear κ vs. $\underline{Q}$ relation is no longer valid and κ quickly assumes its Newtonian value. The intercept of the reduced position-reduced velocity plot also tends to its Newtonian value, and the suspension velocity profiles become indistinguishable from those of a Newtonian fluid. Examples of $\underline{v}^+ - \underline{s}^+$ plots exhibiting damped turbulent and plug turbulent behavior may be found in Fig. 15 and 16.

The experimentally determined values of von Kármán constant are given in tabular and graphical forms in Appendix V.

Shear stresses characterizing the plug boundaries in plug turbulence are listed in Table VI. The only comparison possible (see Table II) shows reasonable

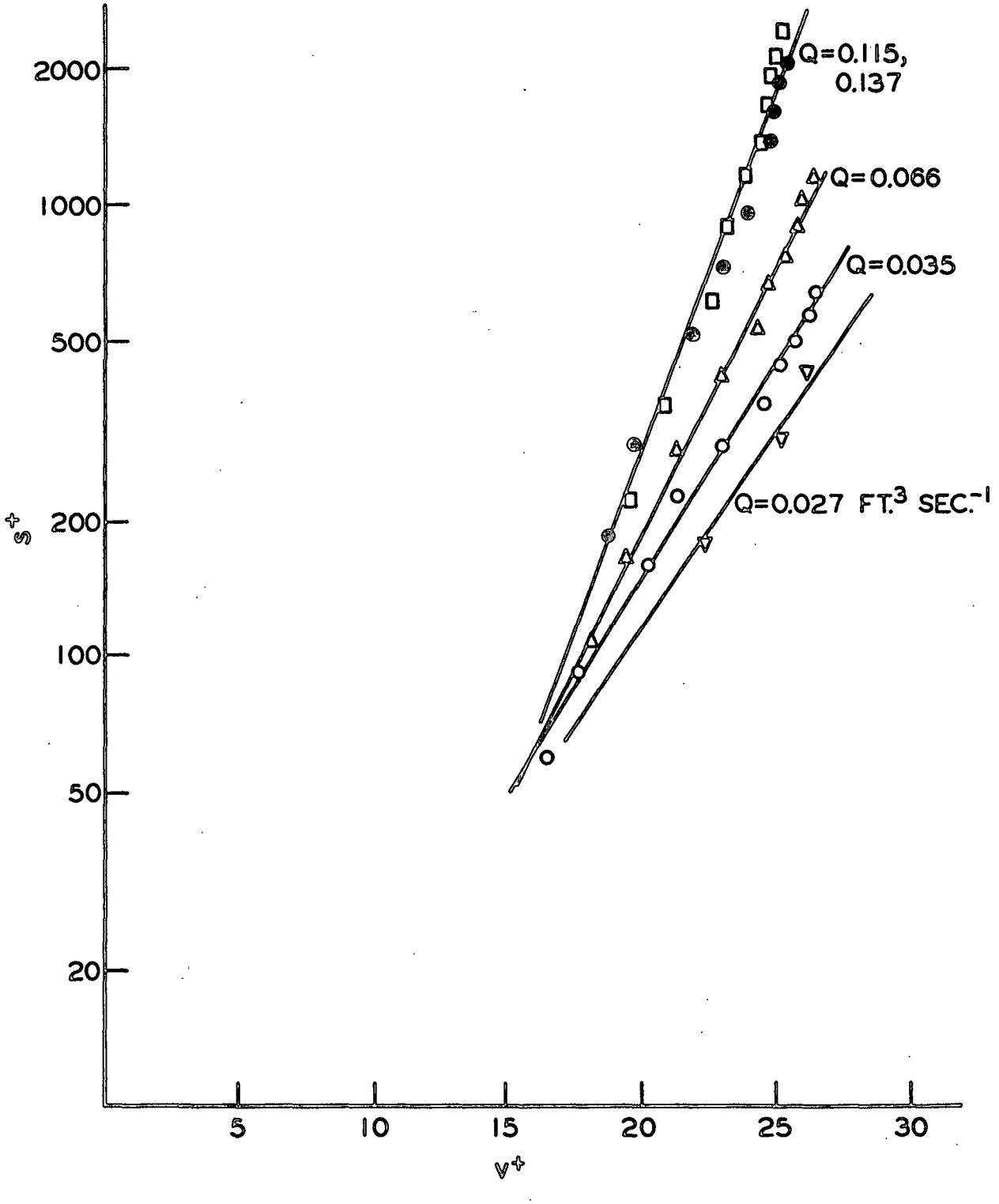

Figure 15. Reduced Position vs. Reduced Velocity; Γ = 0.157 g./100 ml., D = 1.875 in. (Sample 2578)

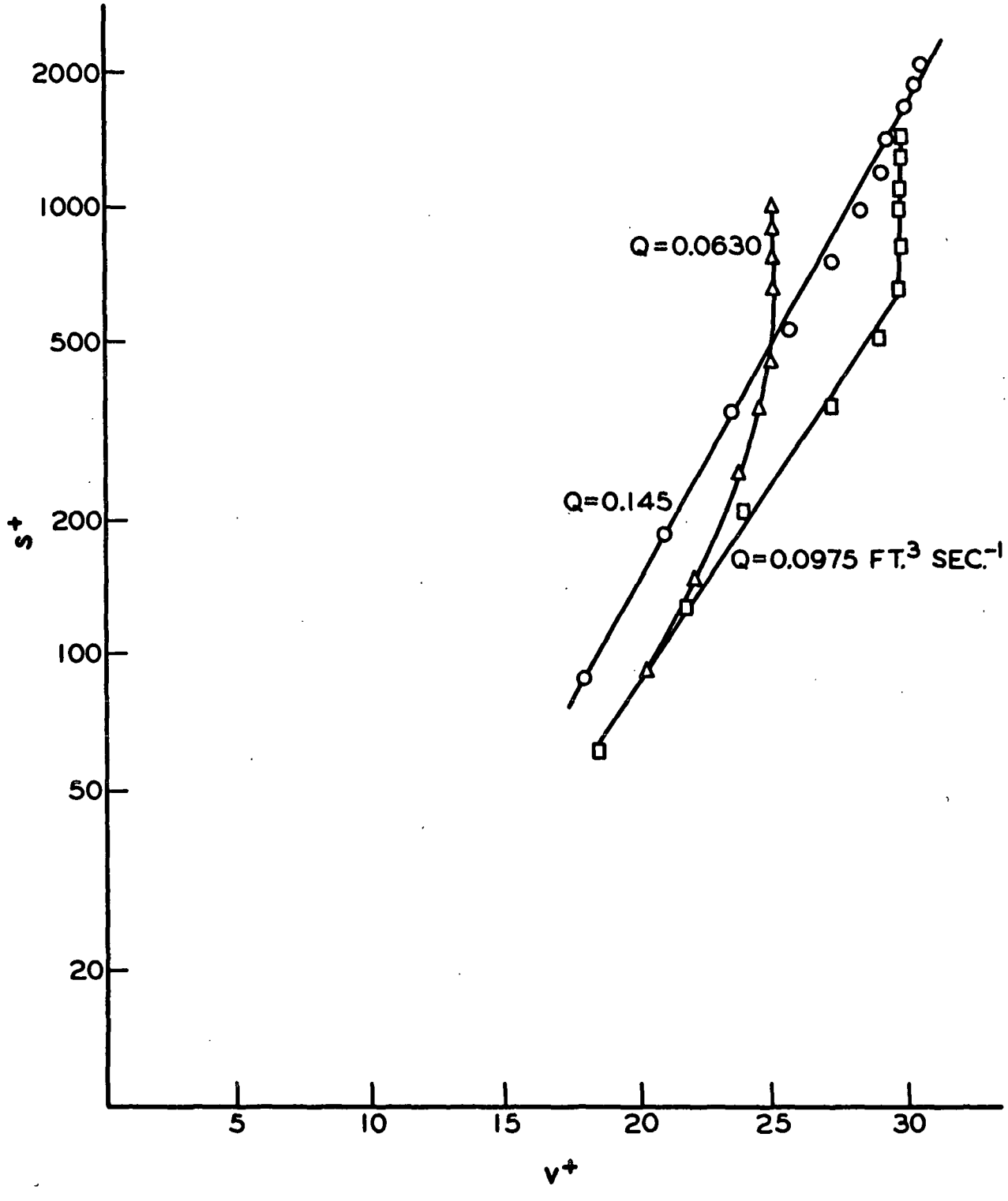

Figure 16. Reduced Position vs. Reduced Velocity; Γ = 0.58 g./100 ml., D = 1.875 in. (Sample 2578)

agreement between these stresses and the yield stress determined in the hyperbolic flow device. In addition, τ_p appears to be independent of tube diameter while depending strongly on consistency and fiber length. These observations seem to argue strongly in favor of the network idea.

TABLE VI

PLUG TURBULENCE-SHEAR STRESS AT PLUG BOUNDARIES

Sample	Γ, g./100 ml.	D, inches	r_p/r_o	τ_o g. cm.$^{-1}$ sec.$^{-2}$	τ_p	Mean Length, mm.
2578	0.313	1.875	0.55	3.65	2.00	1.07
2578	0.585	1.875	0.705	19.3	13.6	
			0.536	40.5	21.7	
			0.390	62.6	24.4	
2	0.277	1.875	0.656	8.45	5.55	1.58
			0.560	16.3	9.15	
			0.410	27.6	11.3	
			0.305	39.7	12.1	
2	0.273	1.400	0.615	15.8	9.71	
			0.444	27.5	12.2	
			0.256	52.8	13.5	

Unfortunately, a systematic increase in τ_p with decreasing plug radius makes acceptance of a simple yield stress model difficult. It is necessary to postulate a small increase in consistency or possibly a change in fiber orientation, etc., of the plug network with decreasing plug diameter. While this is not an unreasonable suggestion, there is no direct evidence to support it.

Mih and Parker (8) have offered essentially the same observations concerning the plug region as are made above. In addition, they present independent quantitative data consistent with the observations.

EMPIRICAL TREATMENT OF THE TUBE FLOW DATA

Review of the experimental data lead to the proposal of empirical relationships to describe observed behavior. The initial part of the following discussion is applicable to the region of damped turbulence.

Within the damped turbulence region, some new flow parameters are defined:

$$\frac{\bar{v}}{\sqrt{\tau_o/\rho}} = g(\langle\bar{v}\rangle, \Gamma, \zeta, D) + \frac{1}{\kappa} \ln \left(\frac{s\sqrt{\tau_o/\rho}}{\nu}\right) \tag{33}$$

where:

$$\kappa = c(D) + \alpha(\Gamma, \zeta, D)Q \tag{34},$$

$$\tau_o = \beta(\Gamma, \zeta, D) \frac{\rho\langle\bar{v}\rangle^2}{2} \tag{35},$$

$$f = \beta(\Gamma, \zeta, D) \tag{36}.$$

Simple manipulation of these equations yields:

$$\frac{\bar{v}_{max} - \bar{v}}{v_*} = \frac{1}{\kappa} \ln \frac{R}{s} \tag{37},$$

$$\langle\bar{v}\rangle = \bar{v}_{max} \frac{3v_*}{2\kappa} \tag{38},$$

$$\langle\bar{v}\rangle = \bar{v}_{max} \frac{3\langle\bar{v}\rangle\sqrt{\beta/2}}{2(c + \alpha Q)} \tag{39}.$$

Thus, knowledge of c, β, α will be sufficient to define the time average parameters of flow for any set of conditions. A typical plot of κ vs. Q is presented in Fig. 17. Picking $\kappa = 0.36$ as the limiting or Newtonian value is a little arbitrary, as some authors prefer 0.40. The data taken here seem to agree with the former value, but with a little reinterpretation would also be consistent with the latter.

The region of damped turbulence may be roughly bounded by the criteria:

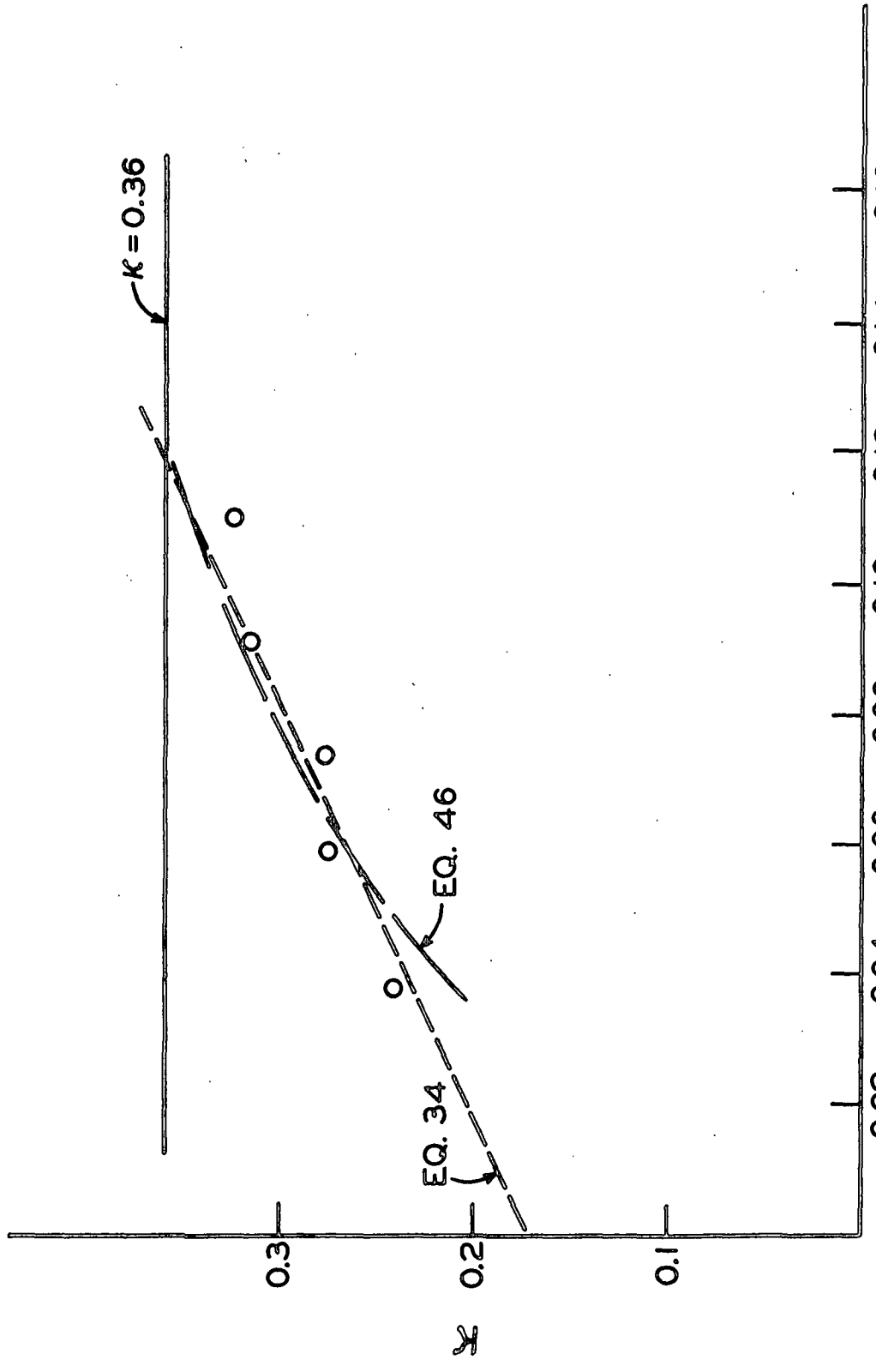

Figure 17. κ vs Q, Sample 2 in 1.875-in. i.d. Loop; Γ = 0.112 g./100 ml.

$$\tau_o \geq 10\tau_p(\Gamma, \zeta) \tag{40}$$

$$c(D) + \alpha(\Gamma, \zeta, D)Q \leq 0.35 \tag{41}$$

It follows that if plug turbulence is observed, its domain is the region $\tau_o < 10\tau_p$, while Newtonian turbulence exists whenever

$$c(D) + \alpha(\Gamma, \zeta, D)Q > 0.35 \tag{42}$$

Combining values of β measured in these experiments with some of those reported by M.I.T. and by Mih and Parker for quite different fibers, it becomes evident that β depends upon Γ and D, but is virtually independent of fiber length. Table VII and Fig. 18 summarizes β values and indicate the form of dependence on Γ and D.

TABLE VII

VALUES OF α, c, AND β

Sample	D, inches	Γ, g./100 ml.	α, ft.$^{-3}$ sec.^{1}	c	β
2578	1.875	0.0995	1.82	0.17	4.9×10^{-3}
		0.157	1.55	0.17	4.5×10^{-3}
		0.313	1.12	0.17	3.9×10^{-3}
		0.585	0.52	0.17	3.2×10^{-3}
2578	1.400	0.100	1.85	0.21	4.9×10^{-3}
		0.208	1.25	0.21	4.4×10^{-3}
2	1.875	0.112	1.60	0.17	4.6×10^{-3}
		0.277	1.10	0.17	3.7×10^{-3}
2	1.400	0.064	2.20	0.21	5.35×10^{-3}
		0.124	1.80	0.21	4.70×10^{-3}
		0.273			3.80×10^{-3}

Values of the parameters c and α are available only for the experiments carried out in the course of this thesis. These data are listed in Table VII and Fig. 19. Evidently, these parameters depend only on D and Γ, as indicated: $c = c(D)$, $\alpha = \alpha(\Gamma)$.

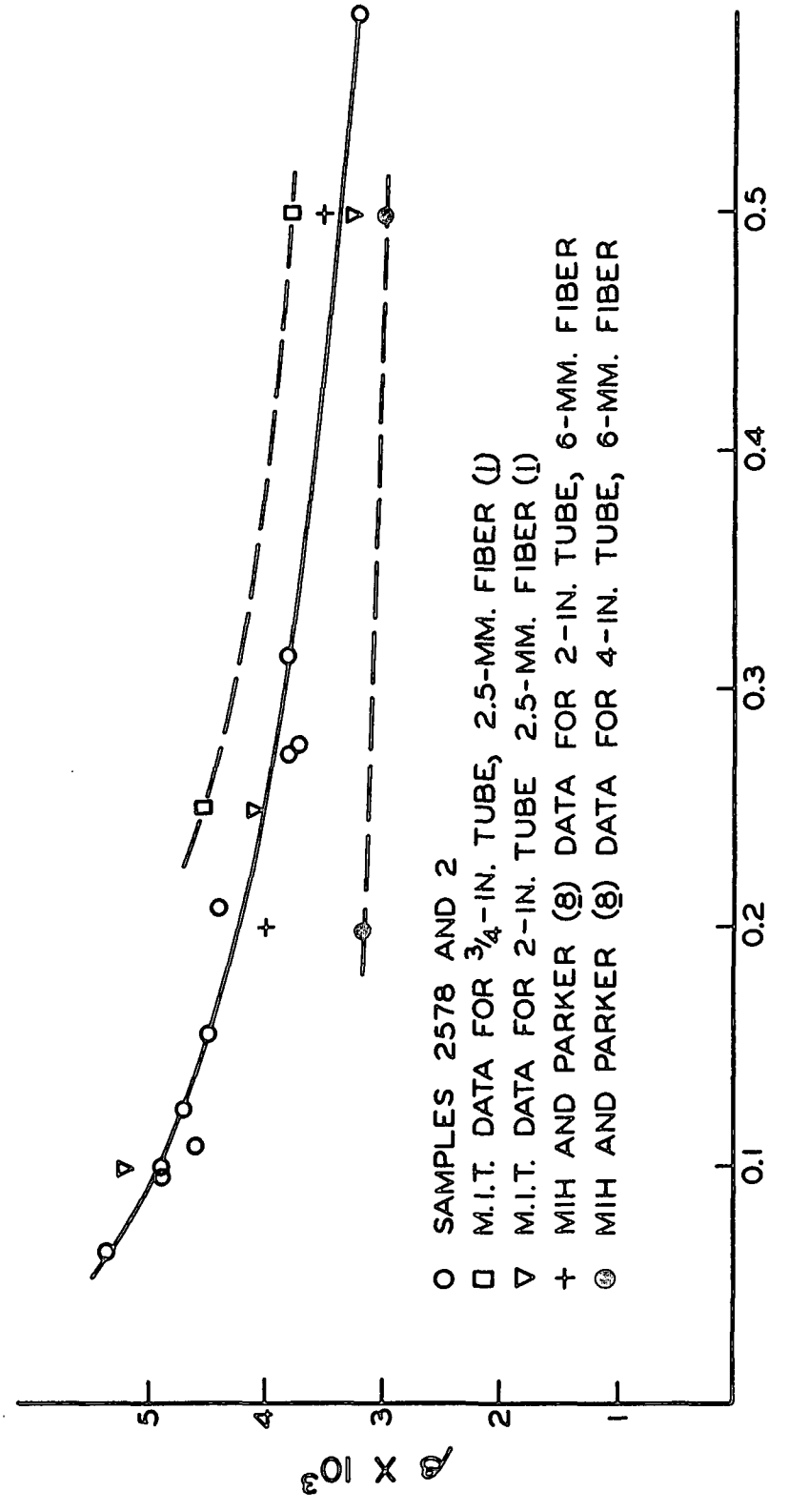

Figure 18. β vs. Γ

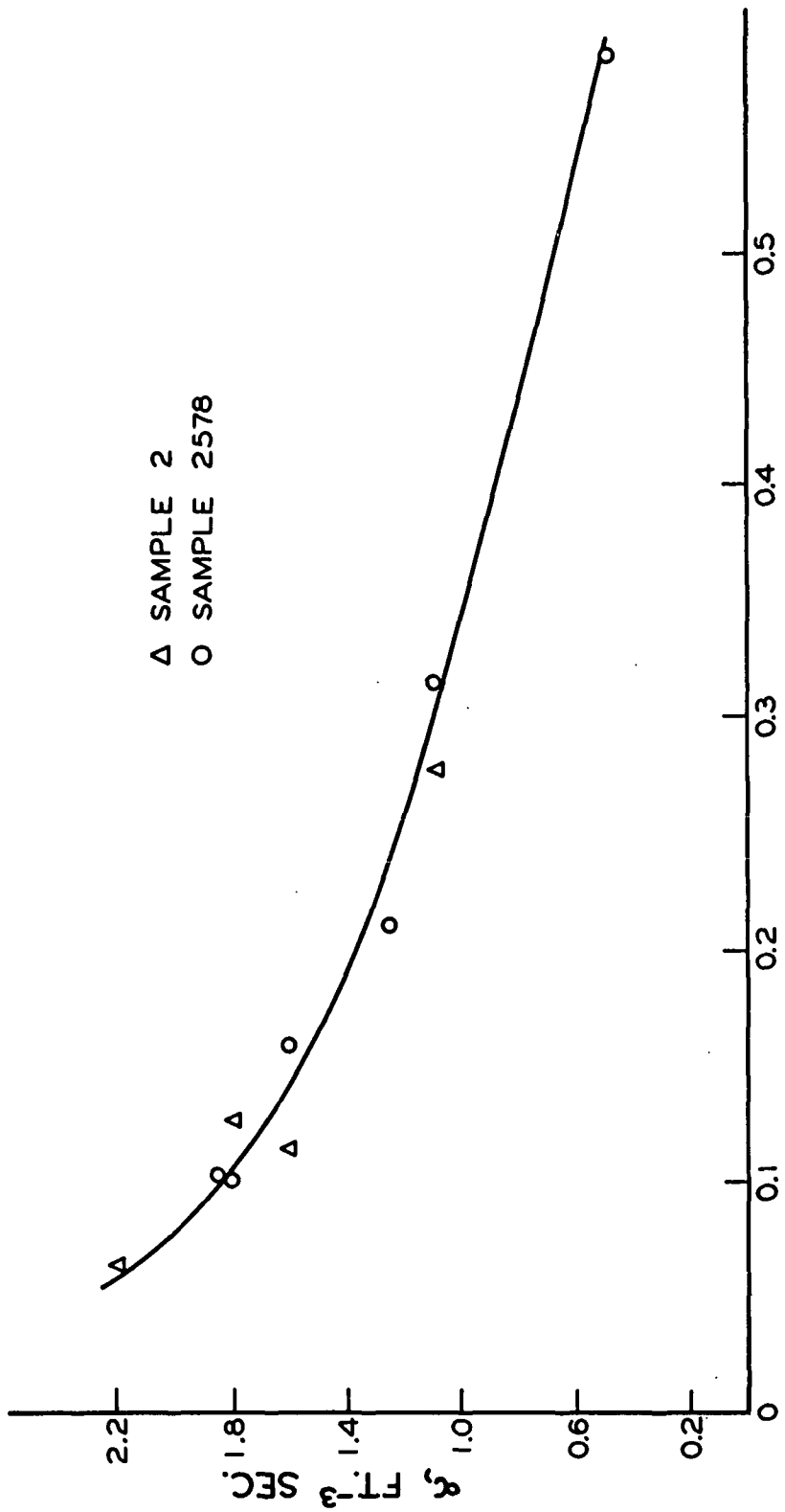

Figure 19. α vs. Q

The lack of dependence of κ and β upon the fiber length or other fiber parameters is somewhat surprising, but in view of the data obtained is hardly challengeable. On the other hand, one may find in the literature information showing that suspensions of small particles such as tiny spheres exhibit higher values of $\underline{f}$ than do Newtonian fluids (3). One should not suppose that observations made on fiber suspensions are applicable to suspensions in general. Rather, think that fibers are all long and thin. Increasing the $\underline{\ell}/\underline{d}$ ratio beyond an already high value is apparently not likely to alter the manner by which fibers seem to reduce the momentum transfer efficiency of a fluid in turbulent flow.

The parameters describing damped turbulence and their dependence upon independent experimental variables are summarized in the following list:

$$\beta = \beta(D, \Gamma), \quad c = c(D), \quad \alpha = \alpha(\Gamma) ,$$

$$\kappa = c(D) + \frac{\pi D^2}{4} \langle \bar{v} \rangle \, [\alpha(\Gamma)] \qquad (43) .$$

Resorting to the usual engineering practice of presenting results in dimensionless form, an educated guess at significant dimensionless parameters may be made:

$$\frac{\rho D \langle \bar{v} \rangle}{\mu} , \quad \Gamma\xi , \quad \frac{D}{d} , \quad \frac{\ell}{D}$$

and the parameters written in terms of dimensionless variables:

$$\beta = \beta(D/d, \Gamma\xi) \qquad (44) ,$$

$$\kappa = c(D/d) + \left(\frac{\rho D \langle \bar{v} \rangle}{\mu}\right) \left(\frac{D}{d}\right) \alpha'(\Gamma\xi) \qquad (45) .$$

There is no justification for this procedure, but it does seem to give a little more insight into what is going on.

For the moment, we shall leave this development and turn to the other regions of flow. Newtonian turbulence is easily dismissed. In this region, the parameters

used to describe turbulent flow of a pure fluid are adequate to describe dilute fiber suspensions as well.

Plug turbulence is necessarily the most complicated region since an additional mechanism of momentum transfer is present.

To begin with, plug turbulence may or may not be observed, depending apparently upon whether the consistency is high enough and the fibers long enough to make a strong coherent network. The reasons for supposing that the plug is really a coherent network have already been mentioned. In the turbulent annulus surrounding the plug, fibers reduce the effectiveness of momentum transfer in the fluid, almost certainly by the same mechanism as in damped turbulence. Qualitatively, as has been remarked, the effect upon κ is the same as for damped turbulence. Quantitatively, however, the linear correlation of κ vs. $\underline{Q}$ does not appear to be valid. There are not enough data available for this region to permit the proposal of a different correlation to describe it, so the matter must be at least temporarily retired.

Now that a reasonably complete model has been built up, it might be worthwhile to try a few simplifying assumptions.

In turbulent tube flow, the laminar sublayer and buffer zone are thin compared to the tube diameter. In fact, the thickness of these layers is generally somewhat less than the length of a wood fiber. Further, in the immediate vicinity of the wall, momentum transfer rates are relatively high and of a predominantly molecular nature. Assume that the position of the boundary between the buffer zone and the turbulent core remains uninfluenced by fibers and that the momentum transfer mechanisms in the buffer zone and laminar sublayer are unaffected by the presence of fibers. Then the unusual behavior of the friction factor must be explained in terms of the altered momentum transfer behavior in the turbulent core, and it should be possible to derive an additional relation between κ and β.

The experimental data suggest that this approach may be close to correct since most of the $\underline{v}^+$-$\underline{s}^+$ plots intersect one another somewhere near $\underline{s}^+ = 30$, particularly in the more dilute cases. (See Appendix IV for some examples.)

Assuming that the buffer zone boundary is located at $\underline{s}^+ = 30$, $\underline{v}^+ = 13$, as for a Newtonian fluid, the following relation between κ and β for damped turbulence is obtained:

$$\kappa = \frac{\sqrt{\beta/2}}{1 - 13\sqrt{\beta/2}} \ln \frac{Re\sqrt{\beta/2}}{60} - \frac{3}{2} \qquad (46).$$

The friction factor β is assumed to be constant, though this may not exactly be the case.

The above equation comes reasonably close in predicting the experimental values of κ given β, as can be seen in Appendix V. It does not fit the data as well as does the empirical straight-line correlation. Deviations are particularly noticeable at the lower flow rates. Probably the assumptions used in building the model are less valid at low flow rates or Reynolds numbers, where the buffer zone thickness begins to be appreciable. In addition, at $Re < 10^4$, the universal velocity profile is not likely to be valid even for Newtonian fluids.

The equation does a sufficiently good job of representing the data to make one think the assumptions leading to it are nearly correct. If so, it appears that the behavior of the friction factor in turbulent flow may be solely attributed to the systematic reduction of Reynolds stresses by fibers in the turbulent core region.

A curious added observation is that the equation appears nearly correctly to predict κ values well into the plug turbulent region using values of β from the damped turbulent region.

If for β the friction factor $\underline{f}$ of a Newtonian fluid were inserted in the equation, the usual value of κ would be produced. Thus, the equation is valid in Newtonian turbulence as well, provided β is replaced by the friction factor associated with the Reynolds number under consideration.

Since there is more information available concerning β than κ, the equation provides some possibilities for extending κ values.

In one case, a cross check of sorts is available: this is Mih and Parker's ($\underline{8}$) observations of 0.2% rayon suspension in a 4-in. pipe. They report $\beta \approx 0.00317$ and present velocity profiles in the range $1.76 \times 10^5 < Re < 3.5 \times 10^5$. The suggested formula yields for κ: $0.263 < \kappa < 0.316$, while they report an apparent κ value of 0.28. Under the circumstances, this should be considered fair agreement.

CONCLUSION

Within a somewhat limited framework, the foregoing discussion has characterized the turbulent tube flow of dilute fiber suspensions.

Three regions of flow are identifiable by their particular characteristics and are designated plug turbulence, damped turbulence, and Newtonian turbulence.

Plug turbulence is simply the flow of a central plug region at uniform velocity with a turbulent annular flow in the region between the plug boundary and the tube wall. The plug region may be thought of as a more or less continuous fiber network with included water, the network being capable of supporting the shear stress applied to it. The boundary of the plug is the point where the shear stress becomes too great for the network to support and the mechanism of momentum transfer shifts immediately to Reynolds stresses in the fluid.

It has been shown that the shear stress characterizing the plug boundary is strongly dependent on consistency and fiber length, while being independent of tube diameter. Furthermore, the response of fiber networks to another sort of hydrodynamic shear was observed and measured. The results showed that the yield stress of a fiber network in a hyperbolic field in creeping motion is similar in magnitude to the stress characterizing the plug boundary in turbulent flow of the same fiber at the same consistency.

To explain an apparent increase in τ_p as the size of the plug decreases it is necessary to postulate a change in plug consistency or possibly a change in fiber orientation, etc. No experimental data are available to support this idea.

In the turbulent annulus, the fluid Reynolds stresses are reduced by the presence of fiber. Qualitatively, this reduction is like damped turbulence,

but the limited experimental data indicate that the two situations are not quantitatively identical.

Damped turbulence has been thoroughly discussed and described in the previous sections. It has been shown that the ability of the fluid to transfer momentum by Reynolds stresses is reduced in a regular manner throughout the turbulent core, and velocity profiles are correspondingly sharper. At "low" flow rates, the behavior of the buffer zone is also affected, but this apparently becomes negligible at higher flow rates. At the higher flow rates, a definite relation exists between friction factor and apparent von Kármán constant which continues to be valid in the Newtonian turbulence region.

Newtonian turbulence is so designated simply because the suspension flow is in this region indistinguishable from that of the pure fluid (water) in so far as measurable average properties are concerned.

One need not be overimaginative to see possible application for these findings when generalized to other flow systems.

From the momentum transfer information provided here, one may infer some things about mass and heat transfer in fiber suspensions. This, in turn, could lead to new ideas about design of reaction vessels and operating conditions in fiber systems.

There remains the possibility of nearly direct application of the flow equations suggested here to the evaluation and design of headboxes and other common paper mill equipment.

SUGGESTIONS FOR FUTURE WORK

There is room for a considerable amount of additional work on the tube flow of fiber suspensions.

Specifically, it would be useful to establish the dependence of τ_p on fiber length and consistency. The behavior of the annular turbulent flow associated with the plug is also worthy of further investigation.

Extension of the experimental data to include different, particularly larger, tube diameters, and to include more types of fibers would be a reasonable program.

Length scales of turbulence within the suspension remain to be established, whether on Eulerian or Lagrangian bases. With such information one could possibly develop reasonable hypotheses about the mechanism of turbulence damping.

No less important than the structure of the fluid turbulence is the small-scale structure of the suspension. It would be well worth the effort if the local fluctuations in fiber concentration could be measured and correlated with local flow conditions. A recently developed technique involving crossed radiation beams may be useful in developing such a correlation (15).

It is possible that the new information about suspension flow is applicable to commercial papermaking processes. For example, high shear stresses are developed in the slice of a fourdrinier headbox or in the nozzle of a Twinverform machine. Conditions here are not likely to be steady state or necessarily identifiable as a particular type of turbulence. Nevertheless, it is possible that the sort of turbulence found could be identified as analogous to one of the steady-state situations. It may develop that a central plug will help or hinder desired sheet

properties. Similarly, damped turbulence might correlate with small structural anomalies in the sheet or Newtonian turbulence result in severe streaking.

Going further afield, one might think that apparent reaction rates would be different in different flow regimes owing to expected differences in mass transfer rates to and from fiber surfaces.

For example, consider a tube flow reactor and ignore likely thermal variations. In laminar flow a plug consisting of virtually all the fibers exists. Reduction in the size of a diffusion boundary layer about a fiber by fluid shear is likely to occur only at the outer edges of the plug. Diffusion-controlled reactions would be relatively slow. In plug turbulence, the reaction should be rapid in the turbulent annulus and slow in the plug leading to considerable variation in degree of reaction. Uniformity would be expected in damped turbulence, along with a fast rate of reaction. Probably the rate of reaction would increase and uniformity improve as Newtonian turbulence is approached.

Investigation in this direction could modify some existing ideas about bleaching in fiber suspensions or about reaction vessel design.

ACKNOWLEDGMENTS

A number of people have contributed materially toward the completion of this thesis. The importance, extent, and nature of their contributions may vary considerably, but all are significant and all deeply appreciated.

First, I must acknowledge the advice and aid of my Thesis Advisory Committee, H. Meyer, Chairman, members T. M. Grace, R. W. Nelson, and the late W. L. Ingmanson.

No less important were the efforts of B. D. Andrews in helping me to "beg, borrow, or steal" equipment; and the help of S. T. Han whose specialty is making students think.

I must also thank J. D. Parker and W. Mih for generously showing me their work long before they published it, and for their help and advice in my own efforts.

Special thanks go to my father, Harold Seely, whose extraordinary skill as a machinist was needed; and to Ken Hermsen, who converted a pile of pipes and pumps into a workable piece of precision equipment, and made it look easy.

Finally, thanks to Betty Cary, who does a lot of careful typing and proofreading, but isn't always thanked for it.

NOMENCLATURE

$\underline{A}_2$ = coefficient for a spherical harmonic of order 2

$\underline{A}_{-3}$ = coefficient for a spherical harmonic of order -3

$\underline{a}$ = radius of a spherical network

$\underline{B}_{-3}$ = coefficient for a spherical harmonic of order -3

$\underline{b}$ = a term in the universal logarithmic velocity distribution law

$\underline{c}$ = a term in the empirical expression for the apparent von Kármán constant of a flowing fiber suspension

$\underline{D}$ = tube diameter

$\underline{d}$ = fiber diameter

$\underline{f}$ = Fanning friction factor, $\underline{f} = \dfrac{\tau_o}{1/2\rho\langle\underline{\bar{v}}\rangle^2} = \dfrac{\underline{D}(\underline{p}_\rho - \underline{p}_L)}{4\underline{L}(1/2\rho\langle\underline{\bar{v}}\rangle^2)}$

$\underline{k}$ = Darcy's Law permeability coefficient

$\underline{L}$ = length of straight tubing between static pressure taps

$\underline{\ell}$ = fiber length

$\underline{n}$ = a universal constant describing flow in a Newtonian buffer zone

$\underline{\underline{P}}_{rx}$ = traction in $\underline{x}$ direction across a segment of spherical surface of radius $\underline{r}$ with center at the origin. The traction is evaluated at the point $(\underline{x}, \underline{y}, \underline{z})$

$\underline{p}$ = pressure

$\underline{p}_2$, $\underline{p}_{-3}$ = spherical harmonic functions of order 2 and -3, respectively, representing pressure distributions

$\underline{Q}$ = discharge flow rate

$\underline{R}$ = timing belt revolution period in hyperbolic flow device

$\underline{r}$ = radial distance in either spherical or cylindrical coordinate system

$\underline{\underline{Re}}$ = Reynolds number, $\rho\underline{D}\langle\underline{\bar{v}}\rangle/\mu$

$\underline{s}$ = position in tube as measured from the wall toward the tube center:

$$\underline{s} = \frac{\underline{D}}{2} - \underline{r}$$

$\underline{s}^+$ = dimensionless variable in tube flow: $\underline{s}^+ = \frac{\underline{s}\sqrt{\tau_o/\rho}}{\nu}$

$\vec{\underline{V}}$ = velocity, a vector

$\underline{u}$ = $\underline{x}$ component of $\vec{\underline{V}}$ in Cartesian coordinate system

$\underline{v}$ = $\underline{y}$ component of $\vec{\underline{V}}$ in Cartesian coordinate system

$\underline{w}$ = $\underline{z}$ component of $\vec{\underline{V}}$ in Cartesian coordinate system

$\vec{\underline{V}}_*$ = superficial velocity of a fluid in a porous medium

$\vec{\underline{V}}_{\underline{r}}$ = superficial velocity of the fluid relative to the porous medium

$\overline{\underline{v}}$ = time-averaged unidirectional velocity in tube flow

$\langle\overline{\underline{v}}\rangle$ = space-averaged $\overline{\underline{v}}$

$\underline{v}^+$ = dimensionless velocity in tube flow, $\frac{\overline{\underline{v}}}{\sqrt{\tau_o/\rho}}$

$\underline{x},\underline{y},\underline{z}$ = Cartesian coordinates, always right handed, usually dimensional

α = shear rate, sec.$^{-1}$; coefficient of discharge rate in empirical expression for von Kármán constant, ft.$^{-3}$ sec.

β = numerical value of friction factor in damped turbulence

Γ = fiber mass per unit volume of suspension, g./100 ml.

ζ = an undefined parameter or group of parameters characteristic of a particular type of fiber

θ = angular component of a spherical coordinate system

κ = von Kármán constant or apparent von Kármán constant

μ = viscosity; in a fiber suspension, the viscosity of the fluid alone

ν = kinematic viscosity, μ/ρ

ξ = fiber-occupied volume per unit mass of fiber

ρ = density; in suspension, the density of the suspending fluid

τ = shear stress; in fluid flow, equivalently momentum flux

τ_o = wall shear stress in tube flow

$\tau_{\underline{p}}$ = shear stress at a plug boundary in tube flow

τ_y = yield shear stress in hyperbolic flow experiments

φ = angular component of a spherical coordinate system

φ_2, φ_{-3} = spherical harmonics of order 2 and -3 representing irrotational flows which are not pressure induced

χ_1 = spherical harmonic of order 1 representing a rotational flow

$\Rightarrow$ = implies

$\mathbb{C}$ = center line

LITERATURE CITED

1. Daily, J., and Bugliarello, G. M.I.T. Hydrodynamics Laboratory Report No. 30. Cambridge, Mass., Massachusetts Institute of Technology, 1958.

2. Daily, J., and Bugliarello, G., Tappi 44:497(1961).

3. Daily, J., and Chu, T. M.I.T. Hydrodynamics Laboratory Report No. 48. Cambridge, Mass., Massachusetts Institute of Technology, 1961.

4. Carrasquilla, A. Flow of suspensions of nonspherical particles. Master of Science Dissertation. Cambridge, Mass., Massachusetts Institute of Technology, 1965.

5. Hubley, C., Robertson, A., and Mason, S., Can. J. Research B 28:770(1950).

6. Robertson, A., and Mason, S., Pulp Paper Mag. Can., Convention Issue: 263 (1954).

7. Wollwage, J. An investigation of the flocculation of papermaking fibers. Doctoral Dissertation. Appleton, Wis., The Institute of Paper Chemistry, 1938.

8. Mih, W., and Parker, J., Tappi 50:237(1967).

9. Schlichting, H. Boundary layer theory. 4th ed. Ch. XIX. New York, McGraw-Hill, 1960.

10. Taylor, G., Proc. Roy. Soc. A146:501(1934).

11. Lamb, H. Hydrodynamics. 6th ed. Ch. XI. New York, Dover, 1945.

12. Einstein, A., Ann. Physik 19:289(1906); 34:591(1911).

13. Seely, T., J. Polymer Sci., in press.

14. Forgacs, O., and Mason, S., J. Colloid Sci. 14:457, 473(1959).

15. Fisher, M., and Krause, F., J. Fluid Mech. 28:705(1967).

APPENDIX I

PHYSICAL PROPERTIES OF FIBERS*

SAMPLE 2578

Length:

$$\frac{\Sigma n\ell}{\Sigma n} = 1.07 \text{ mm.}$$

$$\frac{\Sigma n\ell^2}{\Sigma n\ell} = 1.75 \text{ mm.}$$

Width:

$$\frac{\Sigma nw}{\Sigma n} = 35.2\ \mu$$

$$s_w = 9900 \text{ cm.}^2/\text{g.}$$

$$v_w = 2.42 \text{ cc./g.}$$

Average number of fibers, parenchyma, and ray cells > 0.1 mm. = 5,720,000 fibers/g.

Average number of fibers only > 0.1 mm. = 4,660,000 fibers/g.

SAMPLE 2

Length:

$$\frac{\Sigma n\ell}{\Sigma n} = 1.58 \text{ mm.}$$

$$\frac{\Sigma n\ell^2}{\Sigma n\ell} = 2.15 \text{ mm.}$$

*Data supplied by J. Hankey.

Width:

$$\frac{\Sigma nw}{\Sigma n} = 38.1\ \mu$$

Average number of fibers, parenchyma, and ray cells > 0.1 mm. = 4,060,000 fibers/g..

Average number of fibers only > 0.1 mm. = 3,200,000 fibers/g.

Fiber length distributions for the two samples are shown in Fig. 20 and 21.

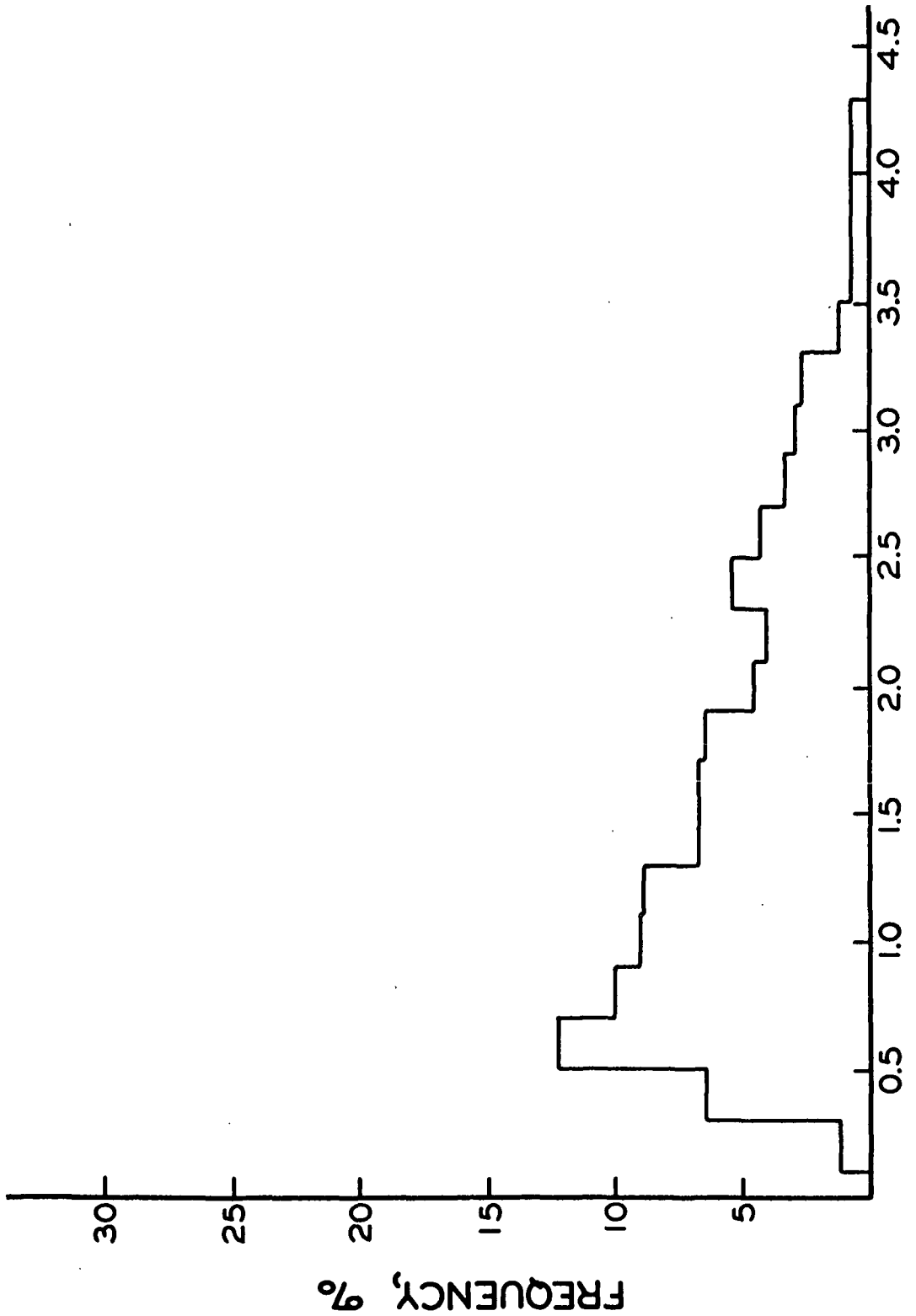

Figure 20. Length Distribution of Sample 2

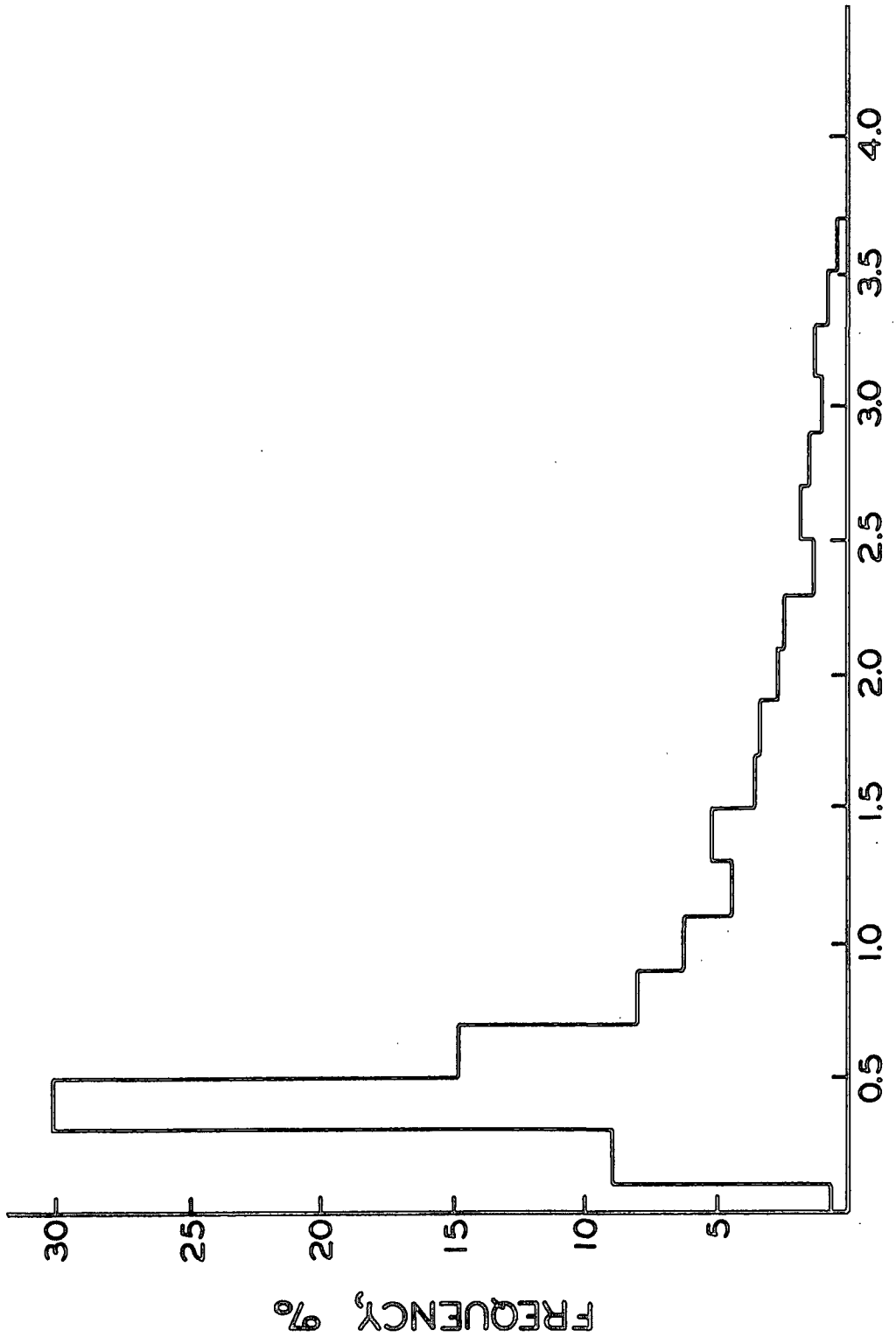

Figure 21. Length Distribution of Sample 2578

APPENDIX II

VELOCITY PROFILE DATA

All pressure drops reported here are in cm. CCl_4/H_2O. Station positions are reported in inches as read on the scale on the probe mounting assembly. Tube center line position ($\underline{\ell}$) is reported for each profile, along with flow rate ($\underline{Q}$), fiber identification, consistency (Γ), and static pressure drop ($\Delta\underline{h}_s$), in cm. CCl_4/H_2O. The distance between static pressure taps is 224 cm. for the 1.875-in. i.d. tube and 226.5 cm. for the 1.400-in. i.d. tube.

Sufficient information is provided herein to allow the reader to perform all the calculations regarding velocity profiles which are discussed in the text. The data are reported in Table VIII.

TABLE VIII

VELOCITY PROFILE DATA

Γ = 0.00 $\Delta\underline{h}_s$ = 8.8 cm.

$\underline{Q}$ = 0.0630 ft.^{3} sec.$^{-1}$

$\underline{D}$ = 1.875 in. $\underline{\ell}$ = 1.43 in.

Station	$\Delta\underline{h}_i$
0.56	6.7
0.58	7.0
0.75	9.0
0.88	10.3
1.00	11.4
1.25	11.8
1.38	11.8
1.50	12.0
1.63	11.7
1.75	11.4
1.88	11.0
2.00	10.0
2.13	8.8
2.25	7.1

Γ = 0.000 $\Delta\underline{h}_s$ = 26.0 cm.

$\underline{Q}$ = 0.1125 ft.^{3} sec.$^{-1}$

$\underline{D}$ = 1.875 in. $\underline{\ell}$ = 1.72 in.

Station	$\Delta\underline{h}_i$
0.84	20.5
0.88	22.7
1.00	29.0
1.13	33.6
1.25	37.0
1.38	39.0
1.50	40.0
1.63	40.3
1.75	40.4
1.88	40.6
2.00	40.3
2.13	39.0
2.25	36.3
2.38	32.1
2.50	25.8

TABLE VIII (Continued)

VELOCITY PROFILE DATA

Γ = 0.00 Δh_s = 12.25 cm.

Q = 0.0350 ft.^{3} sec.$^{-1}$

D = 1.400 in. ℄ = 1.37 in.

Station	Δh_i
0.76	7.15
0.81	8.2
0.88	9.0
1.00	10.6
1.13	11.5
1.25	12.3
1.38	12.65
1.50	12.5
1.63	11.8
1.75	10.5
1.88	8.9
1.94	7.95
2.00	6.6

Γ = 0.00 Δh_s = 32.2

Q = 0.0600 ft.^{3} sec.$^{-1}$

D = 1.400 in. ℄ = 1.37 in.

Station	Δh_i
0.76	2.60
0.88	3.45
1.00	4.10
1.13	4.65
1.25	5.05
1.38	5.3
1.50	4.80
1.63	4.40
1.75	3.85
1.88	3.15
1.94	2.75
2.00	2.25

Γ = 0.00 Δh_s = 5.3 cm.

Q = 0.0217 ft.^{3} sec.$^{-1}$

D = 1.400 in. ℄ = 1.37 in.

Station	Δh_i
0.76	2.60
0.88	3.45
1.00	4.10
1.13	4.65
1.25	5.05
1.38	5.30
1.50	4.80
1.63	4.40
1.75	3.85
1.88	3.15
1.94	2.75
2.00	2.25

Γ = 0.00 Δh_s = 49.7 cm.

Q = 0.0770 ft.^{3} sec.$^{-1}$

D = 1.400 in. ℄ = 1.37 in.

Station	Δh_i
0.76	6.61
0.81	7.11
0.88	7.53
1.00	8.06
1.13	8.30
1.25	8.45
1.38	8.48
1.50	8.46
1.63	8.30
1.75	7.91
1.88	7.22
1.94	6.83
2.00	6.20

TABLE VIII (Continued)

VELOCITY PROFILE DATA

Γ = 0.00 Δh_s = 5.3 cm.

Q = 0.0217 ft.^{3} sec.$^{-1}$

D = 1.400 in. ϕ = 1.37 in.

Station	Δh_i
0.76	2.60
0.88	3.45
1.00	4.10
1.13	4.65
1.25	5.05
1.38	5.30
1.50	4.80
1.63	4.40
1.75	3.85
1.88	3.15
1.94	2.75
2.00	2.25

Γ = 0.00 Δh_s = 49.7 cm.

Q = 0.0770 ft.^{3} sec.$^{-1}$

D = 1.400 in. ϕ = 1.37 in.

Station	Δh_i
0.76	6.61
0.81	7.11
0.88	7.53
1.00	8.06
1.13	8.30
1.25	8.45
1.38	8.48
1.50	8.46
1.63	8.30
1.75	7.91
1.88	7.22
1.94	6.83
2.00	6.20

Sample 2578

Γ = 0.0995 Δh_s = 3.45

Q = 0.0407 ft.^{3} sec.$^{-1}$

D = 1.875 in. ϕ = 1.43 in.

Station	Δh_i
0.54	2.50
1.38	5.65
1.50	5.65
1.63	5.45
1.75	5.20
1.88	4.70
2.00	4.20
2.13	3.45
2.25	2.70

Sample 2578

Γ = 0.0995 Δh_s = 7.8

Q = 0.0610 ft.^{3} sec.$^{-1}$

D = 1.875 in. ϕ = 1.42 in.

Station	Δh_i
0.54	5.8
0.75	9.4
1.00	11.4
1.38	12.2
1.50	12.1
1.63	11.8
1.75	11.4
1.88	10.6
2.00	9.4
2.13	8.1
2.25	6.0

TABLE VIII (Continued)

VELOCITY PROFILE DATA

Sample 2578

Γ = 0.0995 Δh_s = 13.4 cm.

Q = 0.0822 ft.^{3} sec.$^{-1}$

D = 1.875 in. $\mathcal{L}$ = 1.42 in.

Station	Δh_i
0.54	10.5
1.38	21.4
1.50	21.4
1.63	21.0
1.75	20.3
1.88	18.9
2.00	17.3
2.13	14.5
2.25	11.4

Sample 2578

Γ = 0.0995 Δh_s = 16.0 cm.

Q = 0.0907 ft.^{3} sec.$^{-1}$

D = 1.875 in. $\mathcal{L}$ = 1.42 in.

Station	Δh_i
0.54	13.4
1.00	24.5
1.38	26.3
1.50	26.1
1.63	25.8
1.75	24.9
1.88	23.3
2.00	20.9
2.13	18.2
2.25	14.5

Sample 2578

Γ = 0.0995 Δh_s = 27.5 cm.

Q = 0.123 ft.^{3} sec.$^{-1}$

D = 1.875 in. $\mathcal{L}$ = 1.42 in.

Station	Δh_i
0.54	22.9
1.38	45.7
1.50	45.5
1.63	45.0
1.75	43.8
1.88	41.1
2.00	37.3
2.13	32.2
2.25	25.7

Sample 2578

Γ = 0.0995 Δh_s = 36.2 cm.

Q = 0.1415 ft.^{3} sec.$^{-1}$

D = 1.875 in. $\mathcal{L}$ = 1.42 in.

Station	Δh_i
0.54	31.7
1.38	61.2
1.50	61.0
1.63	60.6
1.75	59.0
1.88	55.8
2.00	50.7
2.13	44.1
2.25	34.8

TABLE VIII (Continued)

VELOCITY PROFILE DATA

Sample 2578

Γ = 0.157 g./100 ml.; Δh_s = 1.00 cm.

Q = 0.0227 ft.^{3} sec.$^{-1}$

D = 1.875 in. $\mathbb{C}$ = 1.42 in.

Station	Δh_i
0.58	0.97
1.25	1.27
1.50	1.27
1.75	1.27
2.00	1.27
2.25	1.03

Sample 2578

Γ = 0.157 g./100 ml.; Δh_s = 1.3 cm.

Q = 0.0270 ft.^{3} sec.$^{-1}$

D = 1.875 in. $\mathbb{C}$ = 1.42 in.

Station	Δh_i
1.50	2.1
1.75	2.0
2.00	1.55

Sample 2578

Γ = 0.157 g./100 ml.; Δh_s = 2.6 cm.

Q = 0.0350 ft.^{3} sec.$^{-1}$

D = 1.875 in. $\mathbb{C}$ = 1.42 in.

Station	Δh_i
0.58	1.75
0.75	2.45
0.88	2.8
1.00	3.2
1.25	3.55
1.38	4.00
1.50	4.20
1.63	3.60
1.88	3.10
2.00	2.65
2.13	2.10
2.25	1.70

Sample 2578

Γ = 0.157 g./100 ml.; Δh_s = 8.2 cm.

Q = 0.0661 ft.^{3} sec.$^{-1}$

D = 1.875 in. $\mathbb{C}$ = 1.42 in.

Station	Δh_i
0.56	6.3
0.63	7.4
0.75	9.3
0.88	11.4
1.00	12.3
1.13	12.8
1.25	13.2
1.38	13.3
1.50	13.1
1.63	12.7
1.75	12.1
1.88	10.8
2.00	9.6
2.13	8.7
2.25	6.3

TABLE VIII (Continued)

VELOCITY PROFILE DATA

Sample 2578

Γ = 0.157 g./100 ml.; Δh_s = 25.7 cm.

Q = 0.115 ft.^{3} sec.$^{-1}$

D = 1.875 in. $\mathbb{C}$ = 1.42 in.

Station	Δh_i
0.56	20.8
0.63	25.1
0.75	29.9
1.00	36.2
1.25	38.6
1.38	39.5
1.50	39.7
1.75	38.2
2.00	34.2
2.13	30.1
2.25	25.4

Sample 2578

Γ = 0.157 g./100 ml.; Δh_s = 36.3 cm.

Q = 0.1365 ft.^{3} sec.$^{-1}$

D = 1.875 in. $\mathbb{C}$ = 1.42 in.

Station	Δh_i
0.56	33.2
0.63	37.9
0.75	44.2
0.88	49.0
1.13	53.5
1.38	54.6
1.50	54.7
1.75	52.9
2.00	45.3
2.25	35.5

Sample 2578

Γ = 0.313 g./100 ml.; Δh_s = 1.2 cm.

Q = 0.0277 ft.^{3} sec.$^{-1}$

D = 1.875 in. $\mathbb{C}$ = 1.42 in.

Station	Δh_i
0.56	2.7
0.75	3.2
1.00	3.3
1.25	3.4
1.50	3.7
1.75	3.6
2.00	3.4
2.13	3.3
2.25	2.2

Sample 2578

Γ = 0.313 g./100 ml.; Δh_s = 5.5 cm.

Q = 0.0595 ft.^{3} sec.$^{-1}$

D = 1.875 in. $\mathbb{C}$ = 1.42 in.

Station	Δh_i
0.56	7.4
1.00	11.6
1.13	11.6
1.38	11.9
1.44	12.0
1.50	11.9
1.75	11.7
1.88	11.3
2.00	10.0
2.13	7.7
2.25	6.5

TABLE VIII (Continued)

VELOCITY PROFILE DATA

Sample 2578

Γ = 0.313 g./100 ml.; Δh_s = 8.1 cm.

Q = 0.0700 ft.^{3} sec.$^{-1}$

D = 1.875 in. $\mathcal{L}$ = 1.42 in.

Station	Δh_i
1.50	15.3
1.75	14.9
2.00	12.2
2.13	10.2
2.25	7.9

Sample 2578

Γ = 0.313 g./100 ml.; Δh_s = 20.6 cm.

Q = 0.111 ft.^{3} sec.$^{-1}$

D = 1.875 in. $\mathcal{L}$ = 1.42 in.

Station	Δh_i
0.53	17.6
0.63	21.1
0.88	29.8
1.13	33.7
1.38	34.7
1.44	35.1
1.50	34.4
1.75	32.0
2.00	25.8
2.13	22.0
2.25	15.9

Sample 2578

Γ = 0.313 g./100 ml.; Δh_s = 35.0 cm.

Q = 0.147 ft.^{3} sec.$^{-1}$

D = 1.875 in. $\mathcal{L}$ = 1.42 in.

Station	Δh_i
1.44	60.6
1.50	60.2
1.75	58.2
1.88	54.3
2.00	50.9
2.13	44.8
2.25	38.2

Sample 2578

Γ = 0.313 g./100 ml.; Δh_s = 14.1 cm.

Q = 0.092 ft.^{3} sec.$^{-1}$

D = 1.875 in. $\mathcal{L}$ = 1.42 in.

Station	Δh_i
1.44	25.0
1.50	24.3
1.75	22.7
2.00	18.8
2.13	16.7
2.25	12.5

TABLE VIII (Continued)

VELOCITY PROFILE DATA

Sample 2578

Γ = 0.585 g./100 ml.; Δh_s = 13.3 cm.

Q = 0.0975 ft.^{3} sec.$^{-1}$

D = 1.875 in. $\mathcal{C}$ = 1.42 in.

Station	Δh_i
0.54	13.4
0.62	18.4
0.75	24.8
0.88	27.0
1.00	27.6
1.13	27.6
1.25	27.6
1.38	27.7
1.50	27.6
1.75	27.8
2.00	26.8
2.13	22.3
2.25	15.5

Sample 2578

Γ = 0.585 g./100 ml.; Δh_s = 20.5 cm.

Q = 0.123 ft.^{3} sec.$^{-1}$

D = 1.875 in. $\mathcal{C}$ = 1.42 in.

Station	Δh_i
0.54	21.3
0.56	22.1
0.63	30.2
0.75	37.5
0.88	41.3
1.00	43.8
1.13	45.6
1.25	46.2
1.38	46.2
1.50	46.2
1.68	44.0
2.25	24.2

Sample 2578

Γ = 0.585 g./100 ml.; Δh_s = 6.3 cm.

Q = 0.0630 ft.^{3} sec.$^{-1}$

D = 1.875 in. $\mathcal{C}$ = 1.42 in.

Station	Δh_i
0.63	7.6
0.75	8.9
1.25	9.3
1.38	9.3
1.50	9.5
1.75	9.4
2.00	9.2
2.13	8.6
2.25	6.8

Sample 2578

Γ = 0.585 g./100 ml.; Δh_s = 28.0 cm.

Q = 0.145 ft.^{3} sec.$^{-1}$

D = 1.875 in. $\mathcal{C}$ = 1.42 in.

Station	Δh_i
1.38	61.0
1.50	60.5
1.63	59.9
1.75	58.6
1.88	55.4
2.00	50.2
2.13	42.1
2.25	32.5

TABLE VIII (Continued)

VELOCITY PROFILE DATA

Sample 2578

Γ = 0.100 g./100 ml.; Δh_s = 3.6 cm.

Q = 0.0199 ft.^{3} sec.$^{-1}$

D = 1.400 in. ϕ = 1.37 in.

Station	Δh_i
0.76	1.82
0.81	2.25
0.88	2.68
1.00	3.22
1.13	3.65
1.25	3.95
1.38	4.08
1.50	3.90
1.94	2.05
2.00	1.58

Sample 2578

Γ = 0.100 g./100 ml.; Δh_s = 7.3 cm.

Q = 0.0285 ft.^{3} sec.$^{-1}$

D = 1.400 in. ϕ = 1.37 in.

Station	Δh_i
0.76	4.15
0.81	4.80
0.88	5.55
1.00	6.6
1.13	7.4
1.25	7.9
1.38	8.1
2.00	3.65

Sample 2578

Γ = 0.100 g./100 ml.; Δh_s = 11.0 cm.

Q = 0.0350 ft.^{3} sec.$^{-1}$

D = 1.400 in. ϕ = 1.37 in.

Station	Δh_i
0.76	6.8
0.81	8.0
0.88	9.1
1.00	10.5
1.13	11.6
1.25	12.15
1.38	12.4
1.50	12.05
1.63	11.4
1.75	10.1
1.88	8.4
1.94	7.35
2.00	5.5

Sample 2578

Γ = 0.100 g./100 ml.; Δh_s = 44.3 cm.

Q = 0.0465 ft.^{3} sec.$^{-1}$

D = 1.400 in. ϕ = 1.37 in.

Station	Δh_i
0.76	11.8
0.81	13.9
0.88	15.6
1.00	18.2
1.13	20.2
1.25	21.1
1.38	21.7
1.50	21.1
1.63	19.9
1.75	17.9
1.88	15.2
1.94	13.6
2.00	10.6

TABLE VIII (Continued)

VELOCITY PROFILE DATA

Sample 2578

Γ = 0.100 g./100 ml.; Δh_s = 30.0 cm.

Q = 0.0590 ft.^{3} sec.$^{-1}$

D = 1.400 in. ℄ = 1.37 in.

Station	Δh_i
0.76	20.1
0.81	23.7
0.88	26.2
1.00	30.2
1.13	32.5
1.25	34.4
1.38	34.9
1.50	34.4
1.63	32.4
1.75	29.4
1.88	24.6
1.94	22.0
2.00	17.7

Sample 2578

Γ = 0.100 g./100 ml.; Δh_s = 44.3 cm.

Q = 0.0720 ft.^{3} sec.$^{-1}$

D = 1.400 in. ℄ = 1.37 in.

Station	Δh_i
0.76	29.8
0.81	34.9
0.88	39.0
1.00	44.9
1.13	48.8
1.25	50.5
1.38	51.3
1.50	50.5
1.63	48.4
1.75	44.0
1.88	37.3
1.94	33.3
2.00	25.8

Sample 2578

Γ = 0.208 g./100 ml.; Δh_s = 5.30 cm.

Q = 0.0255 ft.^{3} sec.$^{-1}$

D = 1.400 in. ℄ = 1.37 in.

Station	Δh_i
0.76	2.95
0.81	3.70
0.88	4.35
1.00	5.25
1.13	5.88
1.25	6.25
1.38	6.35
1.50	6.20

Sample 2578

Γ = 0.208 g./100 ml.; Δh_s = 13.0

Q = 0.0398 ft.^{3} sec.$^{-1}$

D = 1.400 in. ℄ = 1.37 in.

Station	Δh_i
0.76	8.4
0.81	10.4
0.88	11.9
1.00	14.3
1.13	15.9
1.25	16.8
1.38	17.4
1.50	16.5

TABLE VIII (Continued)

VELOCITY PROFILE DATA

Sample 2578

Γ = 0.208 g./100 ml.; Δh_s = 19.3 cm.

Q = 0.0480 ft.^{3} sec.$^{-1}$

D = 1.400 in. ϕ = 1.37 in.

Station	Δh_i
0.76	12.6
0.81	15.4
0.88	17.3
1.00	21.0
1.13	23.0
1.25	24.1
1.38	24.8

Sample 2578

Γ = 0.208 g./100 ml.; Δh_s = 29.5 cm.

Q = 0.0615 ft.^{3} sec.$^{-1}$

D = 1.400 in. ϕ = 1.37 in.

Station	Δh_i
0.76	20.2
0.81	24.5
0.88	27.6
1.00	32.0
1.13	35.4
1.25	37.1
1.38	37.9
1.50	37.2
1.75	31.5
1.88	26.3
1.94	22.1
2.00	18.3

Sample 2578

Γ = 0.208 g./100 ml.; Δh_s = 50.0 cm.

Q = 0.0795 ft.^{3} sec.$^{-1}$

D = 1.400 in. ϕ = 1.37 in.

Station	Δh_i
0.76	33.6
0.81	40.2
0.88	44.8
1.00	51.9
1.13	56.0
1.25	57.8
1.38	58.8
1.50	57.8

Sample 2578

Γ = 0.208 g./100 ml.; Δh_s = 78.2 cm.

Q = 0.1005 ft.^{3} sec.$^{-1}$

D = 1.400 in. ϕ = 1.37 in.

Station	Δh_i
0.76	54.4
0.81	64.4
0.88	70.5
1.00	76.9
1.13	78.9
1.25	80.0
1.38	81.3
0.94	74.2

TABLE VIII (Continued)

VELOCITY PROFILE DATA

Sample 2

Γ = 0.112 g./100 ml.; Δh_s = 3.05 cm.

Q = 0.0380 ft.^{3} sec.$^{-1}$

D = 1.875 in. $\mathcal{C}$ = 1.60 in.

Station	Δh_i
1.50	5.50
1.63	5.55
1.75	5.30
1.88	4.90
2.00	4.65
2.13	4.30
2.25	3.70
2.38	3.30
2.45	2.20

Sample 2

Γ = 0.112 g./100 ml.; Δh_s = 6.88 cm.

Q = 0.0590 ft.^{3} sec.$^{-1}$

D = 1.875 in. $\mathcal{C}$ = 1.60 in.

Station	Δh_i
0.75	5.8
0.88	7.75
1.00	8.9
1.25	10.9
1.50	11.5
1.63	11.5
1.75	11.3
1.88	10.0
2.00	10.6
2.13	9.75
2.25	8.7
2.38	7.4
2.45	5.9

Sample 2

Γ = 0.112 g./100 ml.; Δh_s = 10.95 cm.

Q = 0.0745 ft.^{3} sec.$^{-1}$

D = 1.875 in. $\mathcal{C}$ = 1.60 in.

Station	Δh_i
0.77	9.4
0.88	12.3
1.00	14.3
1.13	15.8
1.25	17.0
1.38	17.5
1.50	17.7
1.63	17.8
1.75	17.5
1.88	17.0
2.00	16.3
2.13	15.2
2.25	13.7
2.38	11.3
2.45	8.7

Sample 2

Γ = 0.112 g./100 ml.; Δh_s = 15.65 cm.

Q = 0.0905 ft.^{3} sec.$^{-1}$

D = 1.875 in. $\mathcal{C}$ = 1.60 in.

Station	Δh_i
0.75	14.0
0.88	18.2
1.00	20.8
1.13	23.0
1.25	24.5
1.38	25.5
1.50	25.6
1.63	25.7
1.75	25.3
1.88	24.8
2.00	23.9
2.13	22.3
2.25	19.9
2.38	16.8
2.45	13.5

TABLE VIII (Continued)

VELOCITY PROFILE DATA

Sample 2

Γ = 0.112 g./100 ml.; Δh_s = 22.1 cm.

Q = 0.1095 ft.^{3} sec.$^{-1}$

D = 1.875 in. ϕ = 1.60 in.

Station	Δh_i
0.75	20.7
0.88	26.8
1.00	30.8
1.25	36.2
1.50	36.8
1.63	37.2
1.75	36.7
1.88	36.2
2.00	35.0
2.13	32.8
2.25	29.5
2.38	25.2
2.45	19.8

Sample 2

Γ = 0.277 g./100 ml.; Δh_s = 5.35 cm.

Q = 0.0560 ft.^{3} sec.$^{-1}$

D = 1.875 in. ϕ = 1.60 in.

Station	Δh_i
0.76	4.15
0.88	6.45
1.00	8.35
1.13	9.05
1.25	9.25
1.50	9.25
1.75	9.27
2.00	9.25
2.13	8.75
2.25	8.10
2.38	5.40
2.45	3.65

Sample 2

Γ = 0.277 g./100 ml.; Δh_s = 2.78 cm.

Q = 0.0388 ft.^{3} sec.$^{-1}$

D = 1.875 in. ϕ = 1.60 in.

Station	Δh_i
0.75	2.20
0.88	3.30
1.00	4.23
1.25	4.32
1.50	4.32
1.75	4.32
2.00	4.32
2.25	4.20
2.38	2.85
2.45	1.85

Sample 2

Γ = 0.277 g./100 ml.; Δh_s = 9.10 cm.

Q = 0.0740 ft.^{3} sec.$^{-1}$

D = 1.875 in. ϕ = 1.60 in.

Station	Δh_i
0.76	7.9
0.88	10.8
1.00	13.8
1.13	15.8
1.38	17.2
1.50	17.2
2.00	17.0
2.13	15.0
2.45	7.8
1.25	17.0

TABLE VIII (Continued)

VELOCITY PROFILE DATA

Sample 2

Γ = 0.277 g./100 ml.; Δh_s = 13.05 cm.

Q = 0.0900 ft.^{3} sec.$^{-1}$

D = 1.875 in. ℄ = 1.60 in.

Station	Δh_i
1.25	24.6
1.38	25.9
1.50	26.3
1.63	26.4
1.75	26.4
1.44	26.3
1.88	26.0
2.00	25.0
2.13	23.2
2.25	20.1
2.38	16.2
2.45	12.2

Sample 2

Γ = 0.277 g./100 ml.; Δh_s = 19.65 cm.

Q = 0.112 ft.^{3} sec.$^{-1}$

D = 1.875 in. ℄ = 1.60 in.

Station	Δh_i
0.76	19.8
0.88	26.2
1.00	30.6
1.13	34.3
1.25	36.8
1.38	38.2
1.50	39.7
1.63	40.0
1.75	39.7
1.88	39.1
2.00	36.4
2.13	34.6
2.25	31.0
2.38	25.3
2.45	20.1

Sample 2

Γ = 0.277 g./100 ml.; Δh_s = 28.4 cm.

Q = 0.135 ft.^{3} sec.$^{-1}$

D = 1.875 in. ℄ = 1.60 in.

Station	Δh_i
0.76	25.8
0.88	32.7
1.00	37.5
1.13	41.0
1.25	43.9
1.38	45.0
1.50	46.3
1.63	46.3
2.00	43.9
2.13	40.2
2.25	36.6
2.38	32.7
2.45	24.5

Sample 2

Γ = 0.0636 g./100 ml.; Δh_s = 1.80 cm.

Q = 0.0135 ft.^{3} sec.$^{-1}$

D = 1.400 in. ℄ = 1.37 in.

Station	Δh_i
0.76	0.83
0.81	1.15
0.88	1.40
1.00	1.68
1.13	1.85
1.25	2.08
1.38	2.15

TABLE VIII (Continued)

VELOCITY PROFILE DATA

Sample 2

Γ = 0.0636 g./100 ml.; Δh_s = 5.7 cm.

Q = 0.0240 ft.^{3} sec.$^{-1}$

D = 1.400 in. ϕ = 1.37 in.

Station	Δh_i
0.76	3.30
0.81	3.85
0.88	4.42
1.00	5.10
1.13	5.53
1.25	5.80
1.38	6.20

Sample 2

Γ = 0.0636 g./100 ml.; Δh_s = 14.9 cm.

Q = 0.0395 ft.^{3} sec.$^{-1}$

D = 1.400 in. ϕ = 1.37 in.

Station	Δh_i
0.76	8.7
0.81	10.3
0.88	11.5
1.00	13.7
1.13	15.0
1.25	15.7
1.38	16.4
1.50	15.7

Sample 2

Γ = 0.0636 g./100 ml.; Δh_s = 34.4 cm.

Q = 0.0630 ft.^{3} sec.$^{-1}$

D = 1.400 in. ϕ = 1.37 in.

Station	Δh_i
0.76	22.0
0.81	25.7
0.88	29.6
1.00	34.5
1.13	37.4
1.25	38.8
1.38	39.5
1.50	39.0

Sample 2

Γ = 0.124 g./100 ml.; Δh_s = 26.3 cm.

Q = 0.0555 ft.^{3} sec.$^{-1}$

D = 1.400 in. ϕ = 1.37 in.

Station	Δh_i
1.38	30.4
1.50	30.2
1.63	29.2
1.75	26.8
1.88	23.5
1.94	21.2
2.00	17.9

TABLE VIII (Continued)

VELOCITY PROFILE DATA

Sample 2

Γ = 0.124 g./100 ml.; Δh_s = 16.6 cm.

Q = 0.0435 ft.^{3} sec.$^{-1}$

D = 1.400 in. $\mathcal{L}$ = 1.37 in.

Station	Δh_i
0.77	11.1
0.81	12.1
0.88	14.0
1.00	16.4
1.13	17.8
1.25	18.5
1.38	18.8
1.50	18.5
1.63	17.7
1.75	16.0
1.88	13.3
2.00	10.6

Sample 2

Γ = 0.124 g./100 ml.; Δh_s = 43.0 cm.

Q = 0.0725 ft.^{3} sec.$^{-1}$

D = 1.400 in. $\mathcal{L}$ = 1.37 in.

Station	Δh_i
1.38	50.0
1.50	49.4
1.63	48.6
1.75	45.0
1.88	39.0
1.94	35.8
2.00	30.8

Sample 2

Γ = 0.124 g./100 ml.; Δh_s = 70.3 cm.

Q = 0.0945 ft.^{3} sec.$^{-1}$

D = 1.400 in. $\mathcal{L}$ = 1.37 in.

Station	Δh_i
1.38	81.7
1.50	81.2
1.63	78.8
1.75	74.0
1.88	65.5
1.94	59.9
2.00	50.6

Sample 2

Γ = 0.273 g./100 ml.; Δh_s = 7.0 cm.

Q = 0.0280 ft.^{3} sec.$^{-1}$

D = 1.400 in. $\mathcal{L}$ = 1.38 in.

Station	Δh_i
1.25	7.8
1.38	7.8
1.50	7.8
1.63	7.8
1.75	7.8
1.88	6.6
1.94	5.6
2.01	4.4
1.81	7.5

TABLE VIII (Continued)

VELOCITY PROFILE DATA

Sample 2

Γ = 0.273 g./100 ml.; Δh_s = 12.2 cm.

Q = 0.0395 ft.^{3} sec.$^{-1}$

D = 1.400 in. $\mathcal{C}$ = 1.38 in.

Station	Δh_i
1.18	15.9
1.25	16.0
1.38	16.0
1.50	16.0
1.63	15.8
1.69	15.4
1.75	14.6
1.88	12.8
1.94	11.1
2.01	8.4

Sample 2

Γ = 0.273 g./100 ml.; Δh_s = 23.4 cm.

Q = 0.0565 ft.^{3} sec.$^{-1}$

D = 1.400 in. $\mathcal{C}$ = 1.38 in.

Station	Δh_i
1.18	31.0
1.25	31.4
1.38	31.7
1.50	31.6
1.56	31.5
1.63	30.7
1.75	28.2
1.88	24.3
1.94	21.6
2.02	16.7

APPENDIX III

REYNOLDS NUMBER-FRICTION FACTOR DATA FOR VARIOUS SUSPENSIONS

This appendix is simply a presentation of the relation between static pressure drop and flow rate at various consistencies. Since tube diameter and the distance between static pressure taps are well known, the data are easily converted to Reynolds number-friction factor tabulations. The viscosity and density of the suspension are taken to be those of pure water at the operating temperature (20°C.). Data for pure water are included for the sake of comparison. Table IX summarizes the results while Fig. 22-31 represent them graphically.

TABLE IX

REYNOLDS NUMBERS AND FRICTION FACTORS FOR VARIOUS SUSPENSIONS

Sample No.	Γ, g./100 ml.	D, inches	Q, ft.^{3} sec.$^{-1}$	Δh_s, cm. CCl_4/H_2O	Re	f
	0.00	1.875	0.0107	0.38	0.814×10^4	7.8×10^{-3}
			0.0165	0.85	1.25×10^4	7.1×10^{-3}
			0.0293	2.30	2.22×10^4	6.32×10^{-3}
			0.0395	3.60	3.00×10^4	5.50×10^{-3}
			0.0560	7.35	4.26×10^4	5.50×10^{-3}
			0.0767	12.5	5.83×10^4	5.00×10^{-3}
			0.108	23.6	9.36×10^5	4.78×10^{-3}
			0.132	33.5	1.14×10^5	4.52×10^{-3}
			0.174	53.7	1.51×10^4	4.18×10^{-3}
		1.400	0.0217	5.3	2.29×10^4	6.12×10^{-3}
			0.0350	12.25	3.67×10^4	5.42×10^{-3}
			0.0507	23.8	5.33×10^4	4.93×10^{-3}
			0.0600	32.2	6.30×10^4	4.88×10^{-3}
			0.0770	49.7	8.09×10^4	4.57×10^{-3}
			0.0810	53.6	8.50×10^4	4.47×10^{-3}
			0.0975	76.9	1.02×10^5	4.41×10^{-3}
			0.120	5.05[a]	1.26×10^5	4.10×10^{-3}
			0.1765	10.3[a]	1.85×10^5	3.86×10^{-3}
			0.231	17.1[a]	2.43×10^5	3.74×10^{-3}

[a] (Hg/H_2O).

TABLE IX (Continued)

REYNOLDS NUMBERS AND FRICTION FACTORS FOR VARIOUS SUSPENSIONS

Sample No.	Γ g./100 ml.	D, inches	Q, ft.^{3} sec.$^{-1}$	Δh_s, cm. CCl_4/H_2O	Re	f
2578	0.0995	1.875	0.0250	1.25	1.97×10^4	4.70×10^{-3}
			0.0407	3.45	3.09×10^4	4.89×10^{-3}
			0.0475	4.7	3.61×10^4	4.88×10^{-3}
			0.0610	7.75	4.63×10^4	4.91×10^{-3}
			0.0822	13.4	6.25×10^4	4.68×10^{-3}
			0.0907	16.05	6.90×10^4	4.58×10^{-3}
			0.123	27.5	9.35×10^4	4.28×10^{-3}
			0.1415	36.2	10.8×10^5	4.26×10^{-3}
			0.199	67.8	1.51×10^5	4.04×10^{-3}
2578	0.157	1.875	0.0227	1.00	1.72×10^4	4.58×10^{-3}
			0.0270	1.3	2.05×10^4	4.25×10^{-3}
			0.035	2.6	2.66×10^4	5.01×10^{-3}
			0.0661	8.2	5.03×10^4	4.40×10^{-3}
			0.115	25.7	8.75×10^4	4.58×10^{-3}
			0.1365	36.3	1.04×10^5	4.58×10^{-3}
2578	0.313	1.875	0.0277	1.2	2.10×10^4	3.68×10^{-3}
			0.0375	2.3	2.85×10^4	3.86×10^{-3}
			0.0595	5.5	4.52×10^4	3.65×10^{-3}
			0.0700	8.1	5.31×10^4	3.89×10^{-3}
			0.111	20.6	8.45×10^4	3.94×10^{-3}
			0.147	35.0	1.12×10^5	3.81×10^{-3}
			0.227	80.7	1.73×10^5	3.67×10^{-3}
2578	0.585	1.875	0.0215	0.4-0.5	1.64×10^4	1.8×10^{-3}
			0.0305	1.3	2.32×10^4	3.3×10^{-3}
			0.0435	3.2	3.3×10^4	4.00×10^{-3}
			0.0630	6.3	4.79×10^4	3.73×10^{-3}
			0.0680	7.1	5.16×10^4	3.62×10^{-3}
			0.0830	10.3	6.30×10^4	3.62×10^{-3}
			0.0975	13.3	7.41×10^4	3.30×10^{-3}
			0.107	18.3	8.12×10^4	3.78×10^{-3}
			0.123	20.5	9.35×10^4	3.20×10^{-3}
			0.145	28.0	1.10×10^5	3.14×10^{-3}
2578	0.100	1.400	0.0199	3.6	2.09×10^4	4.94×10^{-3}
			0.0285	7.3	2.57×10^4	4.89×10^{-3}
			0.0350	11.0	3.68×10^4	4.90×10^{-3}
			0.0465	18.9	4.88×10^4	4.76×10^{-3}
			0.0590	30.0	6.20×10^4	4.71×10^{-3}
			0.0720	44.3	7.55×10^4	4.66×10^{-3}
			0.0865	61.5	9.09×10^4	4.51×10^{-3}
			0.138	6.7[a]	1.45×10^5	4.12×10^{-3}
			0.180	10.9[a]	1.89×10^5	3.94×10^{-3}

[a] cm. Hg.

TABLE IX (Continued)

REYNOLDS NUMBERS AND FRICTION FACTORS FOR VARIOUS SUSPENSIONS

Sample No.	Γ g./100 ml.	D, inches	Q, ft.^{3} sec.$^{-1}$	Δh_s, cm. CCl_4/H_2O	Re	f
2578	0.208	1.400	0.0255	5.30	2.68×10^4	4.42×10^{-3}
			0.0398	13.0	4.18×10^4	4.48×10^{-3}
			0.0480	19.3	5.00×10^4	4.57×10^{-3}
			0.0615	29.5	6.45×10^4	4.26×10^{-3}
			0.0795	50.0	8.35×10^4	4.32×10^{-3}
			0.1005	78.2	1.06×10^5	4.23×10^{-3}
2	0.0636	1.400	0.0135	1.8	1.42×10^4	5.39×10^{-3}
			0.0240	5.7	2.52×10^4	5.39×10^{-3}
			0.0395	14.9	4.15×10^4	5.20×10^{-3}
			0.0630	34.4	6.61×10^4	4.73×10^{-3}
2	0.124	1.400	0.0260	6.2	2.73×10^4	5.00×10^{-3}
			0.0435	16.6	4.57×10^4	4.79×10^{-3}
			0.0555	26.3	5.83×10^4	4.66×10^{-3}
			0.0725	43.0	7.61×10^4	4.49×10^{-3}
			0.0945	70.3	9.92×10^4	4.29×10^{-3}
2	0.273	1.400	0.0280	7.0	2.94×10^4	4.86×10^{-3}
			0.0390	12.2	4.10×10^4	4.32×10^{-3}
			0.0565	23.4	5.94×10^4	4.00×10^{-3}
2	0.112	1.875	0.022	1.03	1.67×10^4	5.00×10^{-3}
			0.0380	3.05	2.89×10^4	4.97×10^{-3}
			0.0410	3.55	3.12×10^4	4.94×10^{-3}
			0.0590	6.88	4.48×10^4	4.65×10^{-3}
			0.0675	9.10	5.13×10^4	4.70×10^{-3}
			0.0745	10.95	5.66×10^4	4.67×10^{-3}
			0.0905	15.65	6.88×10^4	4.50×10^{-3}
			0.0929	16.4	7.05×10^4	4.47×10^{-3}
			0.104	20.8	7.90×10^4	4.52×10^{-3}
			0.1095	22.1	8.34×10^4	4.34×10^{-3}
			0.1285	30.0	9.78×10^4	4.27×10^{-3}
			0.176	52.0	1.34×10^5	3.94×10^{-3}
			0.277	5.7[a]	2.11×10^5	3.70×10^{-3}
2	0.277	1.875	0.0215	0.60	1.64×10^4	3.05×10^{-3}
			0.0335	2.2	2.55×10^4	4.50×10^{-3}
			0.0388	2.78	2.95×10^4	4.36×10^{-3}
			0.0560	5.35	4.26×10^4	4.20×10^{-3}
			0.0740	9.10	5.61×10^4	3.94×10^{-3}
			0.0846	12.0	6.43×10^4	3.95×10^{-3}
			0.0900	13.05	6.85×10^4	3.80×10^{-3}
			0.1045	17.65	7.95×10^4	3.80×10^{-3}
			0.112	19.65	8.51×10^4	3.70×10^{-3}
			0.135	28.4	1.03×10^5	3.67×10^{-3}
			0.149	34.2	1.13×10^5	3.62×10^{-3}
			0.199	62.2	1.51×10^5	3.69×10^{-3}
			0.273	5.4[a]	2.07×10^5	3.66×10^{-3}

[a] cm. Hg.

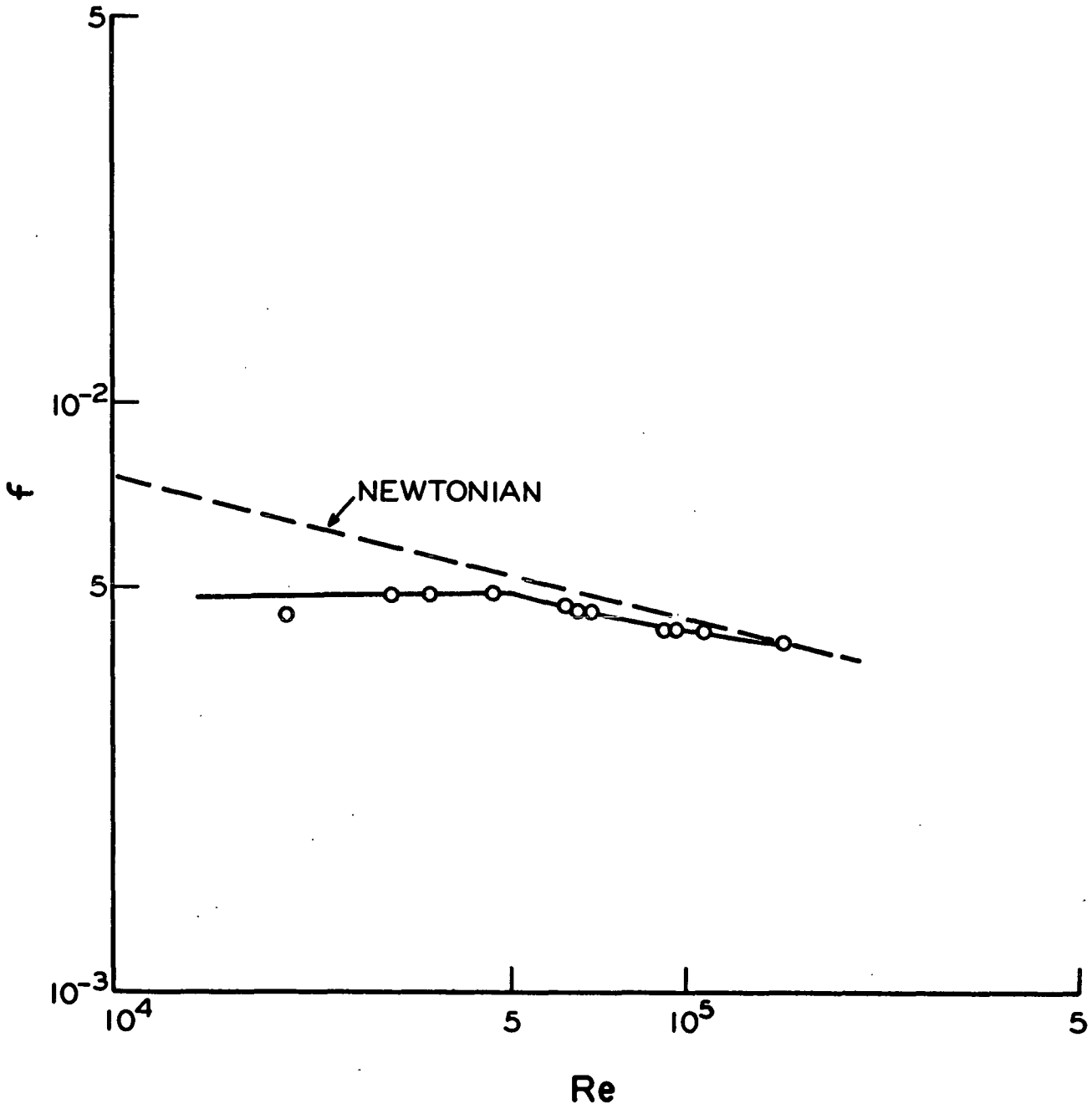

Figure 22. Friction Factor vs. Reynolds Number, Γ = 0.100 g./100 ml. Sample 2578 in 1.875-in. i.d. Tube (20°C.)

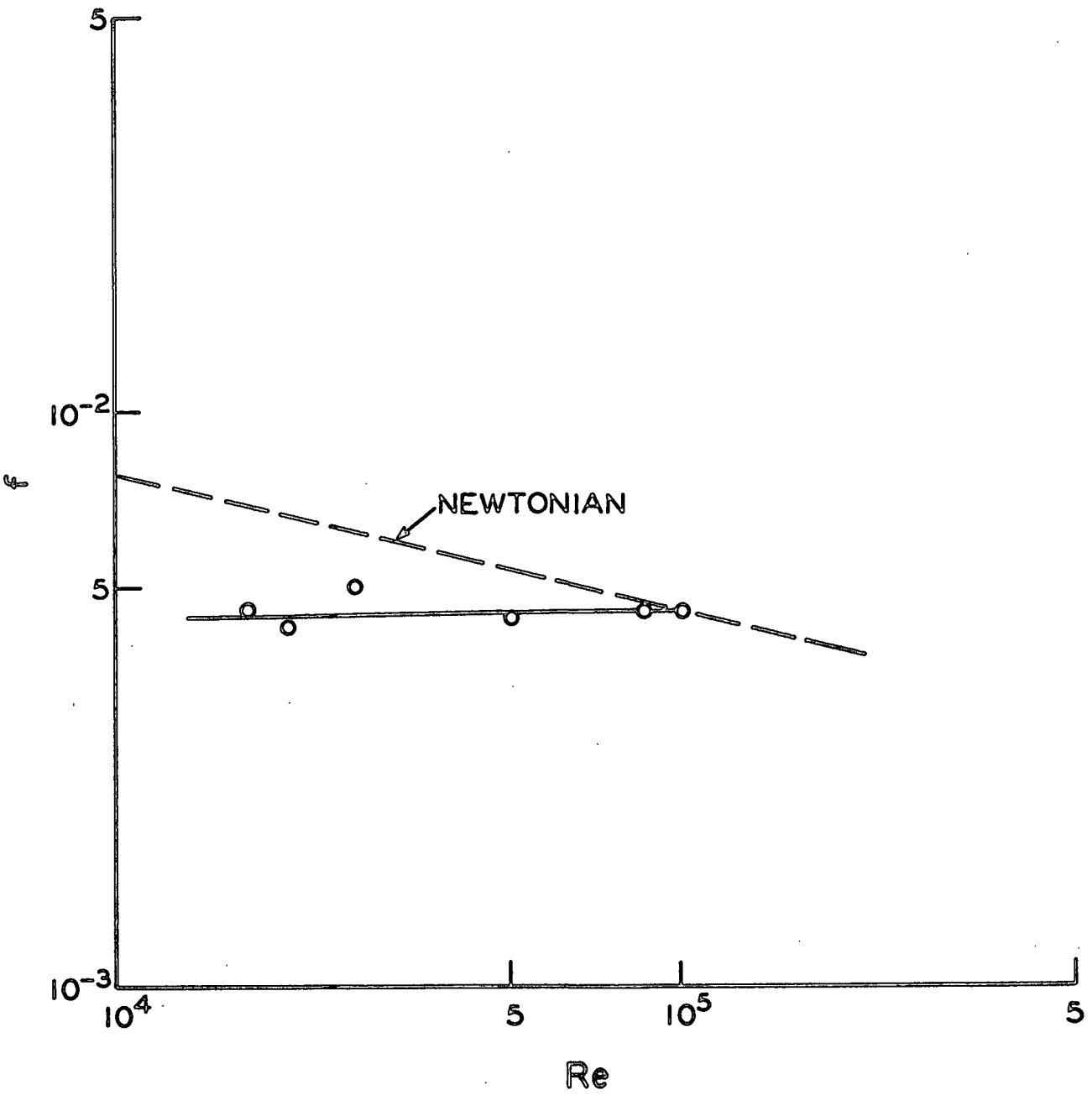

Figure 23. Friction Factor vs. Reynolds Number, Γ = 0.157 g./100 ml. Sample 2578 in 1.875-in. i.d. Tube (20°C.)

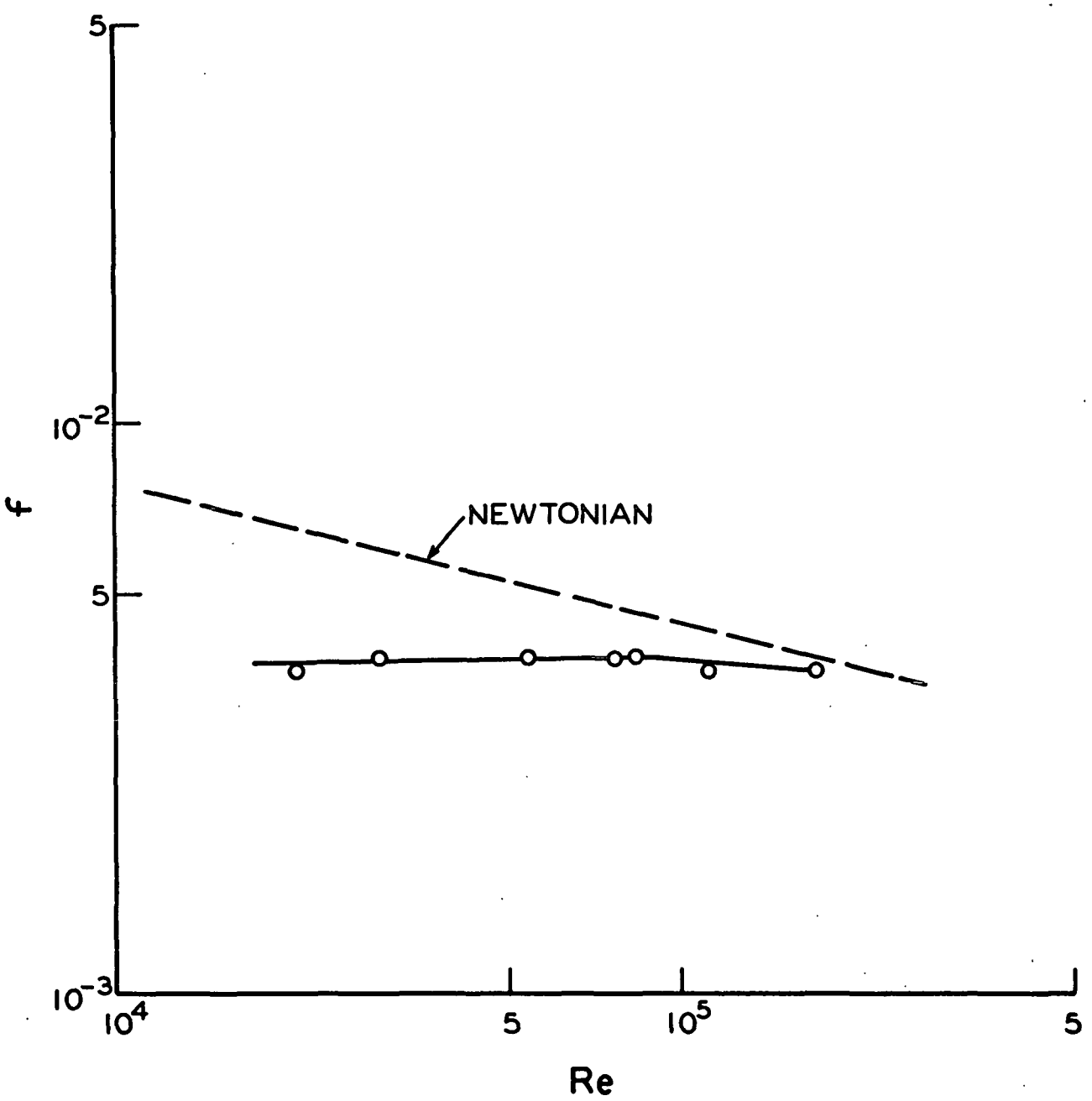

Figure 24. Friction Factor vs. Reynolds Number, Γ = 0.31 g./100 ml. Sample 2578 in 1.875-in. i.d. Tube (20°C.)

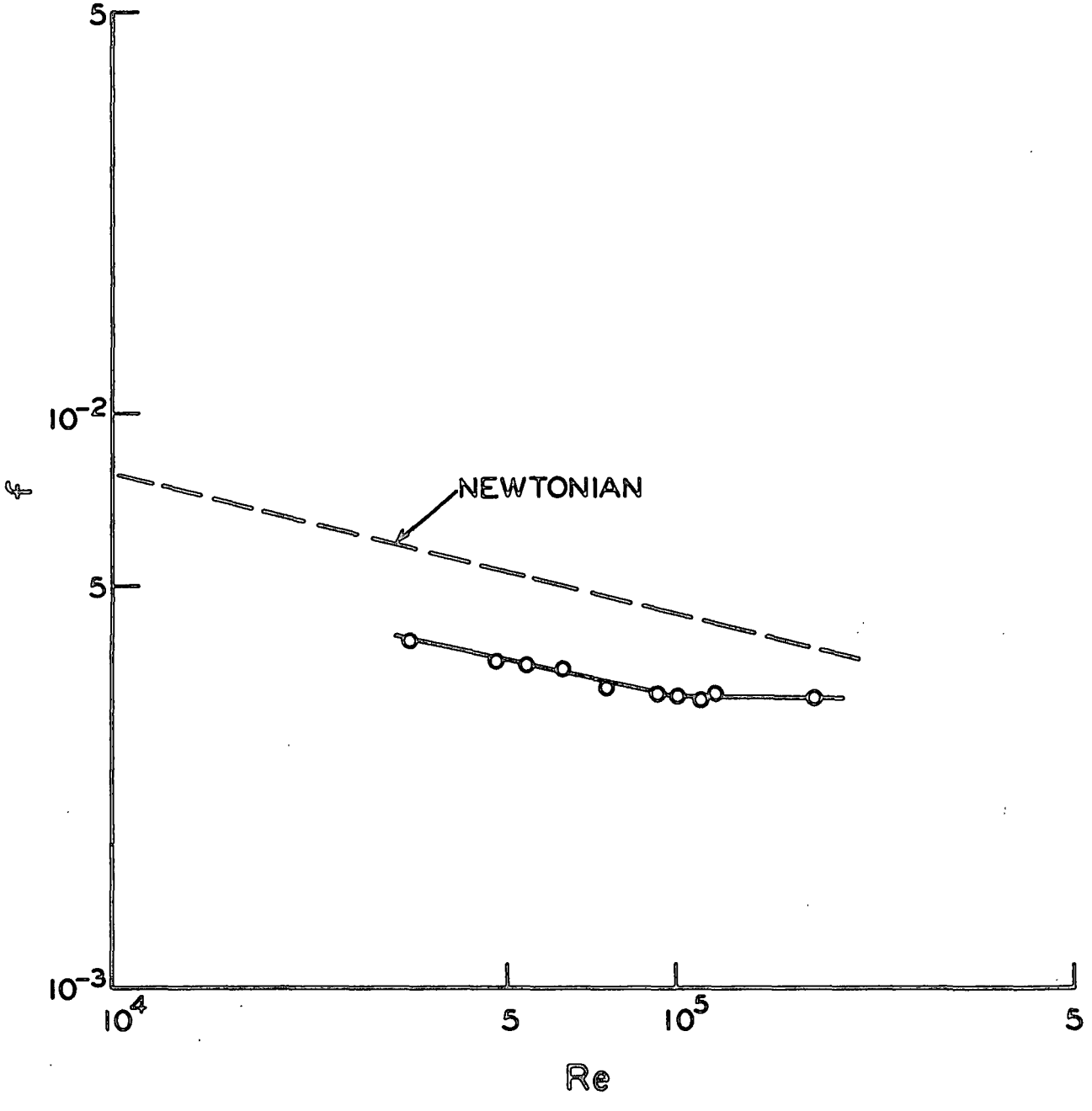

Figure 25. Friction Factor vs. Reynolds Number, Γ = 0.58 g./100 ml. Sample 2578 in 1.875-in. i.d. Tube (20°C.)

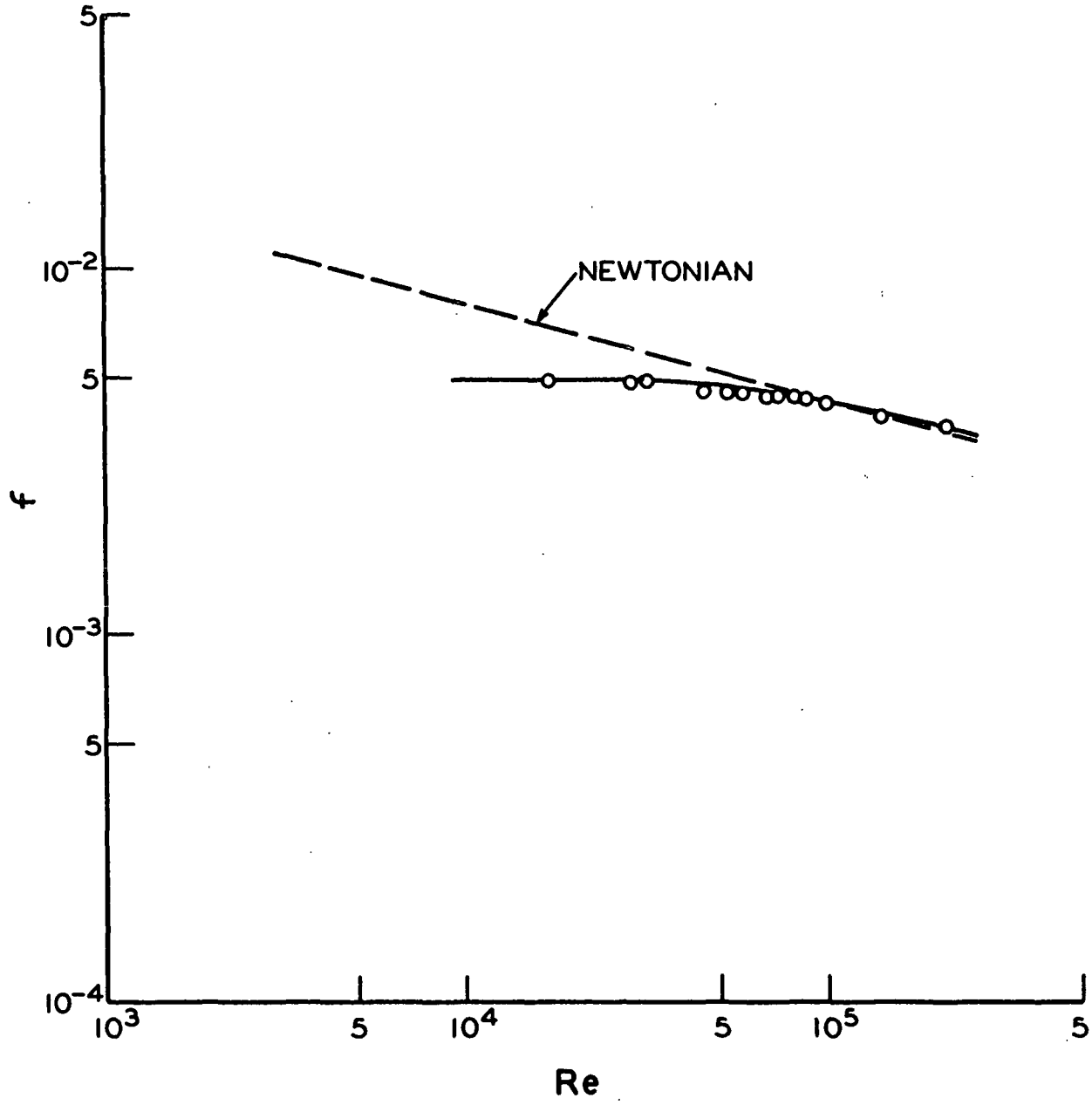

Figure 26. Friction Factor vs. Reynolds Number, Γ = 0.11 g./100 ml. Sample 2 in 1.875-in. i.d. Tube (20°C.)

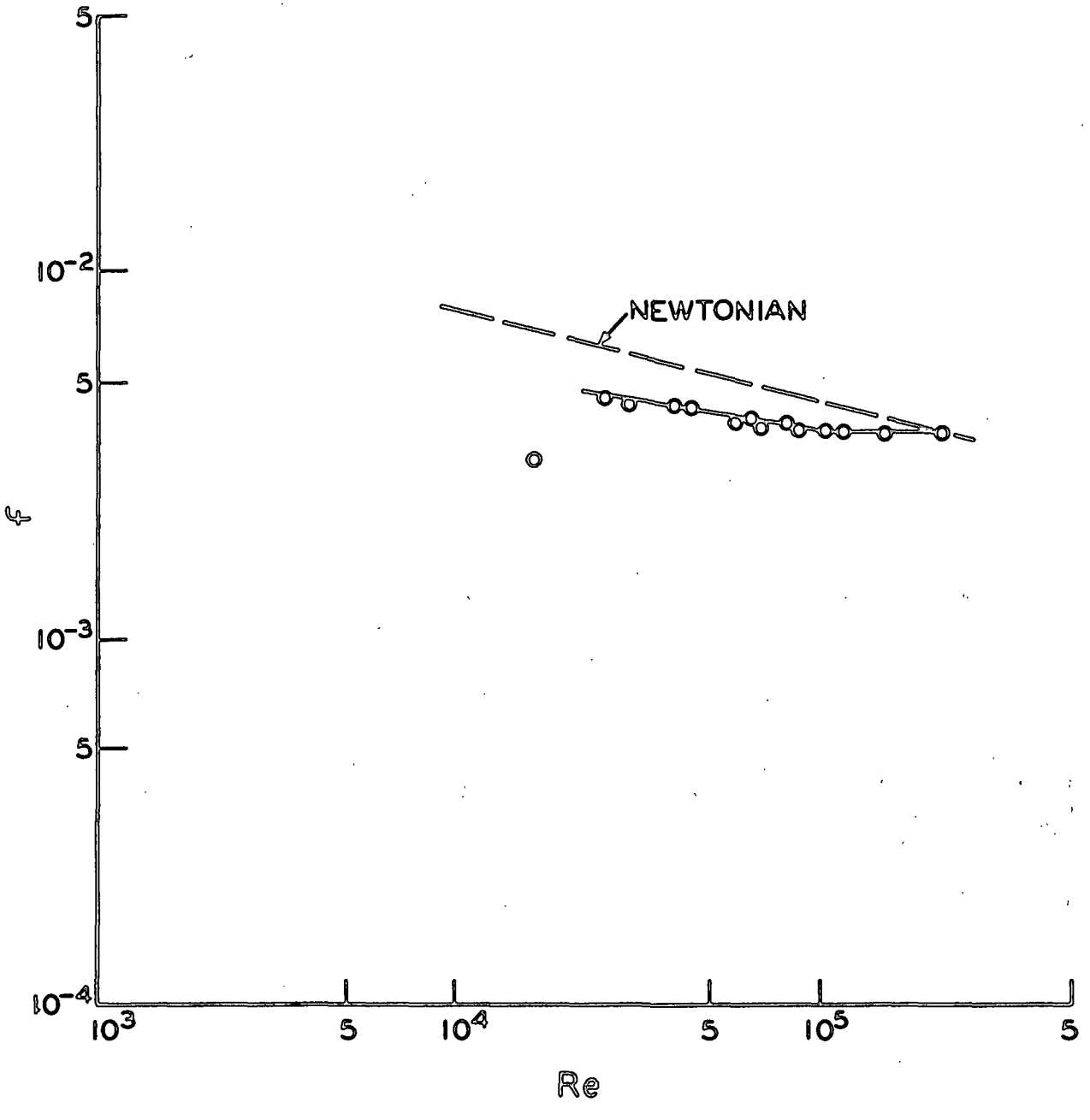

Figure 27. Friction Factor vs. Reynolds Number, Γ = 0.277 g./100 ml. Sample 2 in 1.875-in. i.d. Tube (20°C.)

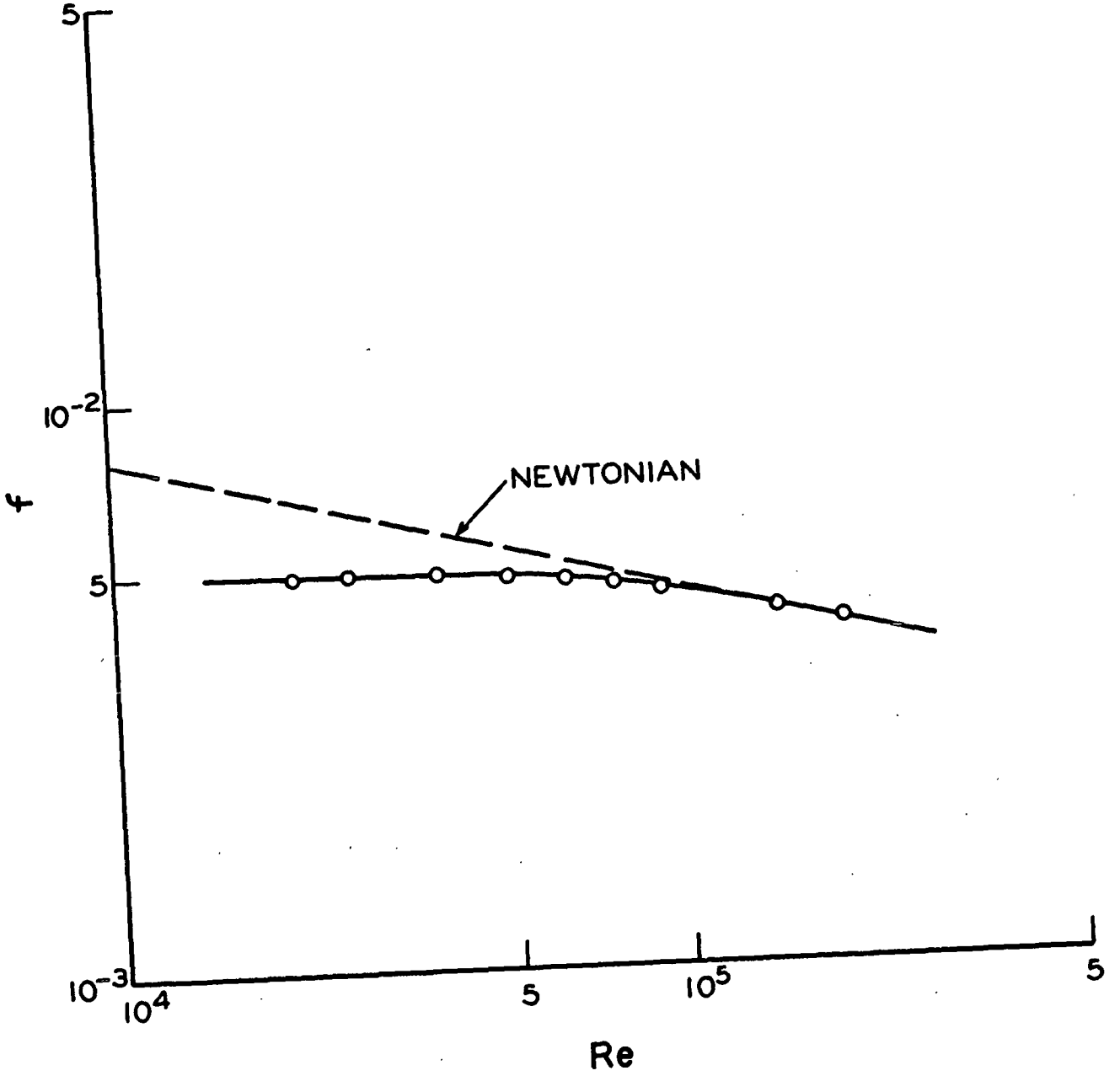

Figure 28. Friction Factor vs. Reynolds Number, Γ = 0.10 g./100 ml. Sample 2578 in 1.400-in. i.d. Tube (20°C.)

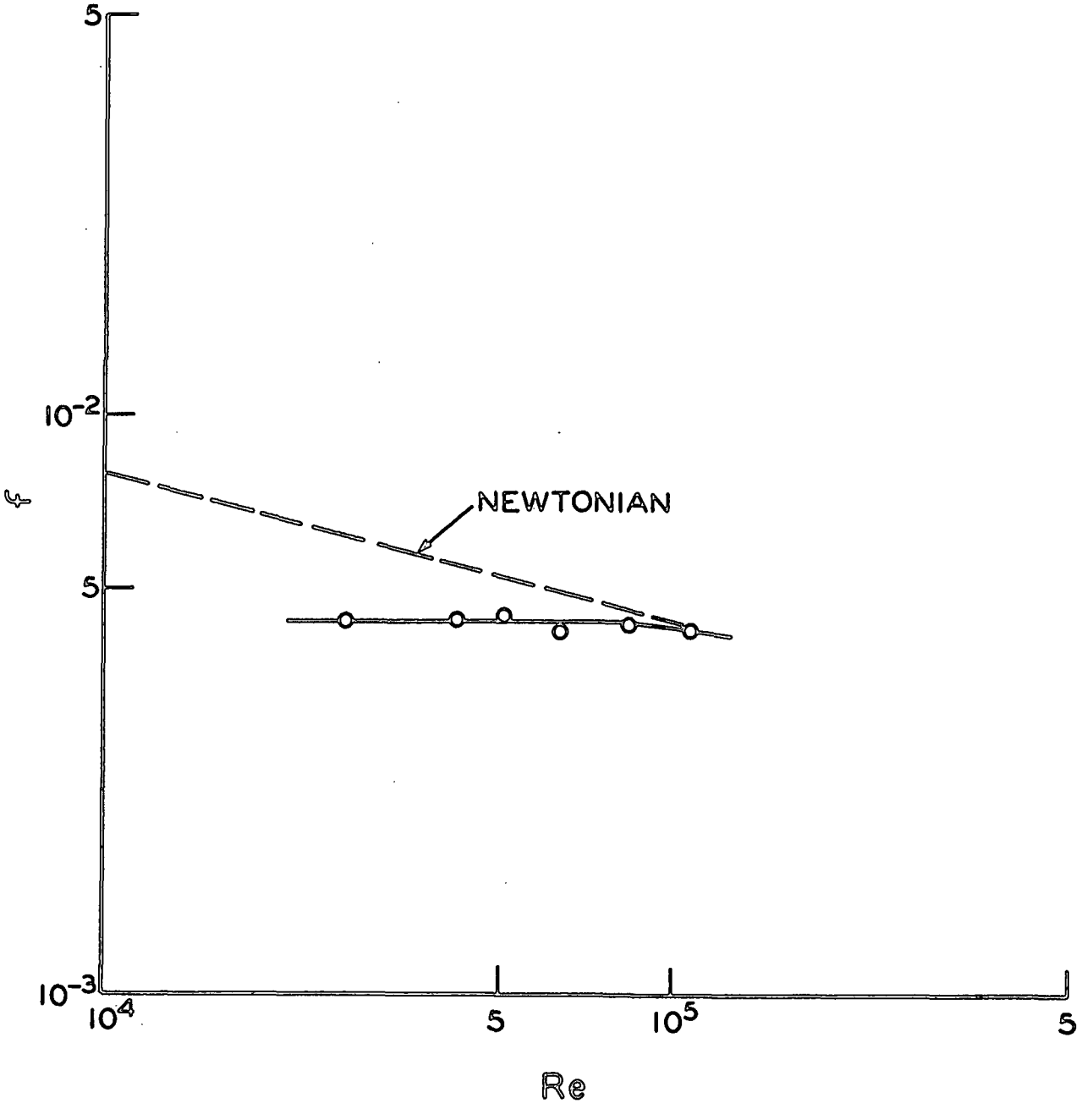

Figure 29. Friction Factor vs. Reynolds Number, Γ = 0.21 g./100 ml. Sample 2578 in 1.400-in. i.d. Tube (20°C.)

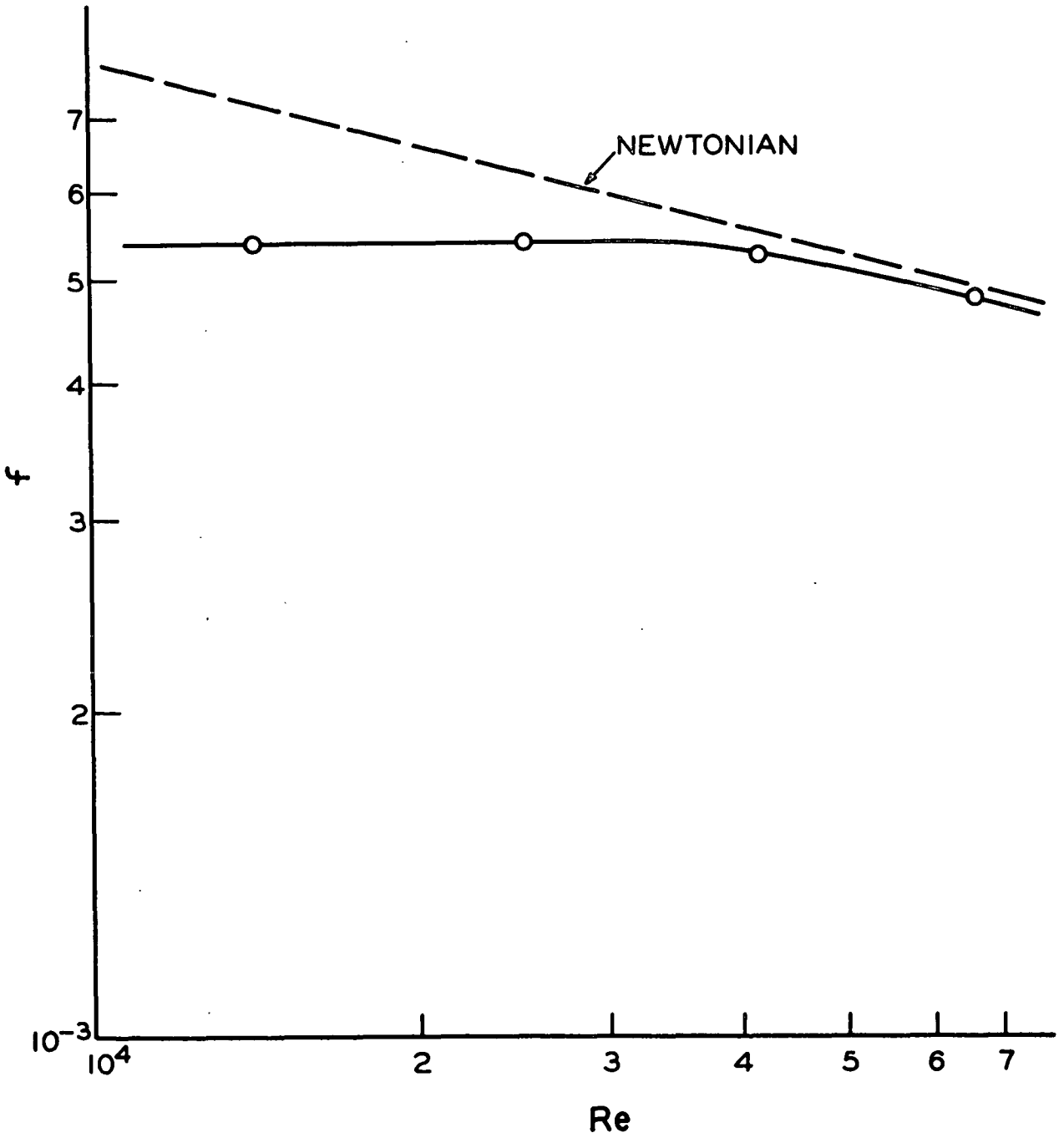

Figure 30. Friction Factor vs. Reynolds Number, Γ = 0.064 g./100 ml. Sample 2 in 1.400-in. i.d. Tube (20°C.)

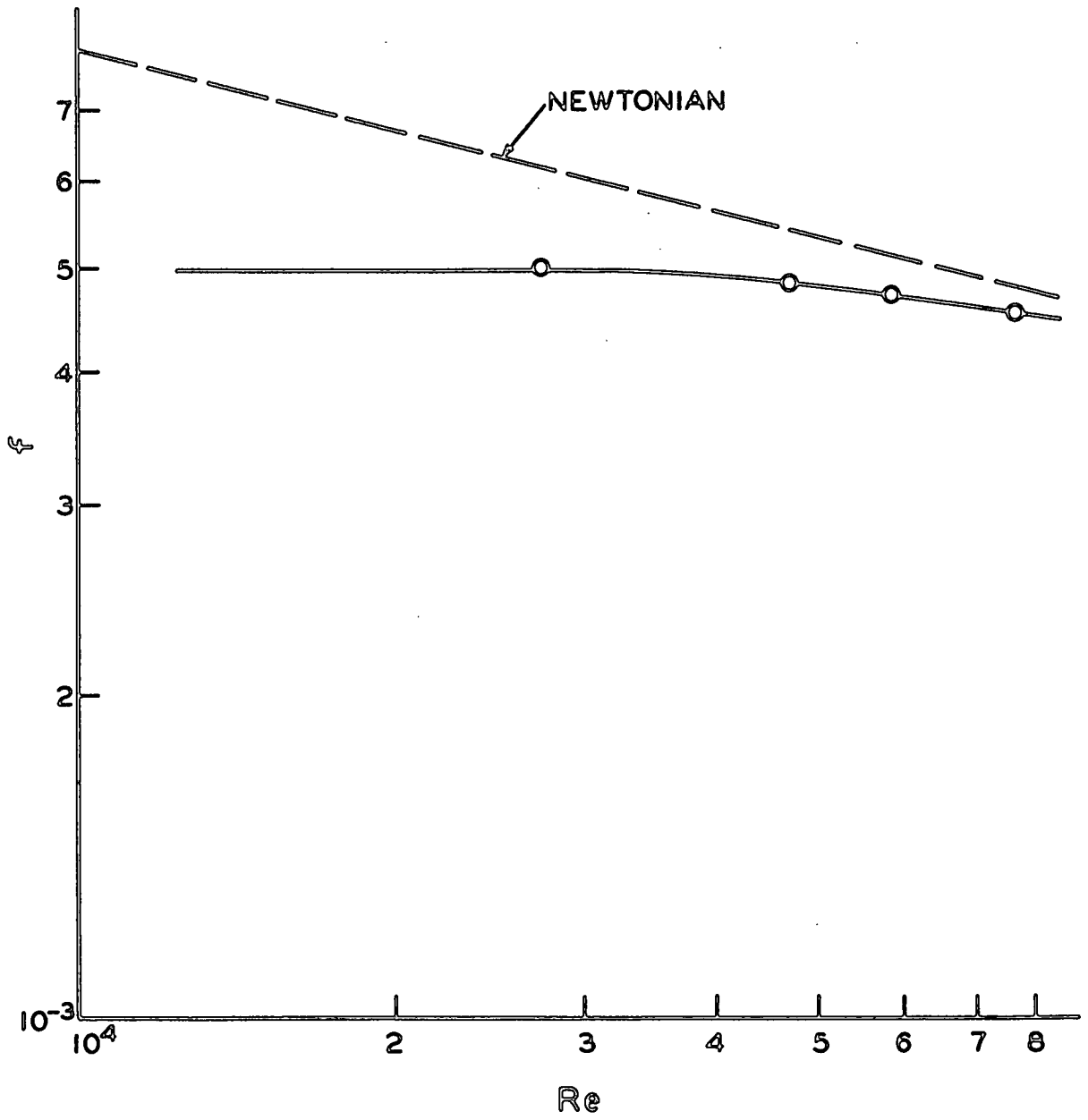

Figure 31. Friction Factor vs. Reynolds Number, Γ = 0.12 g./100 ml. Sample 2 in 1.400-in. i.d. Tube (20°C.)

APPENDIX IV

AN EXAMPLE OF κ DETERMINATION

The following data analysis indicates the method employed in determining κ values from raw data. The example includes the velocity profiles for Sample 2578 in the 1.875-in. i.d. flow loop at 0.157 g./100 ml.

Impact pressures (Table X) are converted to velocities and the velocity profile curve (Fig. 32-33) is constructed. From the curve, velocities are read at selected points and converted to reduced position-reduced velocity tables (Table XI). The apparent von Kármán constant is determined from the slope of the semilogarithmic $\underline{v}^+ - \underline{s}^+$ plot (Fig. 34).

For the small impact probe combined with a CCl_4/H_2O differential liquid-liquid manometer: $\overline{\underline{v}} = 1.113\sqrt{\Delta \underline{h}_i}$ where $\overline{\underline{v}}$ is in ft. sec.$^{-1}$ and $\Delta \underline{h}_i$ is in cm.

Additional examples of $\underline{v}^+ - \underline{s}^+$ plots follow the specific series carried through (Fig. 35-37). Note that one of the addition examples, Fig. 37, indicates plug turbulence.

TABLE X

IMPACT PRESSURES

Station	$\sqrt{\Delta h_i}$	$\bar{v}$, ft. sec.$^{-1}$
Q = 0.0270 ft.^{3} sec.$^{-1}$		
1.50	1.45	1.62
1.75	1.41	1.57
2.00	1.25	1.39
Q = 0.0350 ft.^{3} sec.$^{-1}$		
0.58	1.32	1.47
0.75	1.57	1.75
0.88	1.67	1.86
1.00	1.79	2.00
1.25	1.88	2.10
1.38	2.00	2.24
1.50	2.05	2.29
1.63	1.90	2.12
1.88	1.76	1.96
2.00	1.63	1.82
2.13	1.45	1.62
2.25	1.30	1.45
Q = 0.0661 ft.^{3} sec.$^{-1}$		
0.56	2.51	2.80
0.63	2.72	3.03
0.75	3.05	3.40
0.88	3.38	3.77
1.00	3.51	3.92
1.13	3.58	3.99
1.25	3.63	4.05
1.38	3.65	4.07
1.50	3.62	4.04
1.63	3.56	3.97
1.75	3.48	3.88
1.88	3.29	3.67
2.00	3.10	3.46
2.13	2.95	3.29
2.25	2.51	2.80

Station	$\sqrt{\Delta h_i}$	$\bar{v}$, ft. sec.$^{-1}$
Q = 0.115 ft.^{3} sec.$^{-1}$		
0.56	4.56	5.09
0.63	5.01	5.60
0.75	5.47	6.11
1.00	6.02	6.72
1.25	6.21	6.93
1.38	6.29	7.02
1.50	6.30	7.03
1.75	6.18	6.90
2.00	5.85	6.52
2.13	5.49	6.13
2.25	5.04	5.63
Q = 0.1365 ft.^{3} sec.$^{-1}$		
0.56	5.76	6.42
0.63	6.16	6.87
0.75	6.65	7.41
0.88	7.00	7.80
1.13	7.31	8.16
1.38	7.39	8.24
1.50	7.40	8.25
1.75	7.27	8.11
2.00	6.71	7.50
2.25	5.96	6.65

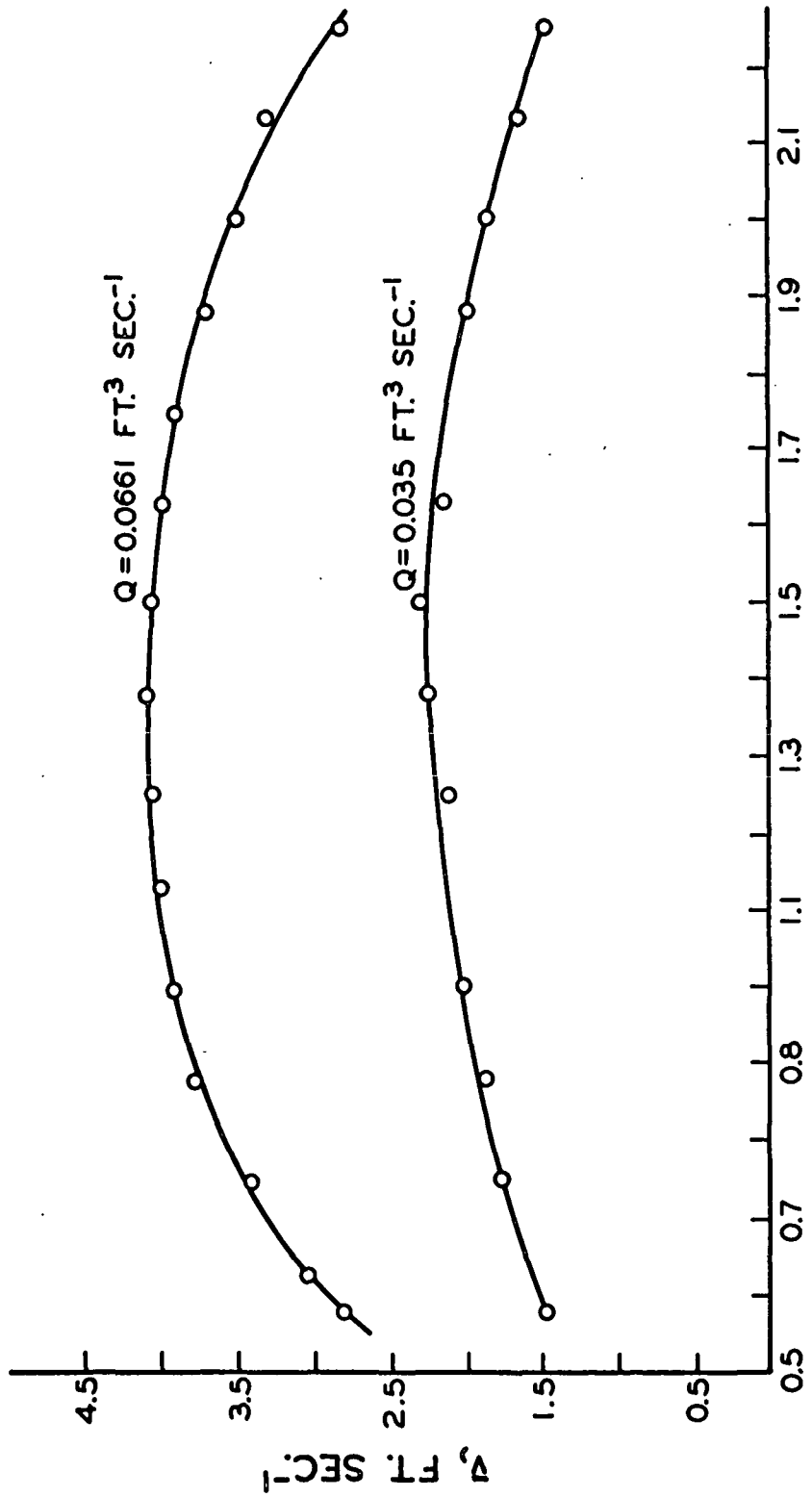

Figure 32. Velocity Profiles

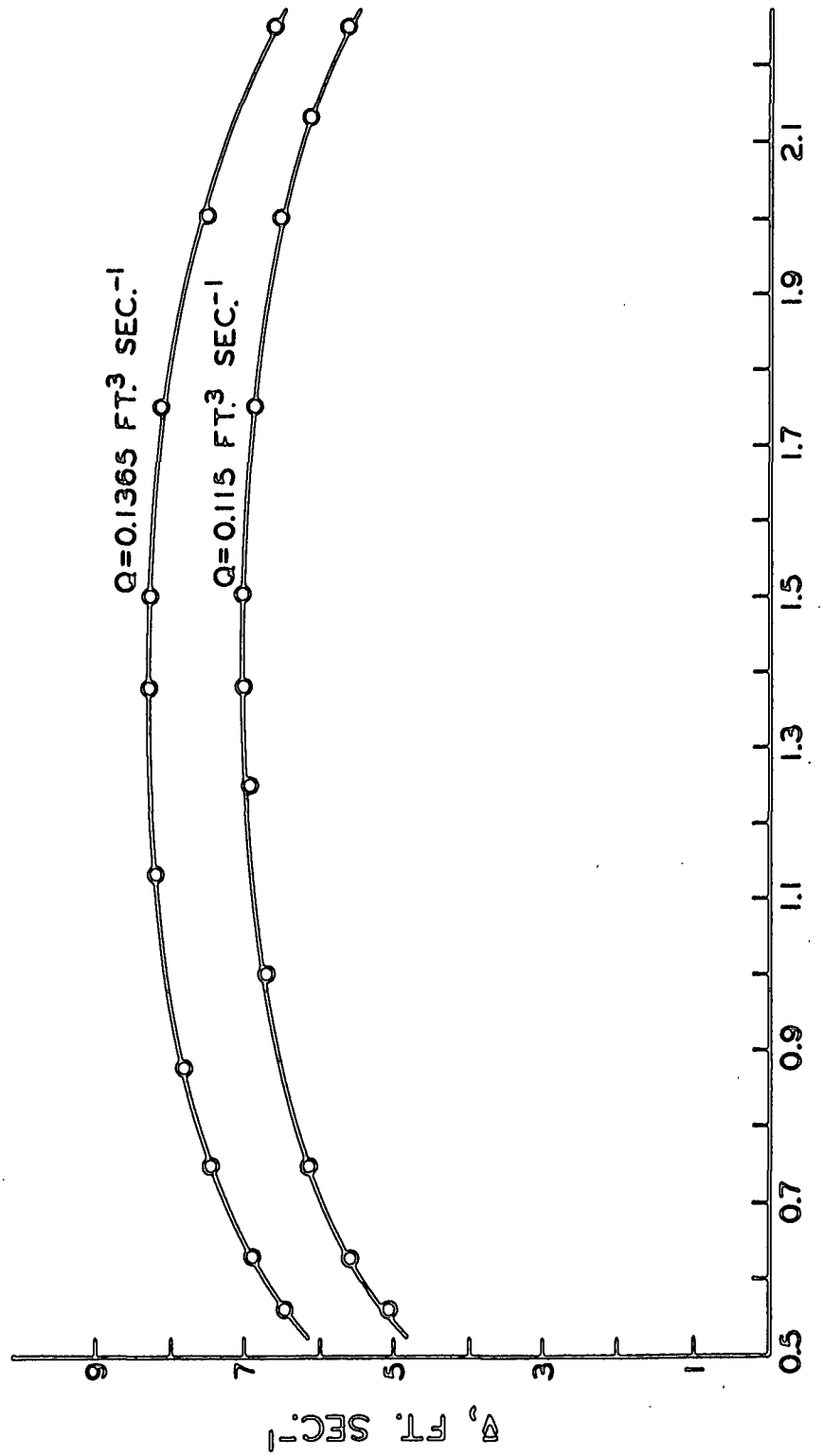

Figure 33. Velocity Profiles

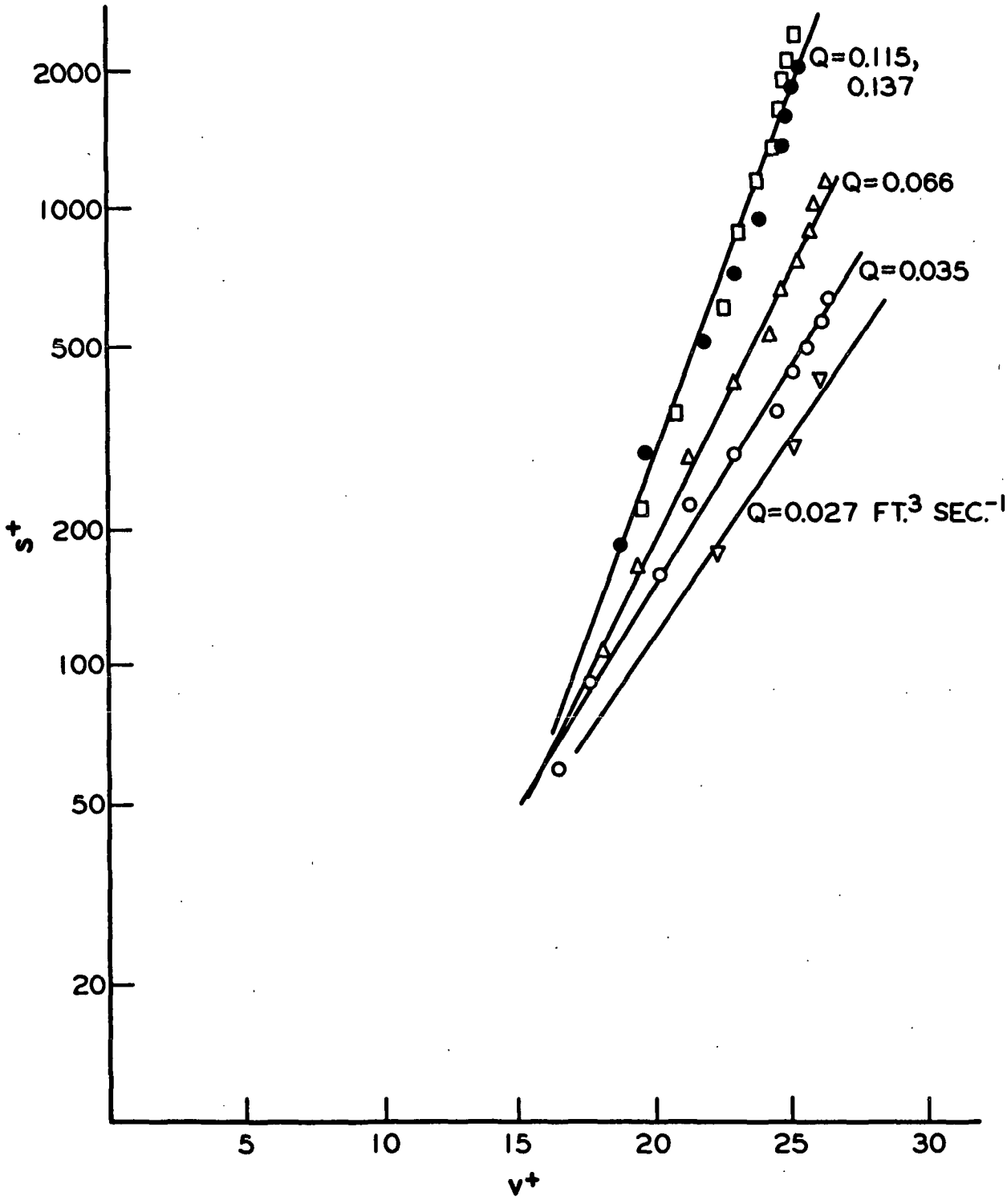

Figure 34. $\underline{v}^+$ vs. $\underline{s}^+$; Γ = 0.157 g./100 ml., $\underline{D}$ = 1.875 in.
(Sample 2578)

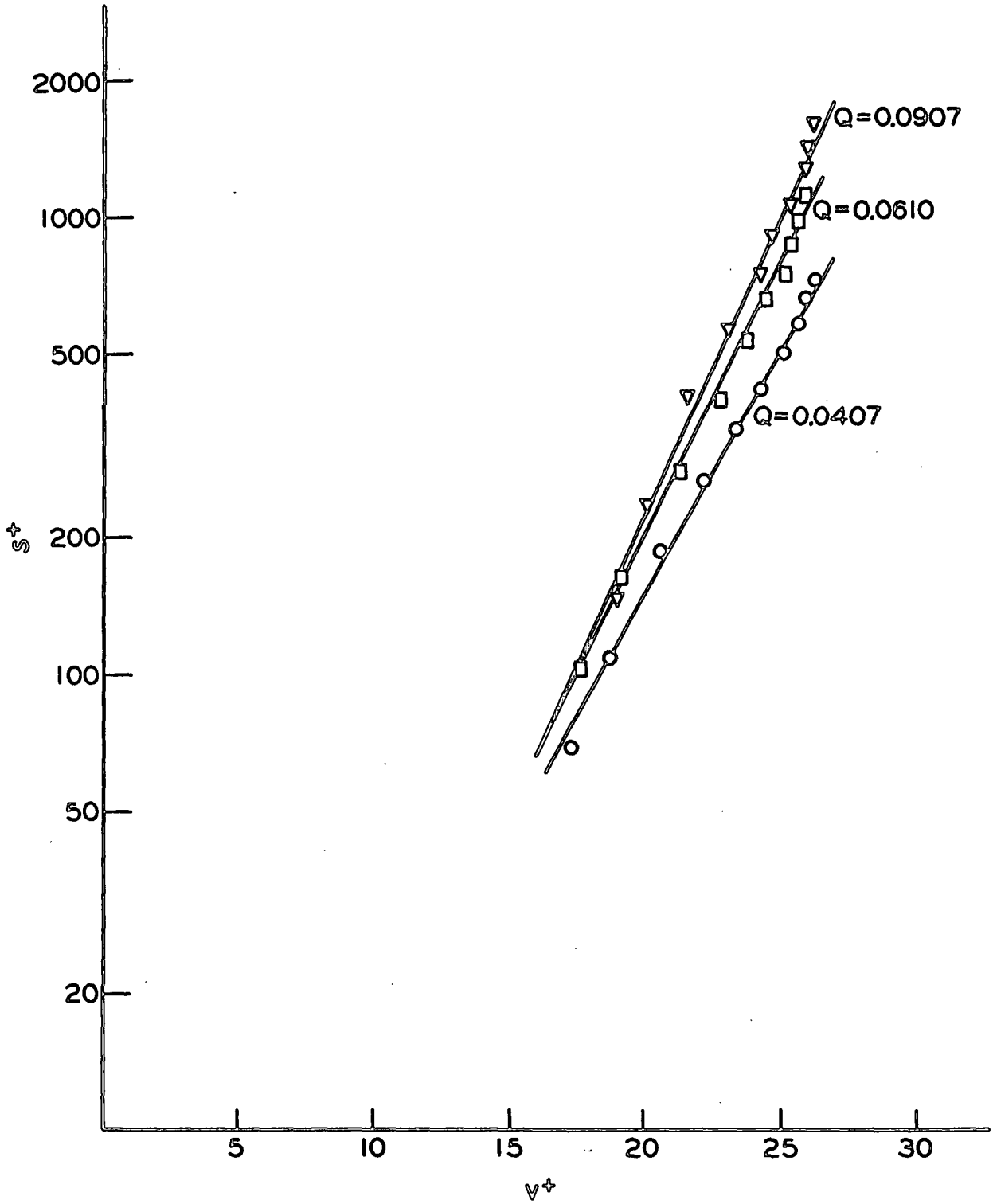

Figure 35. $\underline{s}^+$ vs. $\underline{v}^+$, Γ = 0.100 g./100 ml., $\underline{D}$ = 1.875 in. (Sample 2578)

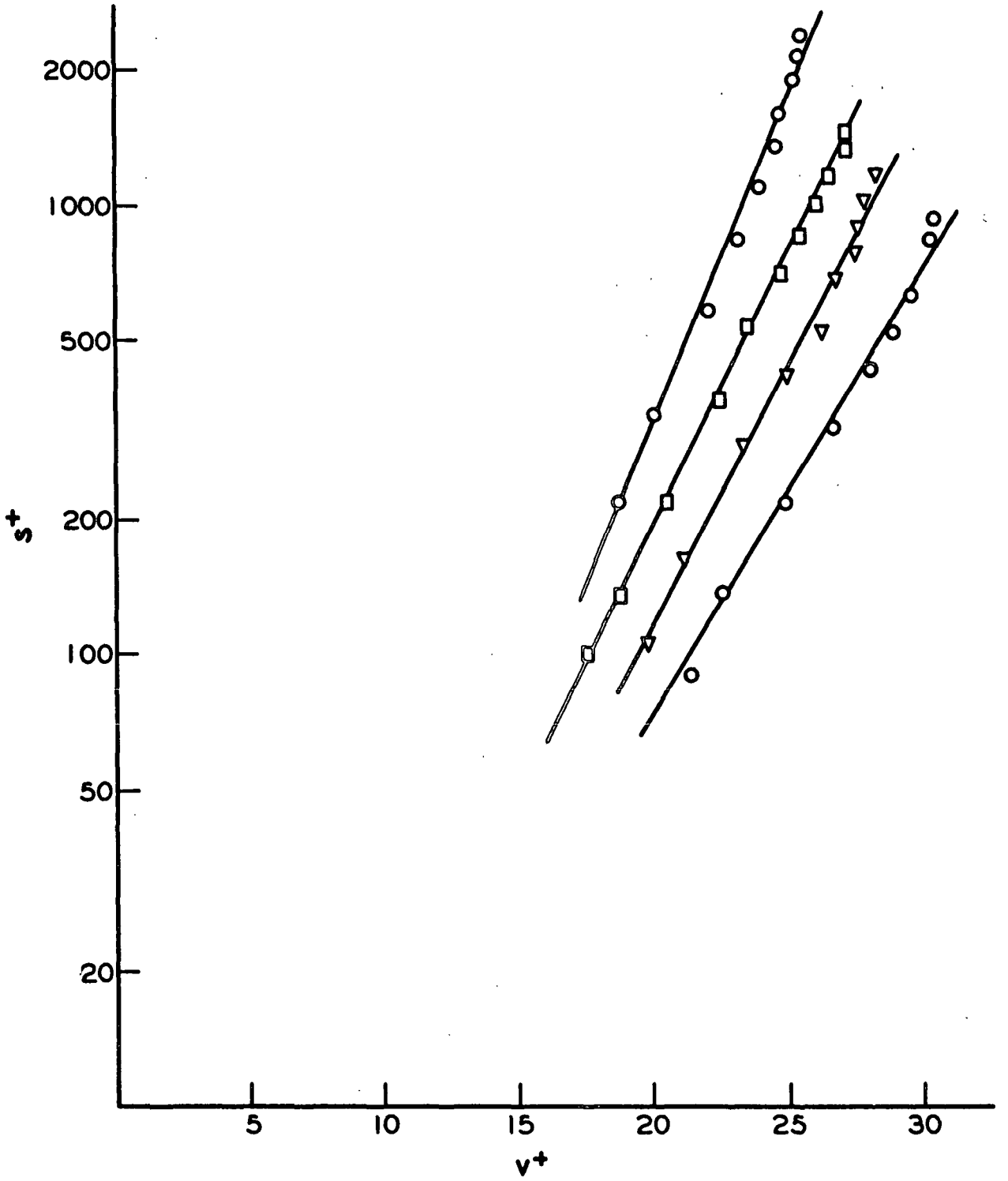

Figure 36. $\underline{s}^+$ vs. $\underline{v}^+$; Γ = 0.31 g./100 ml., $\underline{D}$ = 1.875 in. (Sample 2578)

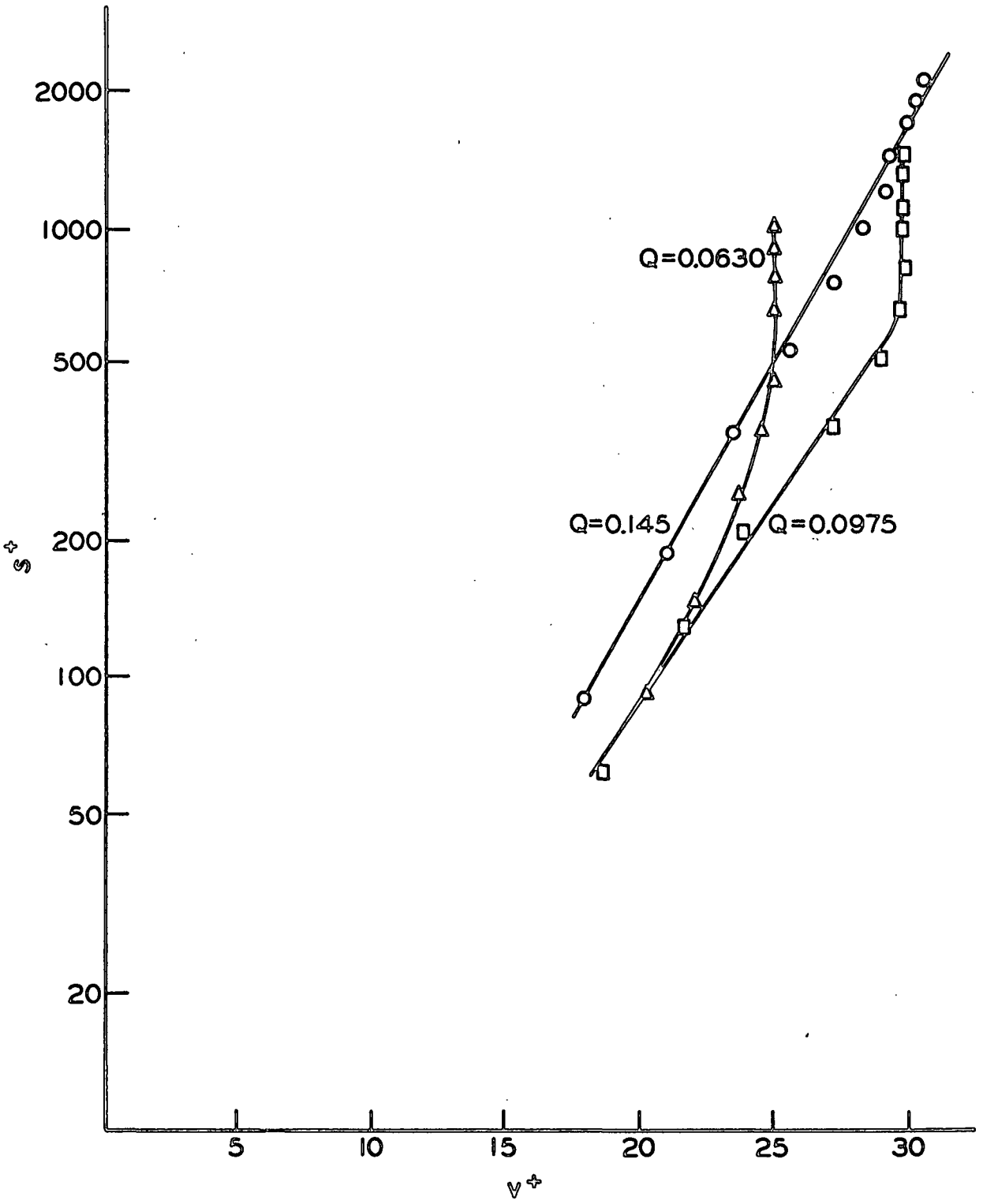

Figure 37. $\underline{s}^+$ vs. $\underline{v}^+$; Γ = 0.58 g./100 ml., $\underline{D}$ = 1.875 in. (Sample 2578)

TABLE XI

REDUCED VELOCITY PROFILES – SAMPLE 2578

Γ = 0.157 g./100 ml., D = 1.875 in.

$$v^+ = \bar{v}/\sqrt{\tau_o/\rho} = \bar{v}/v_*$$

$$s^+ = s\sqrt{\tau_o/\rho}/\nu = sv_*/\nu$$

For water at 20°C.,

$$\nu = 1.00 \text{ cm.}^2 \text{ sec.}^{-1}$$

$$v_* = \sqrt{\tau_o/\rho} = 1.67\sqrt{\Delta h_s} \text{ cm. sec.}^{-1} = 0.0547\sqrt{\Delta h_s} \text{ ft. sec.}^{-1}$$

r, in.	s, cm.	s^+	v, ft. sec.$^{-1}$	v^+
Q = 0.0270 ft.^{3} sec.$^{-1}$				
Δh_s = 1.3 cm.				
v_* = 1.91 cm. sec.$^{-1}$ = 0.0625 ft. sec.$^{-1}$				
0.08	2.18	414	1.62	26.0
0.33	1.54	292	1.57	25.2
0.58	0.91	173	1.39	22.2
Q = 0.0350 ft.^{3} sec.$^{-1}$				
Δh_s = 2.6 cm.				
v_* = 2.70 cm. sec.$^{-1}$ = 0.0882 ft. sec.$^{-1}$				
0.0	2.38	643	2.25	25.5
0.1	2.13	575	2.23	25.3
0.2	1.87	505	2.20	25.0
0.3	1.62	437	2.14	24.3
0.4	1.36	367	2.05	23.2
0.5	1.11	300	1.95	22.1
0.6	0.86	232	1.82	20.6
0.7	0.60	162	1.72	19.5
0.8	0.35	94.5	1.52	17.7
0.85	0.22	59.5	1.42	16.1

TABLE XI (Continued)

REDUCED VELOCITY PROFILES – SAMPLE 2578

Γ = 0.157 g./100 ml., D = 1.875 in.

$$v^+ = \bar{v}/\sqrt{\tau_o/\rho} = \bar{v}/v_*$$

$$s^+ = s\sqrt{\tau_o/\rho}/\nu = sv_*/\nu$$

r, in.	s, cm.	s^+	v, ft. sec.$^{-1}$	v^+
Q = 0.0661 ft.^{3} sec.$^{-1}$				
Δh_s = 8.2 cm.				
v_* = 4.78 cm. sec.$^{-1}$ = 0.157 ft. sec.$^{-1}$				
0.0	2.38	1140	4.09	26.1
0.1	2.13	1020	4.06	25.8
0.2	1.87	895	4.03	25.6
0.3	1.62	775	3.97	25.3
0.4	1.36	650	3.88	24.7
0.5	1.11	530	3.76	23.9
0.6	0.86	411	3.58	22.8
0.7	0.60	287	3.34	21.2
0.8	0.35	167	3.00	19.1
0.85	0.22	105	2.85	18.1
Q = 0.115 ft.^{3} sec.$^{-1}$				
Δh_s = 25.7 cm.				
v_* = 8.47 cm. sec.$^{-1}$ = 0.278 ft. sec.$^{-1}$				
0.0	2.38	2020	7.05	25.4
0.1	2.13	1810	7.00	25.2
0.2	1.87	1580	6.95	25.0
0.3	1.62	1370	6.90	24.8
0.4	1.36	1150	6.80	24.4
0.5	1.11	940	6.65	24.0
0.6	0.86	730	6.40	23.0
0.7	0.60	590	6.05	21.8
0.8	0.35	297	5.50	19.8
0.85	0.22	186	5.20	18.7

TABLE XI (Continued)

REDUCED VELOCITY PROFILES – SAMPLE 2578

Γ = 0.157 g./100 ml., D = 1.875 in.

$$v^+ = \bar{v}/\sqrt{\tau_o/\rho} = \bar{v}/v_*$$

$$s^+ = s\sqrt{\tau_o/\rho}/\nu = sv_*/\nu$$

$\underline{Q}$ = 0.1365 ft.^{3} sec.$^{-1}$

$\Delta h_{\underline{s}}$ = 36.3 cm.

$\underline{v_*}$ = 10.1 cm. sec.$^{-1}$ = 0.331 ft. sec.$^{-1}$

$\underline{r}$, in.	$\underline{s}$, cm.	$\underline{s}^+$	$\underline{v}$. ft. sec.$^{-1}$	$\underline{v}^+$
0.0	2.38	2400	8.30	25.1
0.1	2.13	2150	8.25	24.9
0.2	1.87	1890	8.22	24.8
0.3	1.62	1640	8.20	24.8
0.4	1.36	1370	8.10	24.5
0.5	1.11	1120	7.95	24.0
0.6	0.86	870	7.70	23.3
0.7	0.60	605	7.38	22.6
0.8	0.35	359	6.90	20.8
0.85	0.22	222	6.50	19.6

APPENDIX V

EXPERIMENTALLY DETERMINED VALUES OF κ

This appendix is a summary of experimentally determined values of κ in both tabular and graphical form. Accompanying the graphical representation are curves representing the two proposed empirical representations of κ:

$$\kappa = c(D) + \alpha(\Gamma)Q \tag{34}$$

and

$$\kappa = \left(\frac{\sqrt{\beta/2}}{1 - 13\sqrt{\beta/2}}\right)\left[\ln\left(\frac{Re\sqrt{\beta/2}}{60}\right) - \frac{3}{2}\right] \tag{46}$$

.

Actually, the second equation would do a more complete job if β were replaced by the experimental values of $\underline{f}$, since the equation would then extend into Newtonian turbulence and would adequately handle the transition between damped and Newtonian turbulence.

While the latter equation does a bit more poorly in reproducing experimental data it is in a sense the more useful of the two being easier to apply beyond the range of existing velocity profile data.

Table XII presents the experimental data while Fig. 38-47 present them graphically along with the empirical equations suggested.

TABLE XII

TABULATION OF APPARENT VON KÁRMÁN CONSTANT AS A FUNCTION OF FLOW RATE AND CONSISTENCY

Sample	Γ, g./100 ml.	D, in.	Q, $ft.^3$ $sec.^{-1}$	κ
2578	0.0995	1.875	0.0407	0.252
			0.0610	0.282
			0.0822	0.324
			0.0907	0.330
			0.123	0.340
			0.1415	0.350
2578	0.157	1.875	0.0270	0.207
			0.0350	0.233
			0.0661	0.273
			0.115	0.350
			0.137	0.355
2578	0.313	1.875	0.0595	0.229
			0.0700	0.258
			0.0920	0.280
			0.111	0.286
			0.145	0.327
2578	0.585	1.875	0.0975	0.194
			0.123	0.230
			0.145	0.240
2578	0.100	1.400	0.0199	0.243
			0.285	0.278
			0.0350	0.286
			0.0465	0.300
			0.0590	0.320
			0.0720	0.332
2578	0.208	1.400	0.0255	0.240
			0.0390	0.249
			0.0615	0.275
			0.0795	0.318
2	0.112	1.875	0.0380	0.243
			0.0590	0.275
			0.0745	0.275
			0.0905	0.317
			0.1095	0.320

TABLE XII (Continued)

TABULATION OF APPARENT VON KÁRMÁN CONSTANT AS A FUNCTION OF FLOW RATE AND CONSISTENCY

Sample	Γ, g./100 ml.	D, in.	Q, ft.^{3} sec.$^{-1}$	κ
2	0.277	1.875	0.0388	0.160
			0.0560	0.167
			0.0740	0.187
			0.0900	0.226
			0.112	0.260
			0.135	0.312
2	0.0636	1.400	0.0135	0.232
			0.0240	0.307
			0.0395	0.297
			0.0630	0.316
2	0.124	1.400	0.0435	0.270
			0.0555	0.332
			0.0725	0.355
			0.0945	0.370

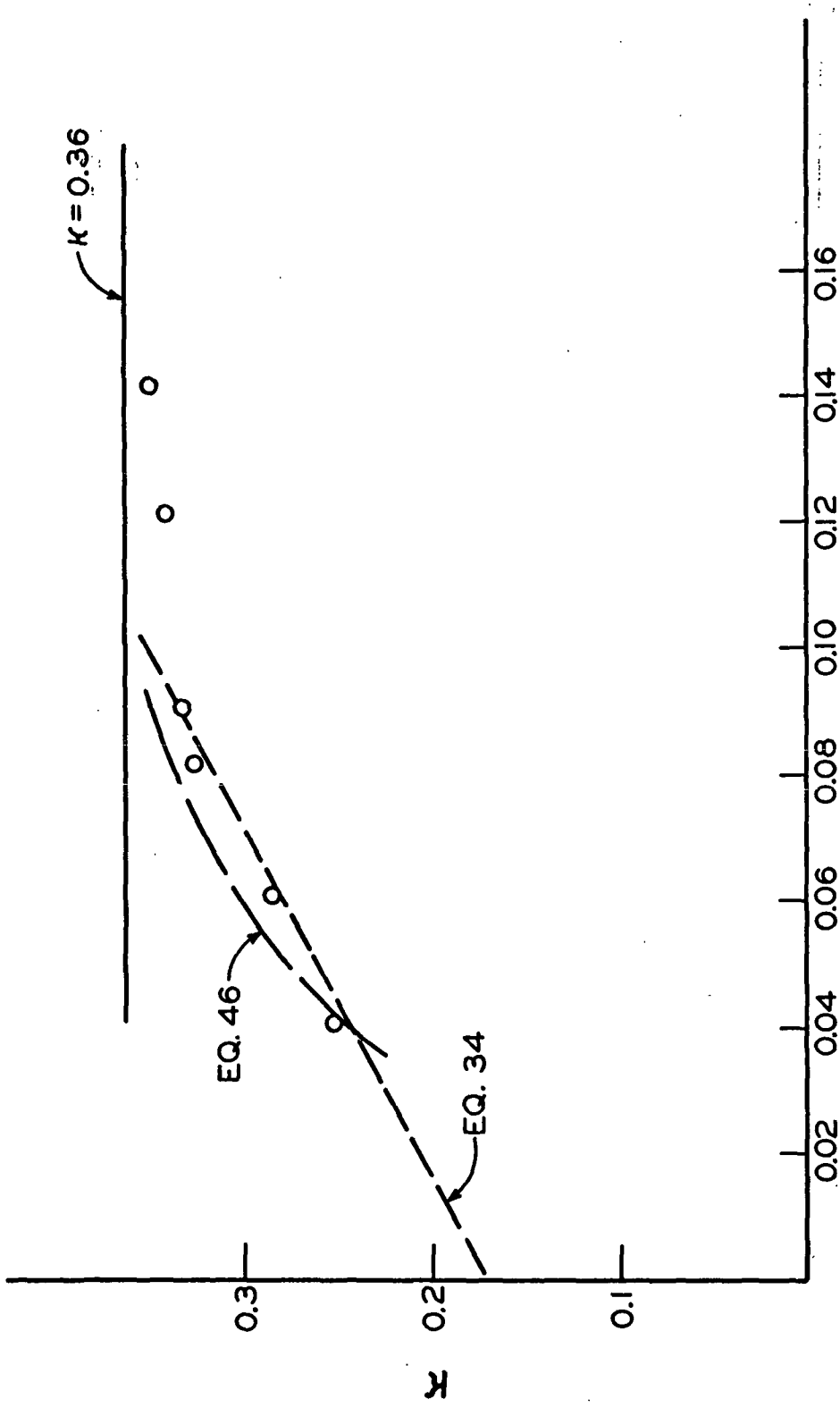

Figure 38. κ vs. Q, Sample 2578 in 1.875-in. i.d. Tube; Γ = 0.0995 g./100 ml.

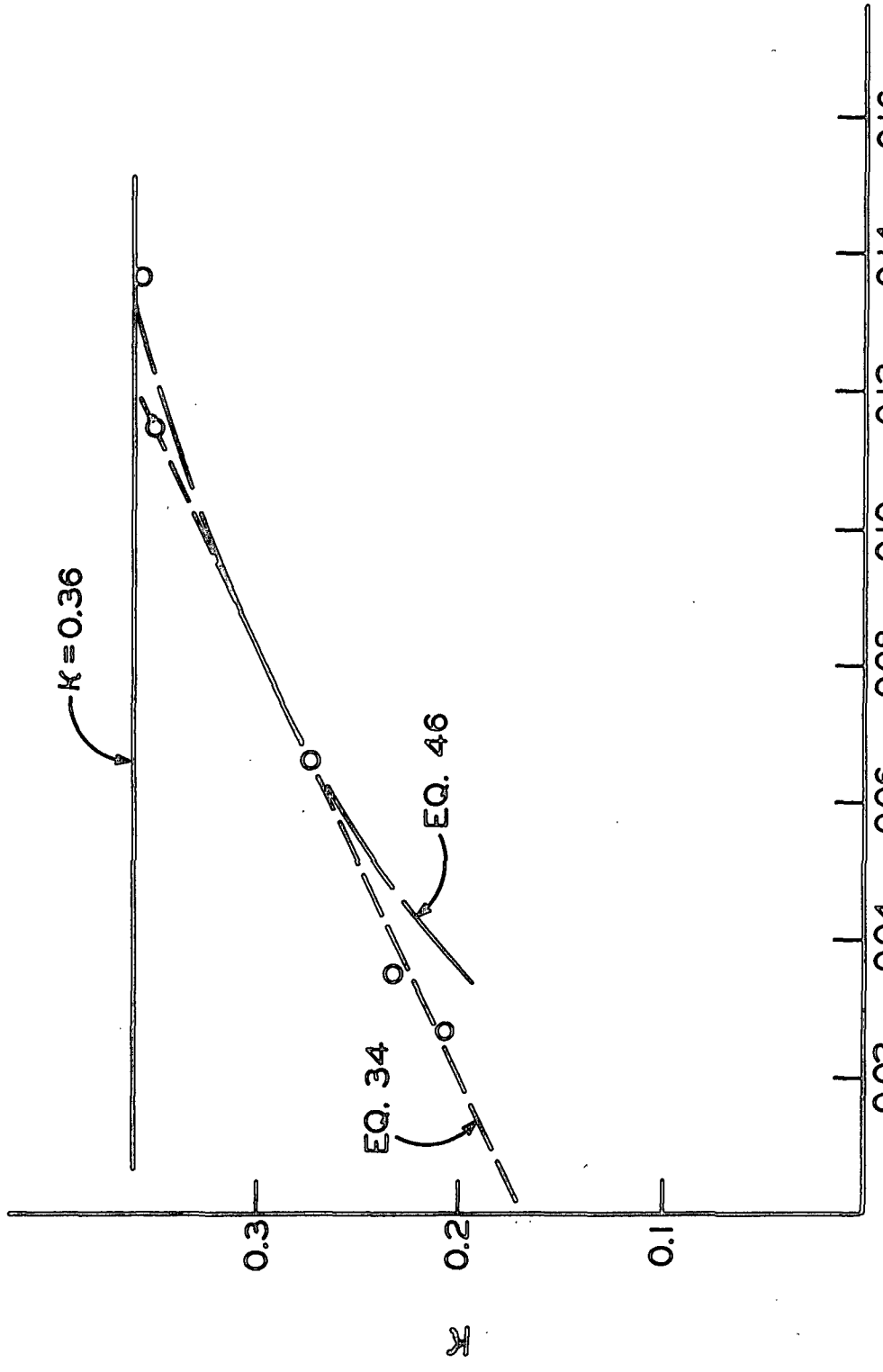

Figure 39. K vs. Q, Sample 2578 in 1.875-in. i.d. Tube; Γ = 0.157 g./100 ml.

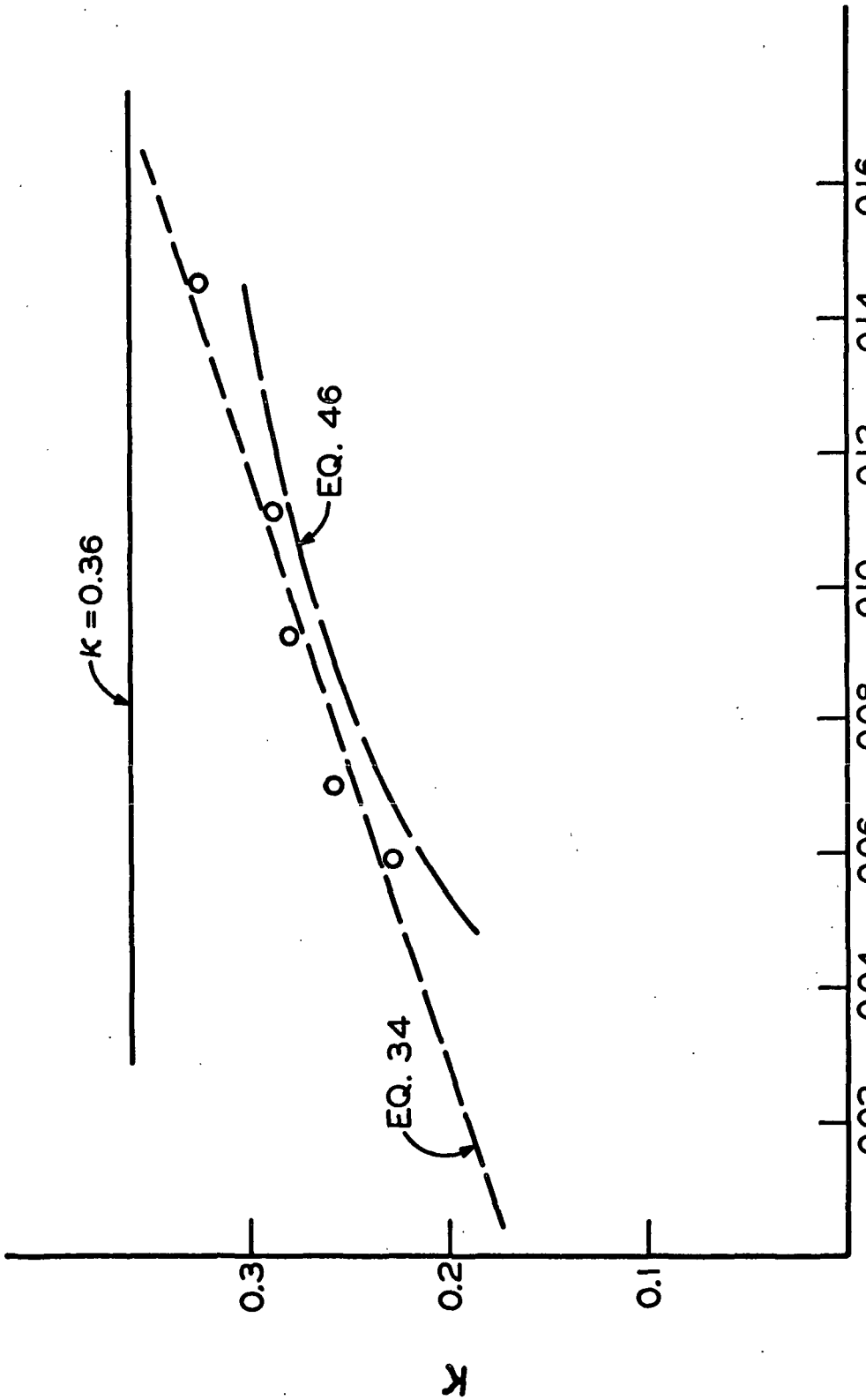

Figure 40. κ vs. Q, Sample 2578 in 1.875-in. i.d. Tube; Γ = 0.313 g./100 ml.

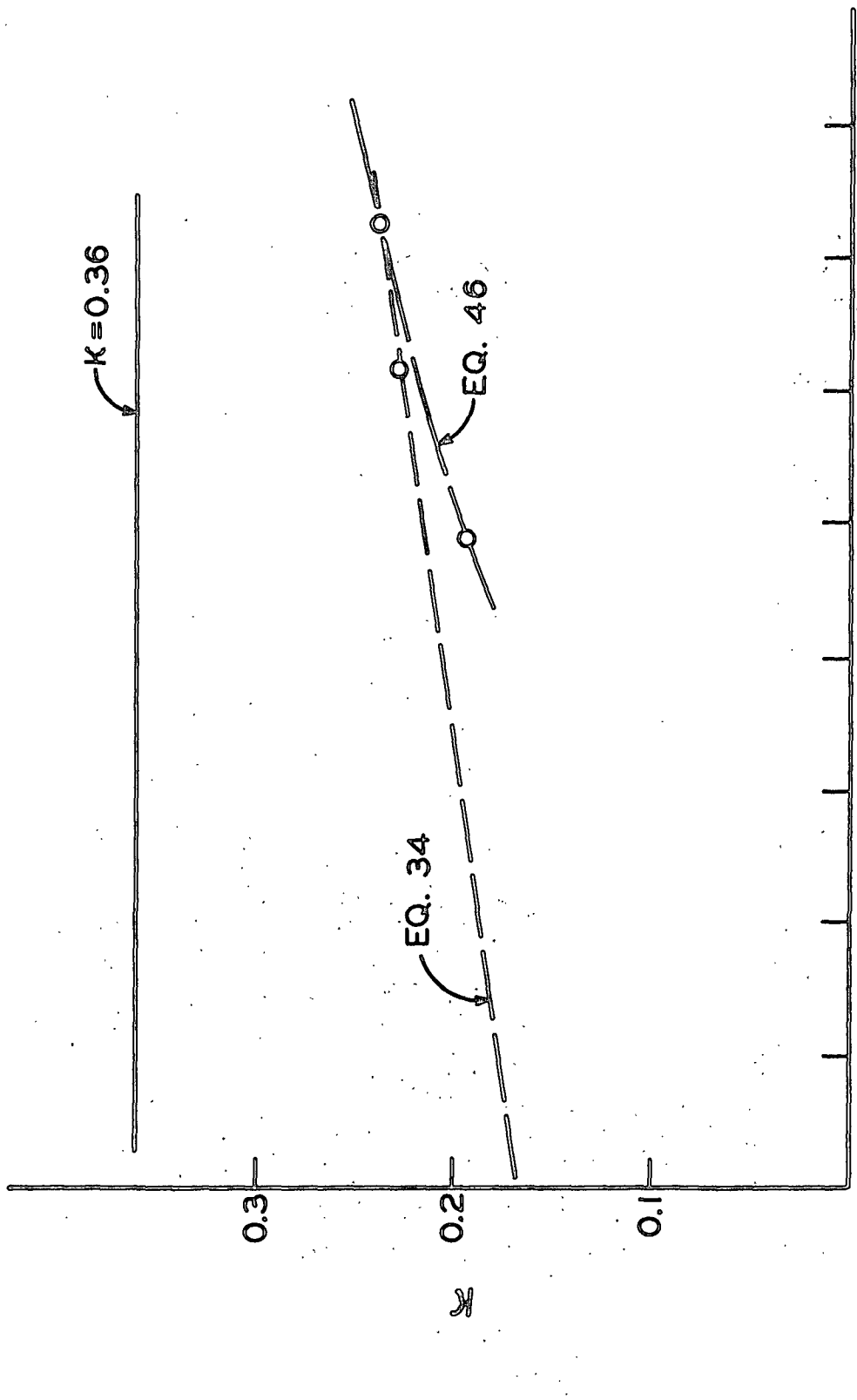

Figure 41. K vs. Q, Sample 2578 in 1.875-in. i.d. Tube; Γ = 0.585 g./100 ml.

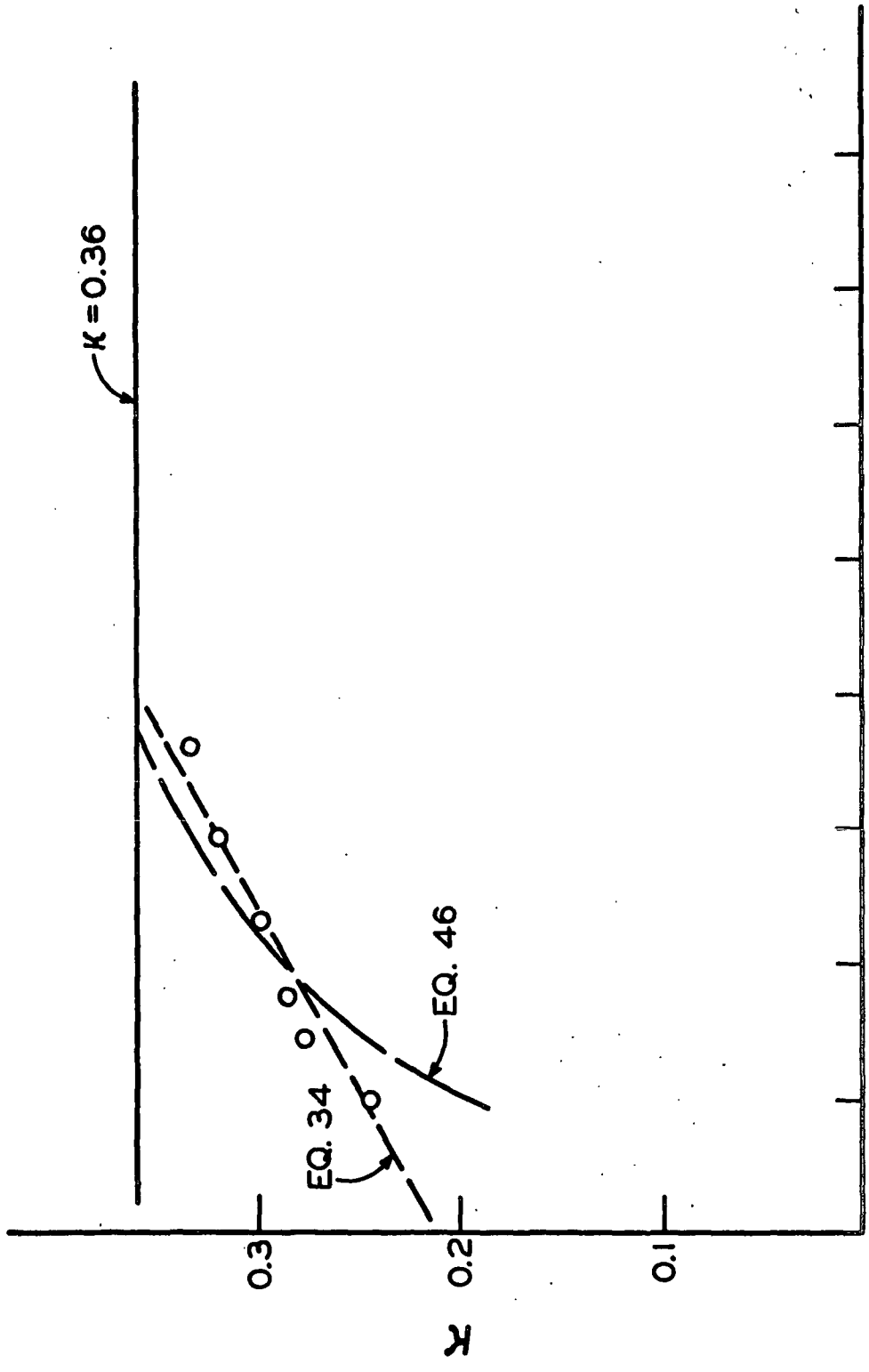

Figure 42. κ vs. Q, Sample 2578 in 1.400-in. i.d. Tube; Γ = 0.100 g./100 ml.

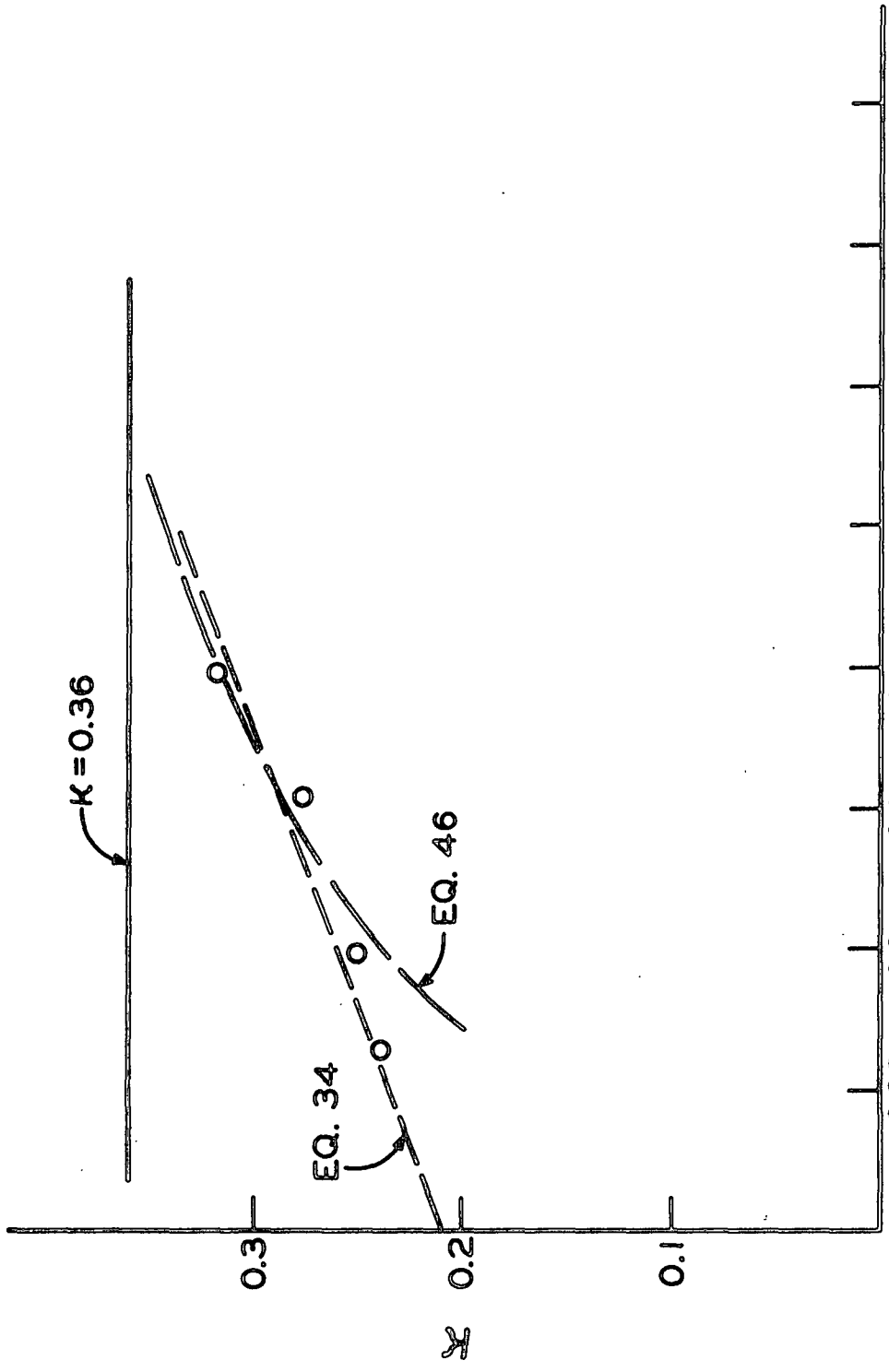

Figure 43. κ vs. Q, Sample 2578 in 1.400-in. i.d. Tube; Γ = 0.208 g./100 ml.

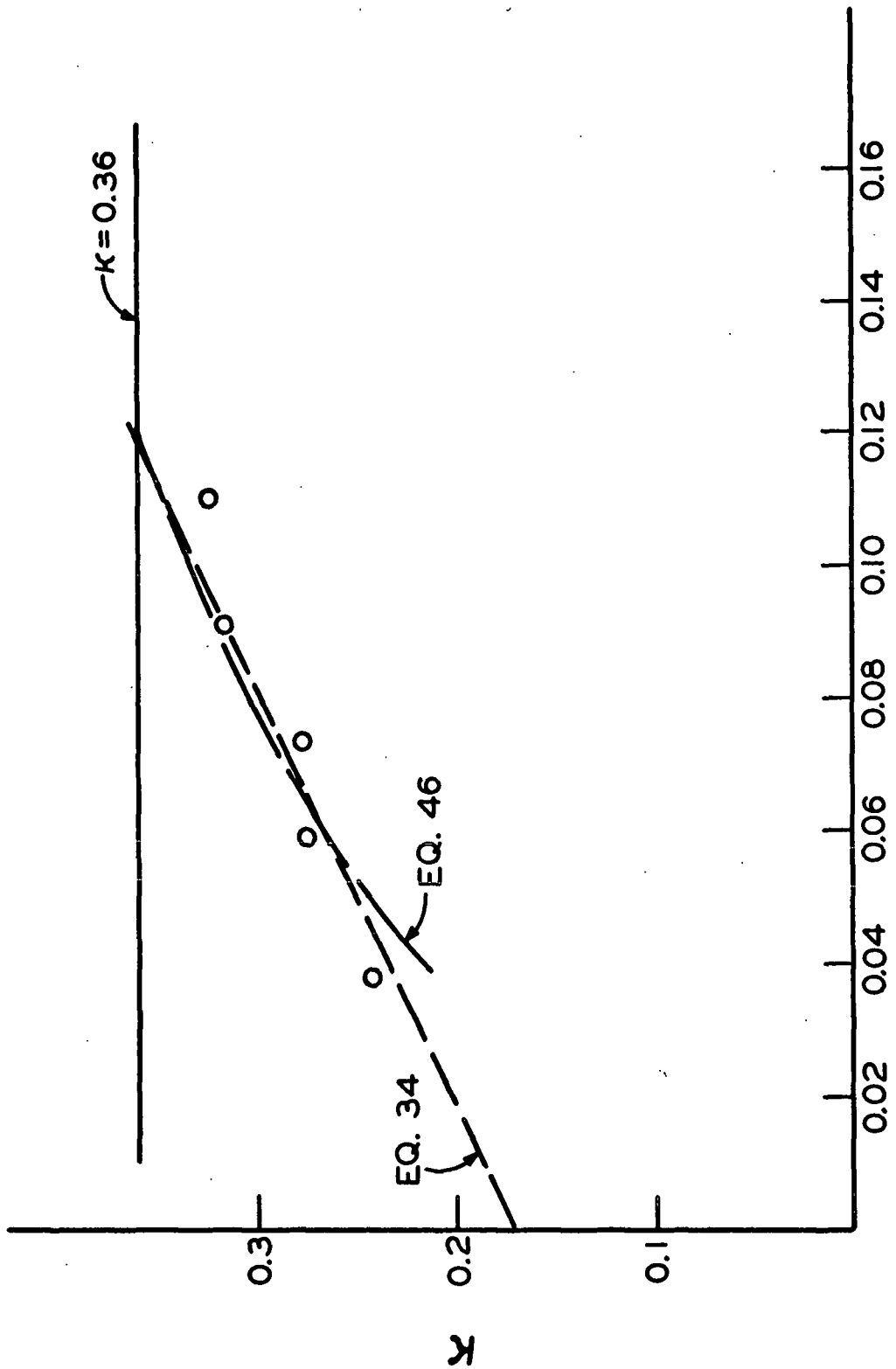

Figure 44. κ vs. Q, Sample 2 in 1.875-in. i.d. Loop; Γ = 0.112 g./100 ml.

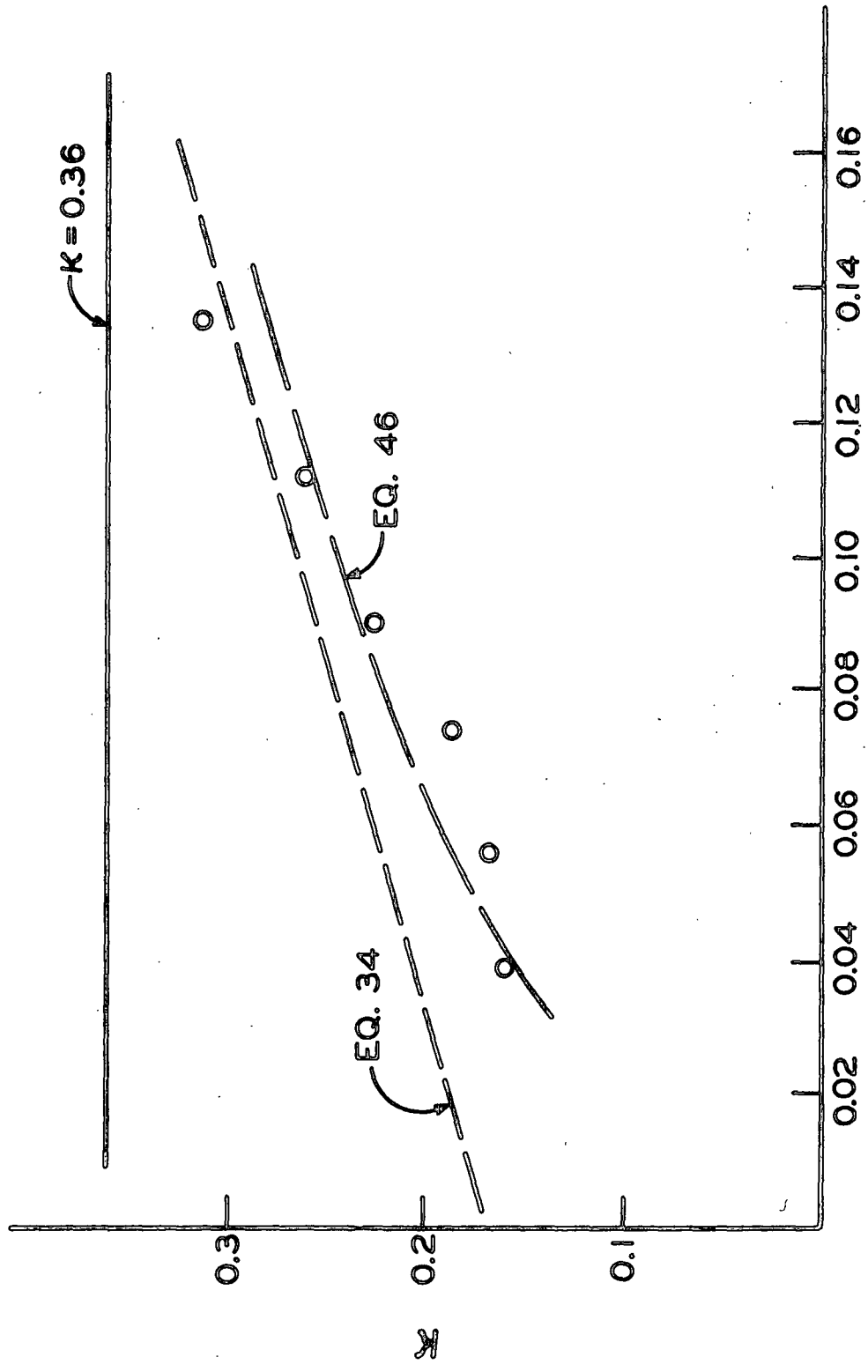

Figure 45. κ vs. Q, Sample 2 in 1.875-in. i.d. Tube; Γ = 0.277 g./100 ml.

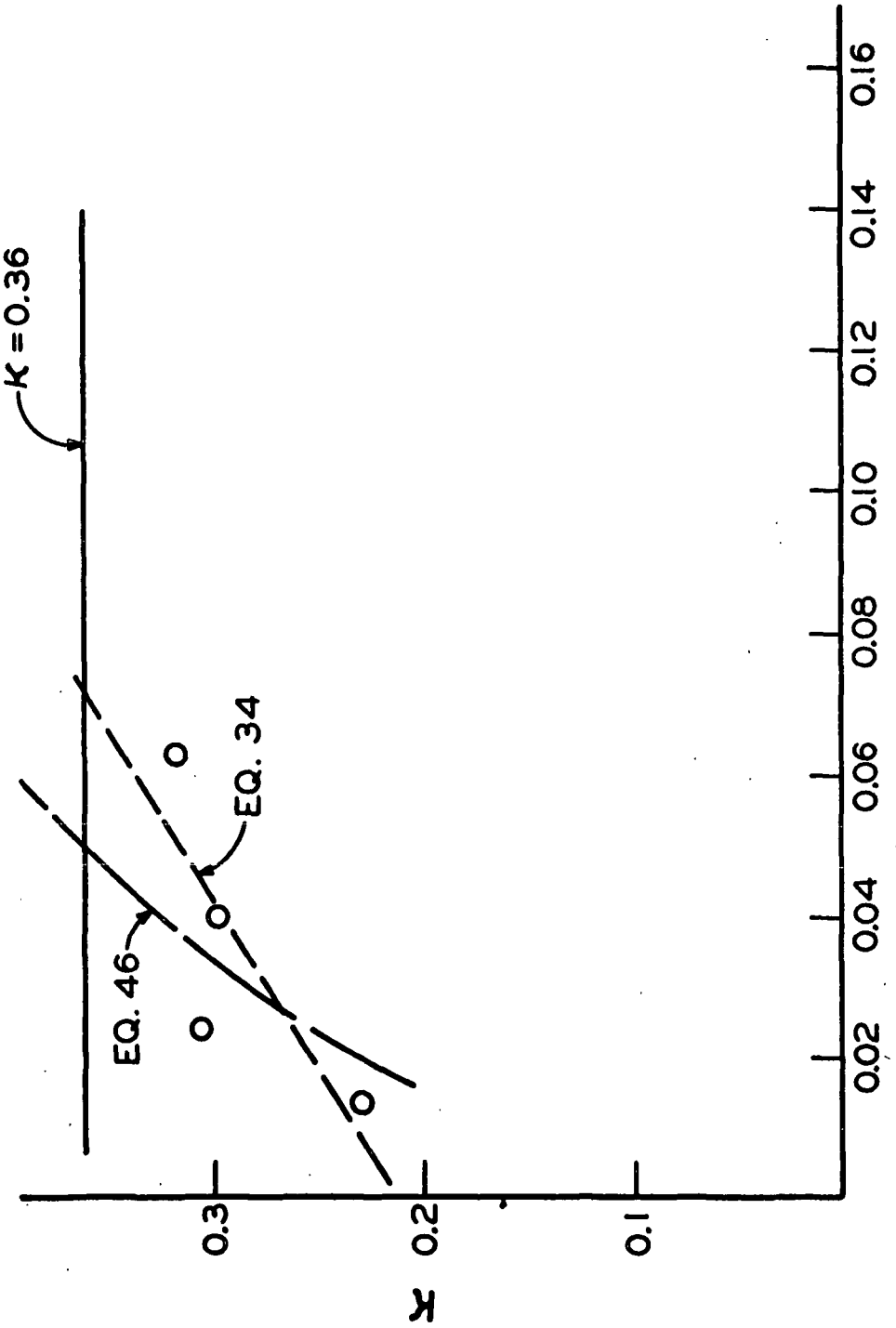

Figure 46. κ vs. Q, Sample 2 in 1.400-in. i.d. Tube; Γ = 0.0639 g./100 ml.

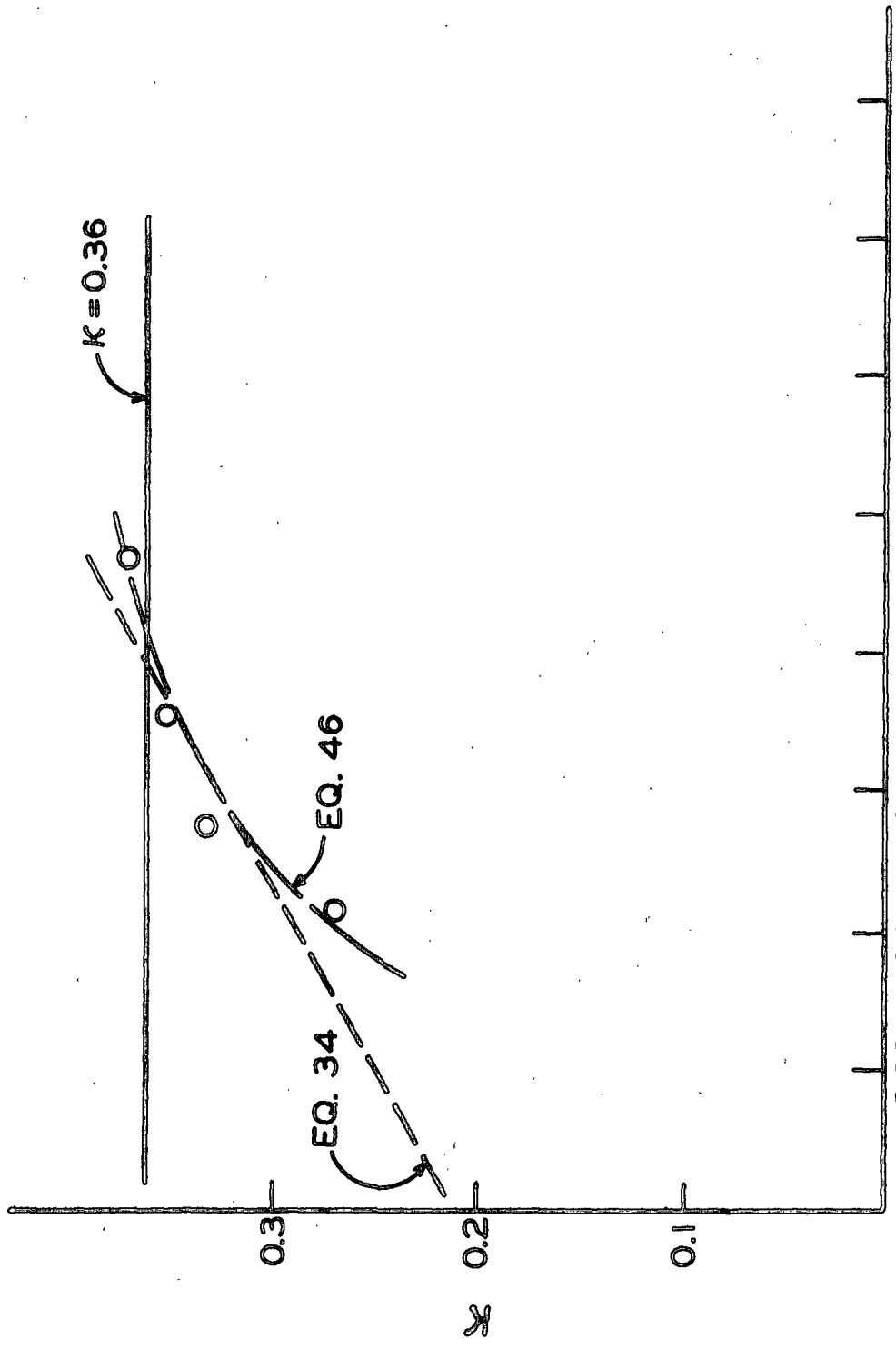

Figure 47. κ vs. Q, Sample 2 in 1.400-in. i.d. Tube; Γ = 0.124 g./100 ml.